PHYSICAL STUDIES OF SOLAR SYSTEM OBJECTS

A Thesis

Submitted for the Degree of

Doctor of Philosophy in the Faculty of Science

BANGALORE UNIVERSITY

By

R. VASUNDHARA

INDIAN INSTITUTE OF ASTROPHYSICS

BANGALORE 560034

INDIA

FEBRUARY 1993

Declaration

I hereby declare that the matter contained in this thesis is the result of the investigation carried out by me at the Indian Institute of Astrophysics, Bangalore and the Department of Physics, Bangalore University, under the supervision of Prof.J.C.Bhattacharyya and Dr.A.R.Hanumanthappa. This work has not been submitted for the award of any degree, diploma, associateship, fellowship etc. of any University or Institute.

R.Vasundhara

Candidate

J.C.Bhattacharyya

Supervisor

A.R.Hanumanthappa

Supervisor

Bangalore 560034
1993 February

Acknowledgement

i

Summary

One of the several key issues in the study of solar system objects concerns the evolution of Jupiter's Galilean satellite system. Volcanic activity on Io and its excess infrared heat flux have been attributed to the tides raised on it by Jupiter. The tidal heating is maintained due to eccentricity forced on its orbit by the Laplace resonance involving the three inner regular satellites, Io itself, Europa and Ganymede. The energy for tidal heating must come from Io's orbit but due to the Laplace resonance between Io, Europa and Ganymede the energy loss is shared among the three satellite orbits. The orbit shrinkage will have the effect of driving the system out of resonance. Tides raised on Jupiter by Io will have the opposite effect as its effect would be to expand the orbits of these satellites. The amount of Jovian torque on the satellite orbits will determine the direction of evolution of the resonance and has been the topic of research during the past decade and the problem is still open.

Accurate measurement of the changes in the mean motion of these satellites holds the key to the solution and has been attempted using existing observations by various researchers using eclipses behind the planet, photographic and mutual events observed during 1973 and 1979. The mutual events are capable of yielding relative astrometric positions at least an order of magnitude more accurate than the photographic or eclipse behind the planet observations. The recent mutual event season of 1991 provided an opportunity to increase the data base of observations from 1973 to 1991. The present investigation concentrates on the observations, analysis and utilization of the astrometric data to obtain the corrections to the constants of motion and look for changes in mean motion of these satellites. Chapter 2 describes the observational set up at the Vainu Bappu Observatory (VBO) and the reduction techniques. A theoretical model was constructed to calculate the synthetic light curves. The salient features of the model are (i)

Calculation of the instantaneous distance between the satellites or the satellite and the shadow centre using Lieske's E-3 ephemeris, (ii) Computation of light loss under the shadow cone or behind the occulting satellite using different light scattering laws to describe the light distribution over the surface of the satellites. Variation in albedo from equator to pole and distinct features like the regiones and ray craters on Ganymede were also included in the model, (iii) Comparison of observed and theoretical light curves using Marquardt's curve fitting techniques. The method of calculating the Heliocentric, geocentric and Joviocentric distances, light time corrections, and the model to calculate the light loss are described in Chapter 3.

All the light curves were fitted using light distributions given by Lommel-Seeliger's law, Lambert's law and Minnaert's law. Most of the occultation light curves were fitted taking into account the albedo variations. Results indicate that in almost all the cases the fitted impact parameter derived by taking into account the albedo variations was closest to the predicted value. This clearly indicates that the relative latitudes predicted by theory (E-3 by Lieske) is quite accurate and further corrections can be effected with realistic albedo maps. Comparison of the observed mid times with the predictions leads to a residual of $\simeq -340$ km along the track of motion of Io relative to Europa. Chapter 4 contains the results of the investigations of the data from VBO. The light curves deposited by others at the data bank in response to the campaigns PHEMU85 and PHEMU91 by J.E.Arlot and his group at the Bureau des Longitude (BDL), France were fitted using the model developed in the present investigation assuming Lommel-Seeliger's law. The published astrometric positions of the mutual events in 1973, 1979 and 1985 were reconstructed to deduce the impact parameter corresponding to Lommel-Seeliger's law of light distribution, and the corresponding phase corrections. The astrometric positions obtained from mutual occultations were combined with photographic observations (1891-1990) to obtain corrections (ε, β) to the constants of motions of the four satellites introduced by Lieske through revitalization of Sampson's theory. The source code developed by J.E.Arlot at Bureau des Longitude, France using Lieske's routines to compute position and partial derivatives of the observable quantities with

respect to the constants was used to derive the new sets of ε-β values. In addition to the new sets of corrections to the constants labelled I-32, the $(O-C)$ values in longitude were analyzed to look for secular variations in the mean motion of the satellites. The present investigation yields to a value of 21.65×10^{-11} for $\dot{n}_1/n_1$ where n_1 is the mean motion of Io. The details of the observational data, the fitting procedure and results are presented in Chapter 5.

Chapter 6 contains the comparison of the new ephemeris with ephemerides obtained by others. The ephemeris reduces considerably the residuals in longitude but the residuals in projected sky plane co-ordinates are only marginally improved. The reason for this may be that mid times are determined accurately but the derived impact parameters are uncertain. This could arise due to improper background subtraction or uncertainty in determining the contribution of the occulting satellite. Problems in including the mutual eclipses with other kinds of data sets for fit to the theory are discussed in this chapter. Further observational plans regarding mutual events of Saturnian satellite are mentioned.

The tables, figures and equations are numbered sequentially in each chapter with the chapter number indicated by suffixes.

Table of Contents

1 Introduction

1.1 Historical Background

The principal goal of planetary science in ancient times was to understand the origin and evolution of our solar system. Several theories have been suggested by various investigators; as early as 280 B.C. Aristarchus of Samos proposed a heliocentric system. This concept which contradicted Aristotle's idea of a fixed Earth was however not accepted by people and soon sank into oblivion. Nicholas of Cusa (1401-1464) made an unsuccessful attempt to convince his contemporaries of the heliocentric theory. The modern concept of the universe was advanced by Nicholas Copernicus (1473-1543) in 1543 in a volume titled 'De revolutionibus orbitum celestium libri VI'. Tycho Brahe (1546-1601), a brilliant observer, constructed far more accurate planetary tables than anyone before him. His student Johannes Kepler (1571-1630) was a keen mathematician. Using Tycho's observations of Mars and his own he formulated the three general laws of the motion of the planets. He could not however find any underlying explanation of these rules. Galileo Galilei (1564-1642) with his telescope discovered the four major satellites of Jupiter. Motion of these satellites gave supporting evidence to Copernican theory. Isaac Newton (1642-1727), used the observational results of Galileo to formulate his 'laws'. With the help of clear ideas and definitions he explained the experimental facts concerning mass, motion and force. He postulated the force of gravity to be governed by the inverse square law. He could account for Kepler's three laws and many other observed features like tides. He published the mathematical proofs in his famous book *'Philosophiae Naturalis Principia Mathematica'* in 1686. The subject of celestial Mechanics was thus born.

An explanation for the existence of the solar system was suggested by René Descartes (1596-1650) in his 'Théorie des vortex' published in 1644. He opposed the idea of vacuum and suggested that the space was filled with

whirling vortices to carry the planets. The model was qualitative and did not explain the existence of the planets close to the ecliptic and was therefore abandoned after the discovery of Newton's laws.

Kant (1724-1804) and Laplace (1749-1827) proposed the concept of a primitive nebula from which the Sun and the planets were born. Laplace's theory suggested that the nebula contracted under the influence of gravitation with an accompanying increase in its rotational velocity until it collapsed into a disk. The planets and the satellites condensed from the rings of gas that were shed. This theory explained all the observational facts known at that time and therefore was accepted for some time until Maxwell (1831-1879) pointed out the difficulty in explaining the accretion of a planet from a ring of planetoids. Another major problem with Laplace's theory was that it failed to explain the observed fact that while 99.8% of the mass is contained in the Sun but most of the solar system's angular momentum is contained in the planets. The models that seem most acceptable at present are those that are derived from Laplace's nuclear model.

1.2 Highlights of Solar System Studies in the 20th Century

The last quarter of the 20th century has been most important in the development of planetary sciences. Improved ground based technology and availability of larger telescopes have helped to probe spectroscopically the atmospheres of the giant planets. Correct interpretation of the complex spectrum especially in the far IR and microwave region was possible as a result of collaboration with laboratory spectroscopists. Advanced technology permitted observations outside the earth's atmosphere, increasing thereby the spectral coverage.

The space missions of the Mariner, Pioneer Venus, Venera, Vega, Pioneer and Voyager series have relayed back information on the physical properties and processes on all the planets except the Pluto - Charon system.

Each encounter of the spacecraft to a planet helped solve many of the issues not understood earlier. The fly-bys also made new findings. These issues are brought to light and discussed in detail in a series of books: *Jupiter*,

2

1976, ed. by T.Gehrels (Pioneer 10 and 11); *Satellites of Jupiter*, 1982, ed. by D.Morrison (Voyager 1 and 2), *Venus*, 1983 ed. by D.M.Hunten, L.Colin, T.M.Donahue and V.I.Moroz (Pioneer Venus and Venera missions), *Saturn*, 1984, ed. by T.Gehrels and M.S.Matthews (Voyager 1 and 2); and several others.

One of the major new findings is the discovery of rings around all the four giant planets. In terms of the origin of solar system this is significant. Saturn's rings were discovered by scientists in the 17th century, but infinitely more details of the structure were discovered from space missions. Uranian rings were first discovered serendipitously during an occultation event in 1977 closely followed by the discovery of Jovian ring system by space probes in 1979. More details of the Uranian ring system were found from Voyager 2 records in 1986, and arcs of Neptunian rings were inferred from occultation observations, which were later confirmed as rings of variable surface density by Voyager 2 in 1989. Ring systems around all four of the major planets have changed our earlier concept. Rings around the massive planets appear now to be a rule rather than an exception.

The Jupiter system was first visited by Pioneer space crafts with the main emphasis on *in situ* measurements of the particles and field environment along the trajectory. The spacecraft trajectory provided improved masses for all the four Galilean satellites. One of the exciting developments in planetary science during the 1970s was the discovery of Io associated neutral and plasma clouds that surround Jupiter (Brown 1974; Kupo et al. 1976; Pilcher and Morgan 1979). Just prior to the encounter of Voyager 1 with the Jupiter system, Peale et al. (1979) suggested that tidal dissipation in Io was likely to have melted a large fraction of its mass. They further predicted widespread and recurrent surface volcanism on this satellite. The existence of volcanic plumes on Io was dramatically confirmed during the encounter of Voyager 1. The plumes seen by Voyager ranged in height from 60 to 300 km.

The Pluto-Charon system is not scheduled to be visited by any space craft as yet but considerable new information has come out as a result of intensive ground-based investigations in recent years. The major discovery which led to further detailed studies was the discovery of its satellite Charon

3

(Christy and Harrington 1978). Harington and Christy (1980, 1981) determined that Charon's orbit is synchronous with Pluto's rotation and is highly inclined to the plane of the ecliptic.

Andersson's (1978) important realization of a possible occurrence of mutual events between Pluto and Charon was very timely. Binzel et al. (1985) reported the first shallow eclipse events. The eclipse season persisted until the end of 1990 and over 100 mutual event observations have been reported by various observers. Analysis of these events have yielded surface maps of Pluto and Charon, revealed information about individual albedos and spectra and improvements in Charon's orbit (Buie and Tholen 1989). From Charon's IR spectrum discerned from the spectra taken outside and during the total events, the presence of absorption feature of water ice and the absence of the volatile frosts of CH_4, CO_2, H_2S, NH_3 or NH_4HS, have been inferred.

Another breakthrough came as a result of a stellar occultation by Pluto on June 9, 1988. Charon during the event was near elongation and therefore well removed. The consistent results of the observation was that the star light dimmmed gradually rather than abruptly inferring thereby the presence of an atmosphere on Pluto.

1.3 Origin of the Present Investigation

The motivation for the present investigations came from the researches of various workers on the investigation of possible changes in the mean motion of the inner Galilean Satellites of Jupiter (deSitter 1928; deSitter 1931; Goldstein 1975; Goldstein and Jacob 1985; Goldstein and Jacob 1986; Lieske 1986, 1987). The prediction by Peale et al. (1979) on the eve of Voyager 1's encounter with Io of widespread and recurrent surface volcanism and its dramatic confirmation during the flyby has evoked considerable interest on the orbital evolution of this satellite. In addition, infrared heat flux from Io has been measured to be $\sim 7.6 \times 10^{13} W$ (McEwen et al. 1985). The source of this heat has been attributed to tidal heating. The energy for tidal heating must come from Io's orbit, but due to the Laplace resonance between Io, Europa and Ganymede the energy loss is shared among the three satellite

4

orbits. The orbit shrinkage will have the effect of driving the system out of resonance. Tides raised on Jupiter by Io will have the opposite effect as its effect would be to expand the orbits of these satellites. The amount of Jovian torque on the satellite orbits will determine the direction of evolution of the resonance, and has been the topic of research during the past decade, and the problem is still open.

The importance of precise estimation of the rate of change of Io's mean motion in understanding the orbital evolution of the Galilean satellites has been stressed by Greenberg (1982, 1986) and Lieske (1986, 1987). The estimations of $\frac{\dot{n}_1}{n_1}$, (where n_1 is the mean motion of Io) by various researchers differ considerably (Table 5.8). Lieske (1987) has used a vast collection of observed data dating from 1652 to the modern optical navigation images on the Voyager mission and mutual events of 1973 and 1979 and used recently determined values for several astronomical constants to derive his E2x3 ephemeris and obtained a small negative value for $\frac{\dot{n}_1}{n_1}$. Since then several observations of Mutual events in 1985 have been analysed and published (Arlot et al. 1992; Franklin and GSO 1991). The three kinds of observational data sets that are used to obtain the constants of motion of these satellites are eclipses by the planet, photographic and mutual events. The photographic data are primarily of value in yielding estimates of the inclinations and nodes. The eclipse observations have the potential of estimating mean motions, eccentricities, periapses and longitudes (Lieske 1980). Extension of the time base of mutual events from 1973 to 1991 enhances the potential of this data set in determining not only the nodes, inclinations and eccentricities but also the mean motions, periapses and longitudes. The astrometric accuracy of mutual event is of the order of 0.03 arcsec whereas visual and photometric observations of eclipses have an accuracy of ~ 0.2 arcsec and ~ 0.11 arcsec respectively. The accuracy of the photographic observations is 0.20 arcsecond when using a short focus astrograph. Photographic observations using long focus (f=10m) refractors can yield relatively better accuracies of about 0.06 arcsec (Arlot et al. 1989). Mutual event data are unaffected by atmospheric seeing conditions. If the photometric observations are carried out carefully by estimating the background contribution due to Jupiter correctly

5

and determining the time of observations accurate to a fraction of a second the accuracy of mutual event data may surpass those from the other kinds of data sets. The recent mutual event season in 1991 provided opportunity for more observations of this kind. The topic of observation and analysis of mutual events of the Jovian satellites and utilization of the astrometric results for obtaining the corrections ε's and β's (Lieske 1977) was therefore taken up. The present investigation utilizes mutual occultation results of 1973, 1979, 1985 and 1991 and therefore increases the time base of this kind of observations.

1.4 Previous Observations of Mutual Events of the Galilean Satellites

The Joviocentric declination of the Sun and the earth become small twice during the planet's orbital period of about 11.6 yr. For a few months around this time pairs of the satellites are frequently aligned with the Sun causing eclipses and with the earth causing the occultations.

Since 1931 these mutual events have been predicted regularly by the British Astronomical Association based on the method by Levin (1931). The first rigorous efforts on predictions (Milbourn and Carey 1973; Brinkmann and Millis 1973; Aksnes 1974) and observations (Aksnes and Franklin 1976; Wasserman et al. 1976; Vermillion et al. 1974; Blanco and Catalano 1974) were made during the 1973 mutual event season. Using a large number of mutual occultation and eclipse data Aksnes and Franklin (1976) obtained solutions to the radii of the satellites along with the impact parameters. The next mutual event season during 1979 was unfavourable due to conjunction of Jupiter with the Sun. Very few events were observed during this mutual event season (Aksnes et al. 1984; Arlot et al. 1982). These events were observed worldwide during the next mutual event season in 1985 in response to the campaign for these observations (Arlot 1984; Aksnes and Franklin 1984). Arlot et al. (1992) published a catalogue of 165 observations of 63 mutual events from 28 sites. Franklin and the 'Galilean Satellite Observers' 1991 reported fitted astrometric parameters of 200 events observed from several

sites. Descamps and Thuillot (1992) analysed 16 eclipses and 25 occultations observed in 1985 using different scattering laws. They also deduced the Hapke's parameters of the leading and trailing sides of the Galilean satellites. They found that the model for mutual occultations was more sensitive than that for the mutual eclipses to the surface characteristics. Vasundhara (1991) fitted the mutual eclipse observations from VBO. Uniform disc, Lommel-Seeliger's law and Lambert's law were used to model the light curves. Analysis of the limited data indicated that Lommel-Seeliger's law describes the light distribution better than Lambert's law.

Goguen et al. (1988) for the first time observed the occultation of Io by other satellites in the infrared (3.8 μm, 4.8 μm, 8.7 μm) region to map the hot spot. The location and area of the region of thermal emission was determined by them. Their observations of 10 July, 1985 in 3.8 μm and 4.8 μm event also lead to the discovery of a new hot spot of $\sim$ 20 km in diameter. Descamps et al. (1992) observed and analysed an occultation of Io by Europa in the infrared band to detect signal from the two volcanoes Loki and Pele.

The recent mutual events during the 1991 season were also observed extensively in response to campaign by Arlot (1990), and Aksnes and Franklin (1990). Mallama (1992) analysed 12 mutual events using Minnaert's law, modelling darker polar areas, brighter leading hemisphere and slightly fainter Jupiter facing hemisphere based on study by Simonelli and Veverka (1986). His astrometric results agree with Lieske's E-3 ephemeris predictions at a 1 σ level of about 0".013 in orbital latitude, but an 0".080 or $\sim$ 308 km residual in relative longitude. From analysis of 1973, 1979, 1985 and 1991, Mallama (1992) found a net error projected along track for Europa relative to Io which increased rather linearly from -12 km in 1973 to -308 km in 1991. Thanks to the extensive PHEMU91 campaign at the Bureau des Longitudes by J.E.Arlot and his group the 1991 mutual events have been extensively observed. Attempts were made at the Vainu Bappu Observatory to observe almost all the events observable from India, of which 17 events were observed successfully.

Wasserman et al. (1975) observed the mutual events in three wavelength bands (0.35, 0.50 and 0.91 μm) with an aim to obtain colour information

about albedo distribution and limb darkening on the satellites. They concluded that before such information would be extracted from the mutual events, values of various geometric parameters such as the radii of the satellites and the impact parameters should be accurately known. Wasserman et al. also included in their model different albedo distributions like uniform disc, bright polarcaps and bright quadrants and concluded that construction of albedo maps if at all possible would require data of extremely high quality. In the post Voyager era one has the distinct advantage of knowledge of accurate radii of the satellites and their albedo maps. This has been fully exploited in the present investigations by including the published albedo boundaries of Io (Simonelli and Veverka 1986) and Ganymede (Squyres and Veverka 1981) to derive the impact parameters.

A curious discordance was noticed by Aksnes and Franklin (1976) in the relative corrections to the longitudes through pairs of mutual occultation and eclipse observations observed in 1973. Both kinds of events follow within a few hours at the most and one expects the corrections to be the same. However they noticed the discrepancy which grew with solar phase angle. Aksnes, Franklin and Magnusson (1986) traced this discrepancy to difference in the brightness distribution due to finite solar phase angle. The predicted time corresponds to the time of close approach of the geometric centre whereas the time of light minimum corresponds to the close approach of the light centre. Aksnes et al. (1986) used Lambert's scattering law and showed that the separation between the two kinds of centres grew with solar phase angle. In the present investigation the phase correction was determined using the three scattering laws by Lambert, Lommel-Seeliger and Minnaert. The influence of the light scattering law on the phase correction has been investigated.

1.5 Lieske's Revitalization of Sampson's Theory

The process of calculating the orbital elements of any solar system object from observations is a tedious process. The entire process needs to be repeated when more observations are available for refinement of the theory. Lieske's (1974, 1977) revitalization of Sampson's (1921) theory which pro-

8

vides means to adjust the constants without having to repeat the process is a major achievement in this field. The approach adopted by him was to redevelop Sampson's method to make it compatible for use with modern day computers. Sampson aimed at an accuracy of one arcsecond in the joviocentric co-ordinates and included all periodic terms larger than 10^{-7} radian and sought to obtain accuracy of 2 km, 3.3 km, 5.2 km and 9.1 km for Io, Europa, Ganymede and Callisto respectively. The current accuracy of Sampson's ephemerides for the satellites is however of the order of 600 km to 1200 km, several times the accuracy sought by him. The main cause of the large residual is due to extrapolation of the orbit solutions which were derived using observations during the years 1878-1903. Some of the solar terms in the longitude (Innes 1910) and 3—7 commensurability between the two outer satellites (de Haerdtl 1892; Lieske 1973) were neglected by Sampson. Lieske's revitalization process included these neglected terms. He corrected arithmetic errors in Sampson's theory and introduced amplitude and phase of the Laplacian free libration as arbitrary constants. Most important of all Lieske's elegant approach provides the means to calculate the partial derivatives of the observable co-ordinates with respect to the arbitrary constants of integrations (ε-β) (Table 5.4 a&b adopted from Lieske 1977). The 28 ε's are the quantities like the masses of the satellites relative to Jupiter, mean motions of satellites I, II and IV (motion of satellite III is constrained via the Laplace resonance), libration phase angle amplitude, mean motion of Jupiter, Zonal harmonic coefficients J_2 and J_4 of Jupiter, its radius, rotation period, primary eccentricities of the satellites I—IV, eccentricity of Jupiter, primary sine inclinations of the four satellites, inclinations of Jupiter to equator and ecliptic, obliquity of ecliptic and mean motion of Saturn. The corrections ε's modify the generic values Ao according to

$$A = Ao(1 + \varepsilon)$$

The ε's are dimensionless constants, except ε_9 which represents the amplitude of free libration which is given in radians.

The 22 β values are the mean longitudes of four satellites, libration phase angle, proper periapses of the satellites (I—IV), longitude of perihelion of

9

Jupiter, proper nodes of the four satellites, longitude of origin of co-ordinates, mean anomalies of Saturn and Jupiter and certain other algebraic quantities. The β's are in degrees and are added to the generic values.

Using the partial derivatives, the ε-β values can be updated when more observations become available. For the revitalized Sampson's theory the ε-β values are zero. Using various observational data sets, several ephemerides (E-1, E-2, G-5, E2x3) have been developed by Lieske (1978, 1980, 1987) and Arlot (1982). This investigation aims at getting a new set of ε-β values using the mutual occultation data of the 1973, 1979, 1985 and 1991 mutual events seasons. Since these events are relatively rare and therefore insufficient photographic data were also used for this purpose. All the ε-β values are not determined, or cannot be determined using astrometric positions of the satellites, 21 of these are fixed via adoption of the physical constants. IAU and Pioneer derived values of rotation period, equatorial radius and the zonal harmonic coefficients J_2 and J_4 for Jupiter Satellite masses. Jupiter related orbital parameters are also not determined during the fit. The 24 fitted parameters are the arbitrary constants in the motion of the four Galilean satellites involving their mean motions, eccentricities, sine inclinations, amplitude and phase of the Laplace libration, mean longitudes, proper periapses and proper nodes.

1.6 Outline of Present Investigation

This investigation concentrates on the observations and analysis of mutual events and to utilize the results to obtain new sets of corrections to the constants of motion of the Galilean satellites. In what follows an outline of the study is given.

Chapter 2 describes the observational technique and the data reduction. Methods to determine the light loss and the time of light minimum and the sources of errors in the estimation of these quantities are discussed.

The geometrical model to calculate the theoretical light curves is described in Chapter 3. The eclipse and occultation geometrics are described separately with emphasis on corrections for light travel times. Method used

10

to calculate the light loss at any instant during the event are explained. The model takes into account the light distribution on the surface of the eclipsed or occulted satellite following the three laws by Lommel-Seeliger,Lambert and Minnaert. Published albedo variations inferred from Voyager images have also been modelled. Expressions for determination of phase corrections have been worked out in this chapter.

Results of the analysis of the data of 1985 and 1991 observed from VBO are presented in chapter 4. The results obtained using different scattering laws are compared.

The occultation light curves from the PHEMU85 and PHEMU91 campaigns by Prof.J.E.Arlot and his group were analyzed using the model developed in Chapter 3. The published astrometric results by others of the 1973, 1979 and 1985 series were reconstructed by applying the phase correction using Lommel-Seeliger's law. The relative astrometric positions derived this way were combined with photographic positions Arlot (1982) and astrometric data by Descamps (1992a) to derive the Lieske's corrections (ε-β) to Sampson's values for the constants of motion of the four satellites. Chapter 4 contains details of the data sets, the methodology and the results. The longitude using the new selected ephemeris I-32 was analyzed to look for secular acceleration in the mean motions of these satellites. The analysis reported in this chapter was carried out at the Bureau des Longitudes, Paris, France using the software developed by Prof.J.E.Arlot.

Chapter 6 contains a comparison of the ephemeris I-32 derived in the present investigation with other ephemerides E-1, E-2, G5 and E2x3. The problems in integrating the mutual eclipse data along with data of other kinds are discussed.

One of the outcomes of the present investigation, using 15 light curves involving occultations or eclipses of Io' is that Lommel-Seeliger's law and Minnaert's law appear to describe the scattering characteristics of Io. The Minnaert's parameter $k(\alpha)$ was determined as a free parameter during the fit. The average value of $k(\alpha)$ derived using good quality light curves in the I band of observation is found to be 0.559 ±0.011, which is compara-

11

ble to the values derived by Simonelli and Veverka (1986). Due to limited data, variation of this constant with solar phase angle could not be estimated. This investigation, however, opens up the possibility of analyzing in a systematic way the mutual event light curves to derive the scattering parameter of these satellites. Good quality light curves can be used to derive the Hapke's parameters (1981, 1984). The new ephemeris labelled I-32 derived using mutual occultation and photographic observations yields lower residuals in longitudes of the three inner satellites, but there is no significant change in the residuals of the sky plane positions ($\Delta\alpha\cos\delta, \Delta\delta$) compared to G-5 ephemeris. The reason for this may be due to better accuracy in determination of mid times as against the impact parameters which is very sensitive to the observing conditions. This chapter concludes with future plans on related topics.

2 Observations and Data Reduction

2.1 The Mutual Events

The transit of Jupiter through the nodes (equator on orbit) twice during its orbital period of 11.6 yr. provides the opportunity for an edge-on view of its equatorial plane from the inner solar system. Inclination of the orbital planes of the Galilean satellites to the planet's equators are very small and the satellites have finite sizes, therefore for a few months around the time of the nodal crossing, the satellites frequently eclipse or occult each other when any two of them are aligned with the sun, or earth respectively. The recent eclipse season commenced in November 1990 and continued till March 1992. Most of the events were observable from the earth during the first half of 1991. Accurate determination of time of light minimum and the depth of the events are the essential requirements of the mutual event observations. In this regard these observations are similar to observations of eclipses of close binaries. Details of the recording system, the observational procedure and the reduction technique are discussed in the following sections.

2.2 The Recording System

The ray path and the block diagram of the recording system are shown schematically in Fig. 2.1. The arrangement used in the present study consist of

1. Light collector (T)
2. Photometer (PMT)
3. Pre-amplifier and discriminator (PAD)
4. Photon counting unit (PCU)
5. Pulse integrator (PI)
6. Strip chart recorder (SCR).

13
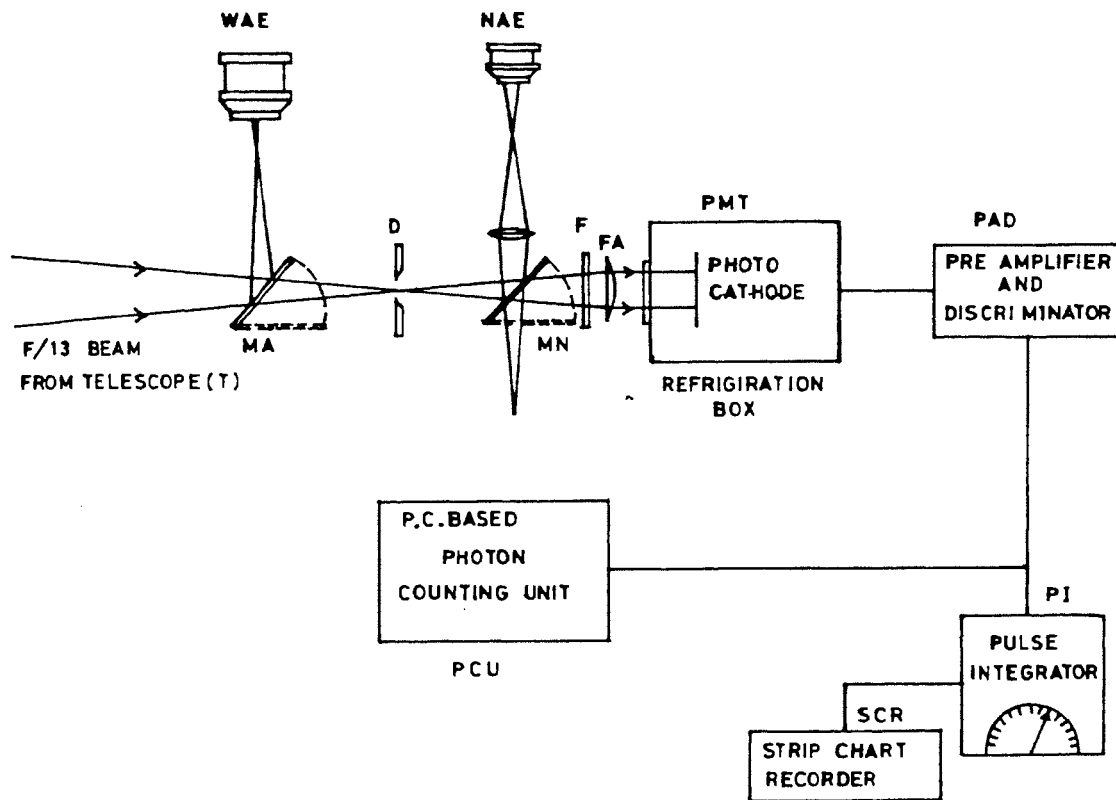
Fig. 2.1 The ray path and the block diagram of the recording system. WAE: Wide angle eyepiece to select the field, MA, MN: flipping 45° mirrors, D: focal plane diaphragm, NAE: narrow angle eyepiece to check centering, F: filter, FA Fabry lens, PMT: photometer. The pulses from the PMT after pre-amplification and discrimination through (PAD) are counted at the photon counting unit (PCU), for real time monitoring the pulses after integration by the pulse integrator PI are fed to the chart recorder(SCR).

The light collectors used in the present study were the 75 cm, 102 cm and 234 cm reflectors in cassegrain mode at the Vainu Bappu Observatory (VBO $78^{deg}49'.58$ E, $12°34.58$ N, 725 m). The focal ratio of the 75 cm telescope is f/13.5. The 102 cm and 234 cm reflectors are both f/13 systems. Standard R or I filters were used. Neutral density filters of suitable transmissions were used to cut down photon incident rate at the detectors.

Two photometer units were available at VBO. One with an EMI 9658R

14

photomultiplier tube refrigerated in a dry ice chamber. This unit was used at the 102 cm telescope. The other unit containing an EMI 9658 B photomultiplier was used at the 75 cm telescope. A water cooled peltier system was used to cool this phototube. One of the two units was used at the 234 cm telescope.

Rest of the recording units were identical. The output pulses from the PMT were fed to a locally built preamplifier and discriminator unit (PAD). The main function of PAD is to transmit all pulses with heights (voltage) larger than a threshold level, irrespective of their actual pulse height. The threshold was set initially at the time of installation to be such that when refrigerated, the dark count rate was about 60 counts per second. The PAD unit also acts as an impedence matcher between the PMT of high output impedence and the pulse detecting units (PCU and PI) of low input impedences.

The working of the PC based photon counting unit used in this study has been discussed elsewhere (Srinivasan et al. 1992). The software for data acquisition is written in turbo pascal. The program utilizes the following procedures:

1. The clock maintained by the disc operating system (DOS) is set at the beginning of observations with reference to the standard time.

2. The PC generates a gate pulse using the delay procedure, the duration of which can be set initially for each run as the required integration time in milliseconds.

3. Before commencing the integration, all counters are cleared and the gate signal is generated. When data acquisition commences the system gets the time from DOS and stores. At the end of each gate signal, the total number of pulses counted during this counting interval are read into a two dimensional array memory (1 .... 16, 1 .... 1000). The data is continuously acquired and stored in a cyclic buffer array until the observation is terminated by pressing any key on the key board. When the buffer of 16 K data points is full, the data points stored at the beginning get successively erased and only the last 16 K data points are accessible. Therefore care

15

was taken to stop the run just before the buffer was full.

4. At the end of the run the program gets the ending time from DOS and stores.

5. The data values are rearranged and the 16K data points are stored on to the disk along with header information giving starting time, ending time and the integration time.

For real time monitoring, the output from PAD was integrated using a pulse integrator (PI). The dc output was recorded using a strip chart recorder (SCR). The pulse integrator has a meter to read the count rate on line.

2.3 The Data Acquisition

The observations commenced whenever possible, atleast an hour before the event and were continued for another hour after the event. Uncertainty in the estimation of the contribution of the sky background in the focal plane diaphragm is the chief source of error in determining the depth of the events. Two dimensional detector arrays like the CCD receptors and video cameras allow accurate modeling of the sky background around the satellites (Thuillot Arlot and Wu 1990; Nakumura and Shibasaki 1990; Colas and Laques 1990; Mallama 1992). While using a conventional photometer the best that is possible would be to measure the sky by positioning the diaphragm at four locations equally spaced along east, west, north and south from the satellites (Fig. 2.2a). The sky background itself can be reduced due to its λ^{-1} and λ^{-4} dependence by carrying out the observations in the longer wavelength bands. Therefore the present series of observations were carried out either through a R or a I filter of Fernie's system. On the 102 cm refractor 9 or 12 arcsecond diaphragms were used while on the 234 cm telescope a 18 arcsecond diaphragm was used. At the 75 cm telescope due to tracking problems a larger diaphragm of 30 arcsecond was used. This leads to higher uncertainty in the estimation of the depth of the events observed at this telescope particularly when the events occurred closer than six Jupiter radii from the planet's centre. The sky counts at the four locations around Europa and Ganymede during the occultation event 203 on 1991 January 23 are

16

shown in Fig. 2.2b. The average sky is shown by the dotted line. The sky south of the satellite was found to be a close approximation to the average value. Whenever it was not possible to sample the sky at all the
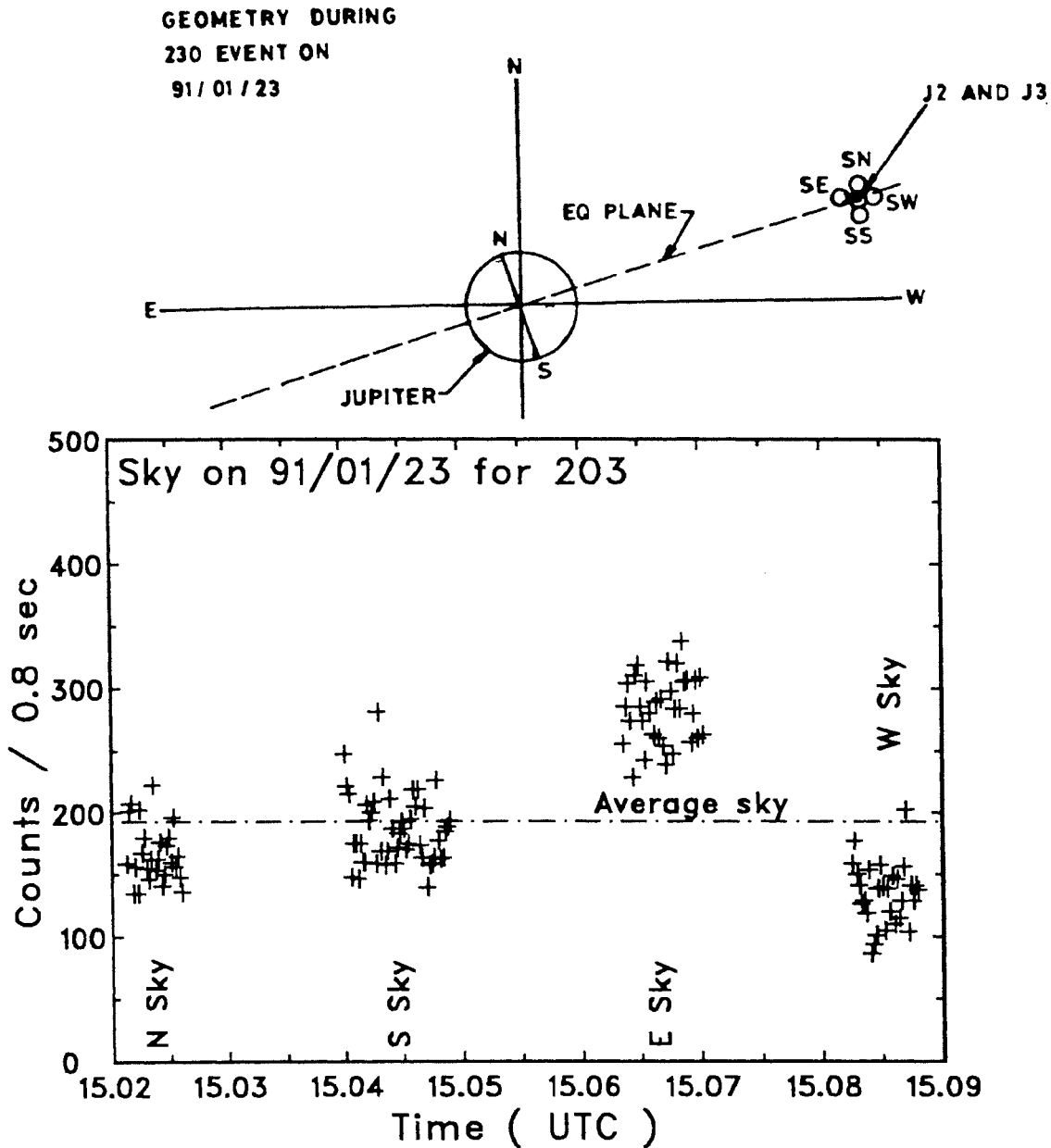
Fig. 2.2(a) The occultation geometry from the earth during the 203 event on 1991 January 23. Both Europa and Ganymede are in the central diaphragm of size 12 arcseconds. SE, SW, SN and SS are locations of the diaphragm for sky sampling at equidistant locations along the four directions. (b) Sky counts at the four locations of the diaphragm. Average value of sky is shown by the dotted line.

four locations, for example just before or after an occultation event when the satellites were close yet could not be accomodated in the same focal plane diaphragm, the sky between the satellites could not be observed, on such occasions only the sky at south was observed.

During an occultation the observer is aligned with the occulting and the occulted satellite. Therefore both the satellites would be close and therefore would be in the diaphragm. During the event, only the occulted satellite would undergo variation in intensity, the contribution of that of the occulting satellite would be constant. In order to remove the contribution of the occulting satellite, the relative contribution of the two satellites to the total light should be carefully estimated. The intensity of the satellites depend on their orbital longitude and the wavelength of observations (Harris 1961; Johnson 1970; Johnson and McCord 1970; Owen and Lazor 1973; Millis and Thompson 1975; Morrison et al. 1974). Therefore the relative contribution should at best be determined for each event just before and after the event and the mean value used. For most events this was possible. The two satellites were observed separately several times. For each observation the sky along the four directions were measured. When the events occurred just after sun set or day break, or when the planet itself was rising or setting, the satellites could only be observed separately either before or after the event.

During an eclipse event, the satellites are aligned with the sun, even during mid event the satellites would in general be well separated. However close to the date of opposition of Jupiter, the earth would also be close to the line joining the satellites and the sun. To a terrestrial observer, therefore the satellites would appear to be very close to each other during the eclipse. Both the objects would have to be accomodated in the diaphragm during such eclipse events. Therefore the eclipse events observed about a month close to the date of opposition would give a light curve containing light from both the satellites. Measurement of their relative contribution would have to be made as in case of occultations.

The main occultation or eclipse events were monitored continuously. The integration time was selected such that the entire event and the four sets of sky measurements before and after the events were captured in the buffer

18

of 16 K data points. The integration times therefore, ranged between 0.15 seconds to 0.3 seconds. While monitoring events longer than one hour, another satellite, mostly Callisto was observed several times to check the sky transparency variations. For example during the 203 event on 1991 January 23, Callisto was observed 6 times. The integration times for the longer events were set between $0.8 - 1.0$ sec. The sky contribution along the four directions was also observed during the long events. The interruptions caused during sky and reference satellite measurements were always negligible compared to the duration of the events.

Standard stars recommended by Nicolet and Nitschelm (1990) were observed on most nights.

2.4 Data Reduction

The various steps involved in the reduction of the data are as follows:

1. Determination of average value of sky.

2. Estimation of the extinction coefficient.

3. Determination of the ratio (R) of the contribution of the occulting or the eclipsing satellite to the total light.

4. Normalization of the light curve after removing the contribution of the occulting/eclipsing satellite. Determination of the time of light minimum of the event.

If $I^{'}$ is the flux from the satellite in counts per second including the contribution of the sky, and S the average value of the flux from the sky as determined from the four sets of sky measurements at east, west, north and south of the object, the flux I from the satellite corrected for extinction will be

$$I = (I^{'} - S)exp(kX) \tag{2.1}$$

where k is the extinction coefficient and X is the air mass in units of thickness

19

at zenith (Hardie 1962) given by

$$X = \sec Z - 0.0018167 \,(\sec Z - 1) - 0.002875 \,(\sec Z - 1)^2$$
$$- 0.0008083 \,(\sec Z - 1)^3 \qquad (2.2)$$

where Z is the zenith distance of the object at the time of observation.

The ratio R was calculated using the relation

$$R = \frac{I_{S1}}{I_{S1} + I_{S2}} \qquad (2.3)$$

where I_{S1} and I_{S2} are the flux of the occulting/eclipsing satellite ($S1$) and the occulted/eclipsed satellite ($S2$) respectively after correcting for extinction and sky background using Eq. 2.1.
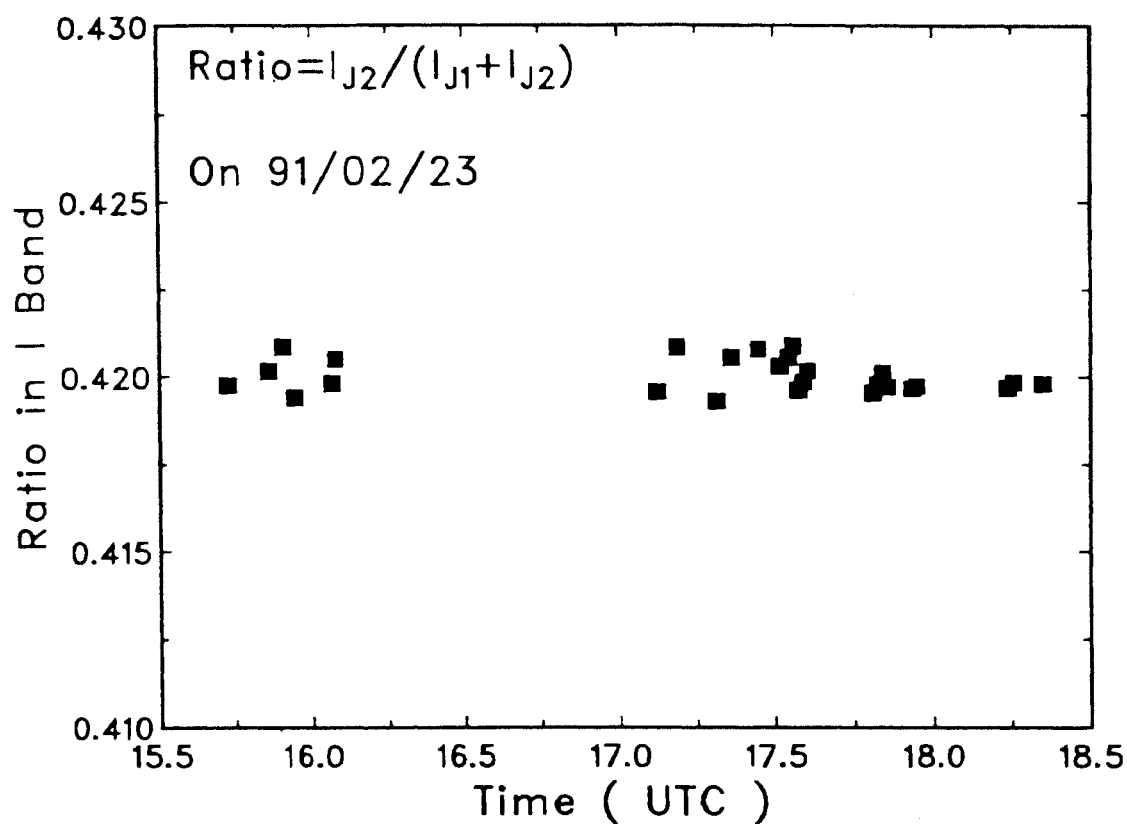
Fig. 2.3 Contribution (R) of light from Europa ($J2$) to the total light with Io ($J1$) during the occultation event (201) on 23 February, 1991.

Since several sets of measurement were made on the two satellites, R was calculated by combining flux measurements of $S1$ and $S2$ taken within 10 minutes apart. Mean value of R was estimated from these values for each night. Fig. 2.3 gives the estimated value of R before and after the event obtained on 23 Feb. 1991.

Normalizing a light curve is carried out with respect to the total light outside the event. As mentioned in Section 2.2, the focal plane diaphragm contains both $S1$ and $S2$ for the occultation events. This is also true for eclipse events close to the date of opposition. In this case there are two ways of normalizing the light curve:

Case I. The normalized intensity with respect to total light $S1$ and $S2$ would be

$$F(S1, S2) = \frac{I(t)}{I_0} \qquad (2.4)$$

where $I(t)$ is the total intensity at any time (t) during the event and I_0 its value outside the event.

Case II. The light curve can also be normalized after removing the contribution of the occulting/eclipsing satellite S1. The normalized flux in this case will be

$$f(S2) = \frac{I(t) - I_0 R}{I_0 - I_0 R} \qquad (2.5)$$

hence

$$f(S2) = \frac{F(S1, S2) - R}{1 - R} \qquad (2.6)$$

The light curve normalized this way is preferred as it can be directly fitted with theoretical light curves. Normalization according to case I can be used for direct comparison with the predicted occultation depth.

It follows immediately that for eclipses away from the date of opposition when S2 alone can be monitored

$$f(S2) = F(0, S2), \qquad \text{since } R = 0.$$

The loss in light obtained from the normalized light curve of case II is given by

$$\Delta f = 1 - f(S2) \qquad (2.7)$$

21

where Δf can vary between 0 for grazing event to 1 for total events.

The time of light minimum was determined by two methods.

(a) Folding the light curve :

The light curve between the first and fourth contact having N data points was examined visually and the approximate lowest intensity point was obtained. The folding was attempted about the data points in the vicinity of this approximate point (Fig. 2.4a) The data point of light minimum (k) should satisfy the relation

$$(\text{Diff})^2 = \frac{1}{n} \sum_{j=1}^{n} \left\{ I(k-j) - I(k+j) \right\}^2 \qquad (2.8a)$$
$$= \text{minimum}$$
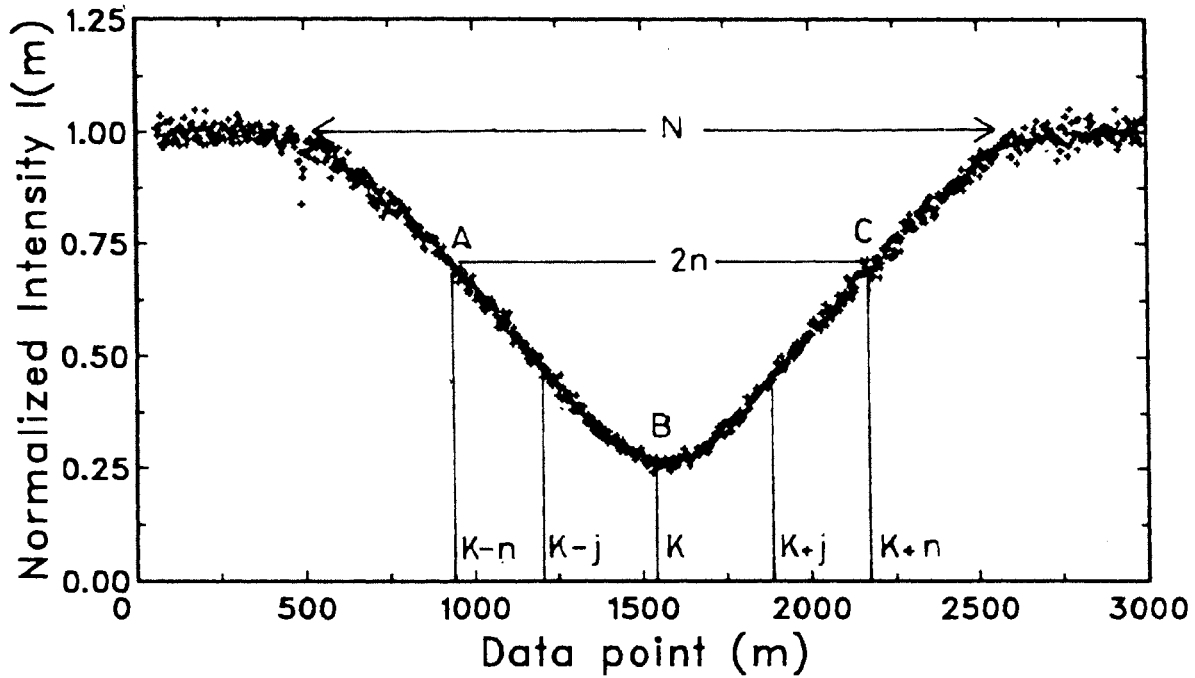
Fig. 2.4(a) Determination of time of light minimum by folding. k: trial mid point, portion of light curve used in folding k—n to k+n
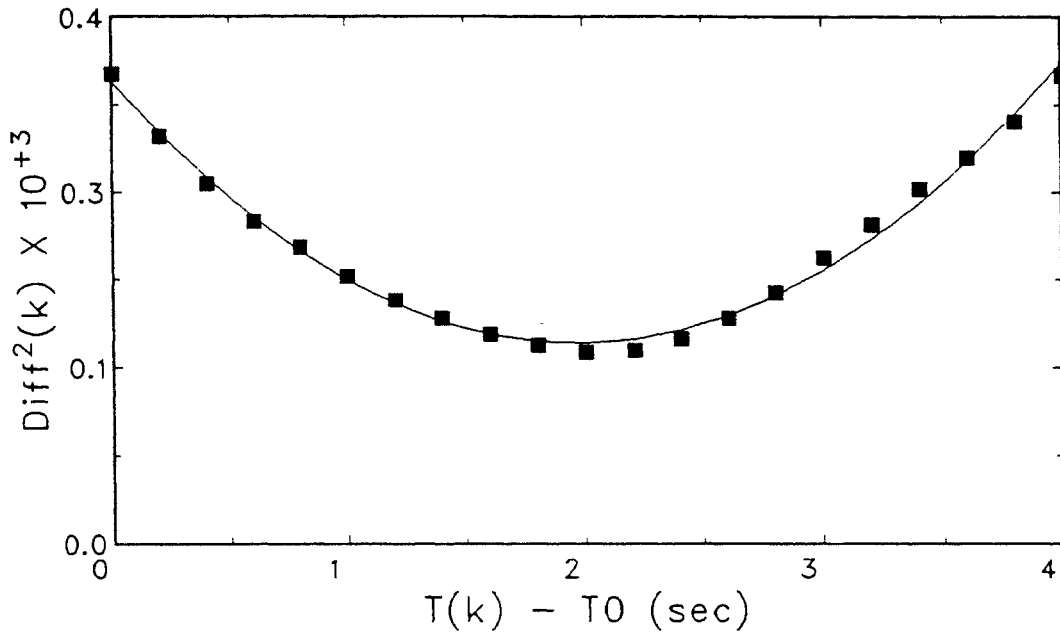
Fig. 2.4(b) The time corresponding to minimum 'Diff^2' is the time of light minimum.
T(0) is an arbitrary reference point.

One essentially finds the difference (Diff) between areas under the portions of the curve AB and BC. When B corresponds to the actual data point of light minimum, Diff^2 would be minimum.

The time corresponding to min (Diff)^2 was obtained by fitting a 3 degree polynomial to the Diff$^2(k)$ vs $T(k)$ curve, (Fig. 2.4b). Where $T(k)$ is the time corresponding to the kth trial mid point.The fitted (Diff^2) is givenby

$$\text{Diff}^2 = a_0 + a_1 T + a_2 T^2 \qquad (2.8b)$$

(b)   Polynomial fit :

A third degree polynomial was fitted to the deep part of the light curve

$$Y = b0 + b1T + b2T^2 \qquad (2.9)$$

23

The time of light minimum corresponding to $\delta y / \delta T = 0$ would be given by

$$T_l = -\frac{b1}{b2} \tag{2.10}$$

Light curves with breaks either due to clouds or while centring the object were analyzed by polynomial fit. The method of folding as described above requires equally spaced continuous set of data points; this method was used only for continuous light curves. The sensitivity of the two methods were compared by analyzing good quality and continuous light curves, using both the methods. Column 2 in Table 2.1 gives T_l for all the observed events. The maximum light loss calculated from the relation in Eq. (2.7) are given in column (3). The telescope aperture, filter used, and the air mass at T_{min} are given in columns (5) $-$ (6) respectively. The sky conditions at the time of observations are indicated in column (7); an entry of 1 indicates good sky conditions and 3 as variable transparency.

2.5 Estimation of Errors

The aim of observing mutual events is to obtain precisely the light loss and the time of light minimum. The uncertainty in the estimation of these two quantities must be evaluated carefully in order to assign weight to each observation, while using the results to further refine the theory of motion of the satellites.

A) The factors affecting the final accuracy of the light loss determined using Eq. (2.7) are:

A1. Uncertainty in sky determination.

A2. Uncertainty in determining the raw counts I_0' outside the event and I' during the event.

A3. Error in estimating the extinction by the earth's atmosphere.

A4. Uncertainty in the determination of the Ratio (R) calculating using Eq. (2.3).

The uncertainty in sky arises mainly due to error in positioning the diaphragm at equal distances in the four directions. The photon statistics noise

is very much smaller. The uncertainty in determination of I_0' and I' may arise due to local fluctuations in sky transparency and the photon statistics noise.

The error in estimating the extinction coefficient would be significant for events of longer durations or occurring at large zenith distances.

Uncertainty in the determination of R basically arises due to uncertainties in measuring intensity of light $I'(S1)$, $I'(S2)$ from individual satellites S1 and S2 respectively and the sky around them. The light variation of the satellite Io near the orbital longitude 270° is steep (Morrison et al. 1974). Europa also shows considerable variation in intensity between about 210° to 270° longitude. For most of the events involving Io and Europa (during the current series) the longitudes of the satellites are in vicinity of those regions. Even though Europa's motion is half of that of Io, changes in intensity with orbital longitude would affect estimation of R. Therefore care was taken to use values of R obtained from measurements taken just before and after the event.

To estimate the standard deviation σ_f of the normalized intensity given by Eq. (2.7), let $\sigma_{I'}$, $\sigma_{I_0'}$, σ_s, σ_k and σ_R be the standard deviations in estimation of I', I_0', S, k and R respectively we note that (Bevington 1962)

$$\sigma_f^2 = \left(\frac{\delta f}{\delta_{I'}}\right)^2 \sigma_{I'}^2 + \left(\frac{\delta f}{\delta_{I_0'}}\right)^2 \sigma_{Io'}^2 + \left(\frac{\delta f}{\delta S}\right)^2 \sigma_s^2 + \left(\frac{\delta f}{\delta R}\right)^2 \sigma_R^2 + \left(\frac{\delta f}{\delta k}\right)^2 \times \sigma_k^2 \quad (2.11)$$

from Eq. (2.6)

$$f(S2) = \frac{F(S1, S2) - R}{1 - R}$$

for simplicity writing f for $f(S2)$ and F for $F(S1, S2)$

$$f = \frac{F - R}{1 - R}$$

using Eqs. (2.2) and (2.4)

$$f = \frac{1}{1 - R}\left[\frac{(I' - S)exp(kX)}{(I_0' - S)exp(kX_o)} - R\right]$$

simplifying further

$$f = \frac{1}{1 - R}\left[\frac{(I' - S)}{(I_0' - S)}exp(k\Delta X) - R\right] \qquad (2.12)$$

25

where ΔX is the difference in airmass between the two sets of measurements I' and I_0'.

The partial derivatives are

$$\frac{\delta f}{\delta_{I_0'}} = \frac{(I'-S)}{(I_0'-S)^2}\frac{exp(k\Delta X)}{(1-R)} \tag{2.13(a)}$$

$$\frac{\delta f}{\delta_{I'}} = \frac{1}{(I_0'-S)}\frac{exp(k\Delta X)}{(1-R)} \tag{2.13(b)}$$

$$\frac{\delta f}{\delta_S} = \frac{(I'-I_0')}{(I_0'-S)^2}\frac{exp(k\Delta X)}{(1-R)} \tag{2.13(c)}$$

$$\frac{\delta f}{\delta k} = \frac{(I'-S)}{(I_o'-S)}exp(k\Delta X).\Delta X \tag{2.13(d)}$$

$$\frac{\delta f}{\delta R} = \frac{1}{(1-R)^2}\left[\frac{(I'-S)}{(I_o'-S)}exp(k\Delta X)-R\right] - \frac{1}{(1-R)}$$

$$= \frac{1}{(1-R)^2}\left[\frac{(I'-S)}{(I_o'-S)}exp(\Delta X)-1\right] \tag{2.13(e)}$$

Substituting the partial derivatives from Eqs. 2.13(a-d) in Eq. 2.11 and simplifying

$$\sigma_f = \left[\left\{\frac{exp(K\Delta X)}{(I_0'-S)(1-R)}\right\}^2\left\{\left(\frac{I'-S}{I_0'-S)}\right)^2\sigma_{I_0'}^2 + \sigma_{I'}^2 + \left(\frac{I'-I_0'}{I_0'-S}\right)^2\sigma_S^2 + \right.\right.$$
$$\left.\left((I'-S)\Delta X\right)^2\sigma_k^2\right\} + \frac{1}{(1-R)^4}\left\{\left(\frac{I'-S}{I_0'-S}\right)exp(K\Delta X)-1\right\}^2\sigma_R^2\right]^{1/2} \tag{2.14}$$

From Eq. 2.13 (a-d) it can be seen that the uncertainty σ_f in the estimation of the normalized intensity f during an event is reduced by decreasing the sky contribution; therefore use of R or I band and a small focal plane diaphragm help in reducing σ_f.

In Eq. 2.13(e) since $\Delta X \sim 0$, the contribution to the final uncertainty in f, due to uncertainty in estimation of R is less for shallow events than the deeper events. Again for events of long durations errors due to uncertainty in estimation of extinction coefficient σ_k is significant.

B)   The sources of error in determining the time of light minimum are:

B1. Error in setting the UT clock with respect to standard time signal.

B2. Error in setting the system clock of the PC of the photon counting unit with respect to the UT clock.

26

B2. Error in setting the system clock of the PC of the photon counting unit with respect to the UT clock.

B3. Drift in the time maintained by the DOS.

B4. Uncertainty in locating the time of light minimum as determined by the two methods discussed in Section 2.4.

The error in setting the UT clock on the observing floor was estimated in the worst case to be $\pm 0'.3$, on most days it was of the order of ± 0.2 seconds. This was judged by checking the UT clock every hour with reference to the standard signal on the wireless equipment.

The uncertainties in setting the system clock of the PC, and the clock rate maintained by DOS were determined as follows:

The PC clock was set at time To at the beginning of the observations. Since the cyclic buffer can store only 16 K data points, the runs were terminated just before the buffer was full. The system reads the ending time from the PC clock and writes it as the header information. The PC clock was found to gain time. As a result the ending time T_{PC} was found to be ahead of the actual ending time T_{UT}. Since several sets of observations were made, it was noticed that the difference

$$\Delta T = T_{PC} - T_{UT}$$

increased linearly through the night, i.e. at any time T

$$\Delta T \quad \propto \quad T - To$$

or

$$\Delta T = C(T - To) + \Delta To \qquad\qquad 2.15$$

where ΔTo is the error in setting the PC clock at time To and C is the time gained by the PC clock per second. Fig. 5 shows the variation of ΔT with $(T - To)$ for the observational runs on 23 February, 1991. The scatter in the data points is due to personal error in stopping the run precisely at T_{UT}. The slope of the fitted line and the intercept on the y axis give the values of C and ΔTo respectively. To ending time T_{PC} was corrected for

27

estimated using the uncertainties σ_c and $\sigma_{\Delta T_o}$ was always found to be about an order of magnitude less than the error in setting the ut clock (B1).

The uncertainty in locating the mid point of the light curve were determined from the coefficients of the fitted polynomial

$$Y = A_0 + A_1 T + A_2 T^2$$

where Y in this equation represents $(\text{Diff})^2$ of Eq. (2.8 b) or Y of Eq. (2.9) corresponding to the two different methods of determining the mid time. In either case the time of light minimum is given by

$$T_l = -A_1/2A_2.$$

The least square solution yields A_1, σ_{A_1}, A_2 and σ_{A_2}, the uncertainty in determination of T_l is therefore

$$\sigma T_l = \left[\left\{ \frac{\delta T_l}{\delta A_1} \right\}^2 \sigma_{A_1}^2 + \left\{ \frac{\delta T_l}{\delta A_2} \right\}^2 \sigma_{A_2}^2 \right]^{1/2}$$
$$= \frac{1}{2A_2} \left[A_2^2 \sigma_{A_1}^2 + A_1^2 \sigma_{A_2}^2 \right]^{1/2}.$$

For light curves of good signal to noise ratio, σT_l (B4) was found to be far less than the uncertainty due to the source of error (B1).

On the other hand σT_l was the main source of undertainty in the determination of time of light minimum for poor quality light curves.

28
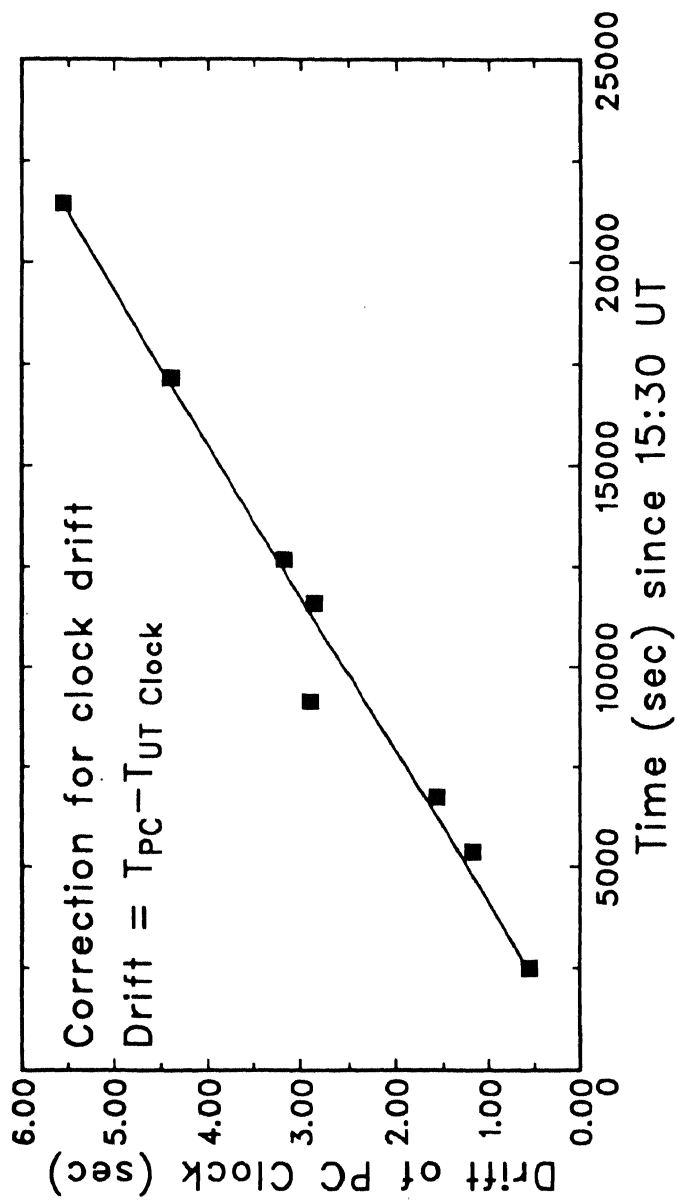
Fig. 2.5 Error in time on the PC Clock maintained by DOS at various instants.

29

Table 2.1 Observed times of light minimum, light loss[1] and journal of observations

UTC Date Event (1)	T_{min} hh:mm:ss (2)	Light loss (3)	Telescope Aperture (4)	Filter (5)	Airmass (6)	Observing condition (7)
91/01/22 2E1	18:23:12.7 +0.5s	0.721 ±.01	102	R	1.04	1
91/01/22 2O1	18:43:52.5 ±0.5s	0.411 ±.01	102	R	1.02	1
91/01/23 2O3	16:42:19.1 ±0.5	0.358 ±.015	102	R	1.29	2
91/01/29 2O1	21:00:32.0 ±0.5	0.651 ±.02	234	R	1.18	1
91/01/29 2E1	21:03:23.6 ±0.5	0.572 ±.02	234	R	1.18	1
91/02/05 2O1	23:13:35.0 ±2s	0.721 ±.04	102	I	2.86	3
91/02/16 2O1	14:29:41.9 ±0.5s	0.685 ±.003	102	I	1.41	1
91/02/16 2E1	15:18:31.7 ±0.5s	0.726 ±.01	102	I	1.18	1
91/02/23 2O1	16:39:16.1 ±0.5s	0.685 ±.01	102	I	1.01	1
91/02/23 2E1	17:42:58.5 ±0.5s	0.739 ±.01	102	I	1.02	1
91/03/09 2O1	20:58:40.5 ±1.5s	0.386 ±.03	102	I	2.81	2
91/03/18 4E2	19:43:25.1 ±3s	0.243 ±.01	75	I	2.11	2
91/03/20 2E1	13:55:45.3 ±1.0s	0.635 ±.004	102	I	1.46	3
91/03/27 2O1	14:26:37.3 ±0.5s	0.106 ±.01	102	I	1.01	1
91/03/27 2E1	16:14:11.7 ±0.5s	0.546 ±.003	102	I	1.07	1
91/04/03 2E1	18:31:49.0 ±2.0s	0.405 ±.011	75	I	2.05	3
91/05/17 1E2	14:49:41.7 ±1.5s	0.772 ±.006	102	I	1.42	2

1. After removing the contribution from the occulting/eclipsing satellite

3 Comparison of Observations with theory

3.1 Introduction

During the mutual event season the Sun, the earth, Jupiter and the Galilean satellites are very nearly in the same plane. Fig. 3.1 shows the geometry when J1 (Io) is passing behind the shadow of J2 (Europa) and J3 (Ganymede) is being occulted by J2. Both these events can not be observed simultaneously by an observer on earth E due to different corrections for the two kinds of events for light travel time.

The observed light curve on reduction using the method described in the previous chapter represents the variation of the fractional area in the shadow cones for eclipses and behind the occulting satellite for occultations.
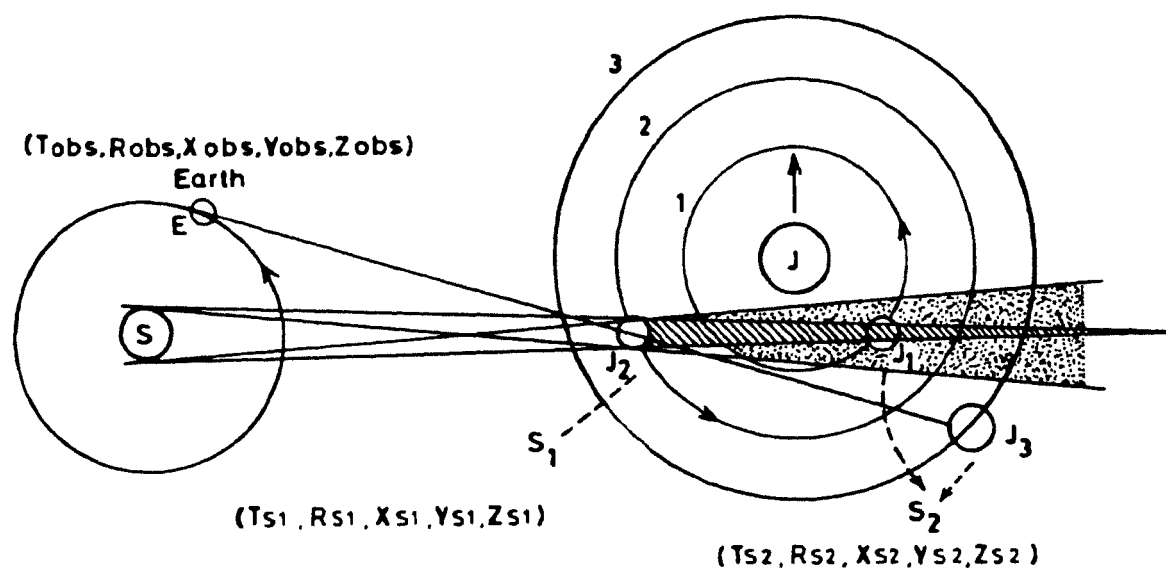
Fig. 3.1. Geometry during a mutual event season. The Sun, the earth, Jupiter, and the Galilean satellite lie very nearly in one plane, leading to the possibility of occurrence of mutual occultations (e.g. here 2O3) and eclipses (e.g. 2E1).

If one assumes a uniform disc for the satellites, the geometric area intercepted would be a direct measure of the light loss. For a realistic approach to the problem one must however take into account the variation of intensity across the disc.

The rate of change of the intercepted area depends on the event geometry. The depth of an event depends on the impact parameter which is the minimum projected distance between the centres of the two satellites for occultations; for eclipses the impact parameter is the closest projected distance of the eclipsed satellite to the shadow centre. The projections are on the sky plane, heliocentric for eclipses and topocentric for occultations. The duration of the event depends on the impact parameter and on the relative velocity of the two objects projected on the sky plane. Using the theory of motion of satellites of Jupiter (Lieske 1978, 1980) to predict the planeto-centric distance and the velocity of the satellites, theoretical model light curves were generated. In the present study it was aimed to fit the observed light curves with theoretical model light curves using Marquardt's curve fitting technique (Bevington 1969) using appropriate models to describe the global reflectance characteristics of the eclipsed or occulted satellite. Because of their simplicity, we used Lommel-Seeliger's law, Lambert's law and Minnaert's law to model the light curves. For light curves of good signal to noise ratio, the effects of non uniform albedo over the surface either from equator to pole or due to difference in nature of terrain have also been investigated. In the following sections, the method to calculate the event geometry and prediction of the light loss are presented.

3.2 Calculation of Event Geometry

3.2.1 The Eclipse Geometry

The geometry of an eclipse is shown schematically in Fig. 3.2. Following the nomenclature used by Aksnes (1974), an occulting or eclipsing satellite is denoted as S1 and the occulted or eclipsed satellite is denoted as S2. In Fig. 3.2. S, S1 and S2 are the Sun, the eclipsing satellite and the eclipsed satellite respectively not drawn to scale. U is the apex of the umbral cone

32

and P is the apex of the penumbral cone. The umbral and penumbral radii at the distance of S2 are given by (Aksnes 1974),

$$R_u = R_1 \frac{R_{s2} - R_{s1} \dfrac{R_s}{R_s - R_1}}{R_{s1} - R_{s1} \dfrac{R_s}{R_s - R_1}} \qquad (3.1)$$

$$R_p = R_1 \frac{R_{s2} - R_{s1} \dfrac{R_s}{R_s + R_1}}{R_{s1} - R_{s1} \dfrac{R_s}{R_s + R_1}} \qquad (3.2)$$

where R_{s1}, R_{s2}, R_1 and R_s are the Sun $-$ S1 distance, Sun $-$ S2 distance, radius of S1 and radius of the Sun respectively.
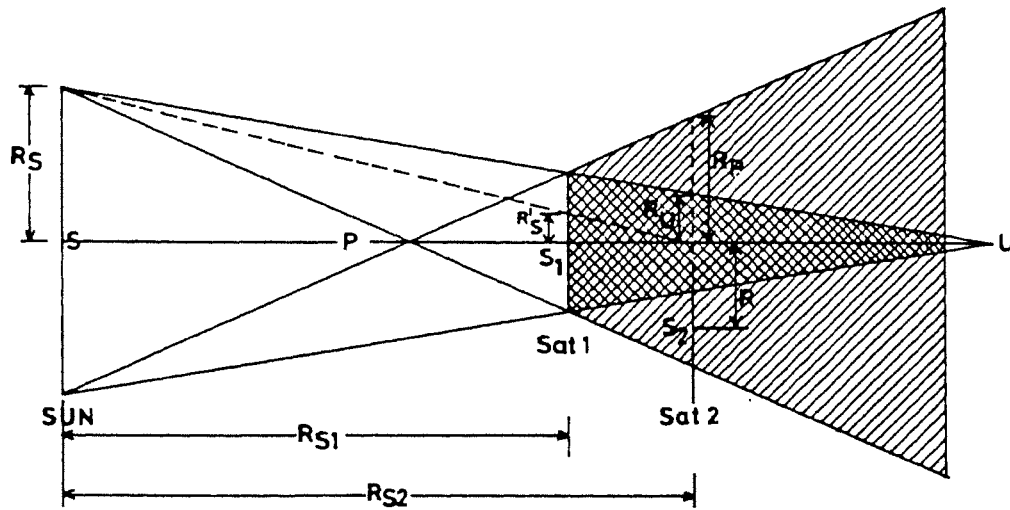
Fig. 3.2. Geometry of an eclipse. The centre S_2 of the satellite S2 is at a distance of R from the shadow axis (SU). R_p and R_u are the radii of cross sections of the penumbral and umbral cones at the location of S_2. R'_S, is the apparent radius of the Sun at the location of S1 as seen from the eclipsed satellite.

33

The expected light loss at any instant during the event can be computed from the predicted values of R_p, R_u and R, the instantaneous separation between S2 and the shadow axis. The light curve can therefore be constructed knowing the time variation of R. During the mutual event season, the planeto-centric declination of the Sun and the earth are small. The orbital planes of the Galilean satellites are close to the equatorial plane of Jupiter. As a result of the grazing view of the orbital plane of the satellites from the sun and the earth, the apparent orbits of the satellites would be flattened to linear motions parallel to each other and perpendicular to the spin axis of Jupiter. The impact parameter during an event is a measure of the latitude separation between the satellites. The instantaneous projected separation R changes owing to the relative longitudinal motion of the satellites. The heliocentric distances R_{s1} and R_{s2} required to calculate the umbral and penumbral radii and the separation R were calculated in the following manner :

The heliocentric earth's equatorial co-ordinates of Jupiter were calculated from the heliocentric distance (R_J), heliocentric longitude (l) and latitude (b) of the planet published in the Indian Astronomical Ephemeris (1991) based on the DE-200 ephemeris at two day intervals, using the well known relations.

$$X_J = R_J \cos b \cos l$$
$$Y_J = R_J(\cos b \sin l \cos \epsilon - \sin b \sin \epsilon)$$
$$Z_J = R_J(\cos b \sin l \sin \epsilon + \sin b \cos \epsilon) \tag{3.3}$$

These co-ordinates were then processed back to 1950.0. The instantaneous position and velocity of the planet were obtained by quadratic interpolation.

The positions and velocity of the satellites with respect to the equator and equinox of 1950.0 were computed using the quick loading routine 'KODQIK' along with 'EPHEM/E-3' and 'GALSAT' of Lieske (1977, 1987a). Corrections for light travel time between the two satellites and the S2 − observer distance were taken into account by combining the position of observer at the time of observation (T_{obs}) with that of the position of the eclipsed satellite at time (T_{s2}) and the position of the eclipsing satellite at time (T_{s1}),

where

$$T_{s2} = T_{obs} - R_{o2}/c$$
$$T_{s1} = T_{s2} - (R_{s2} - R_{s1})/c \tag{3.4}$$

where c is the velocity of light R_{o2} is the observer $-$ S2 (ES2) distance, R_{s2} and R_{s1} are the Sun $-$ S2 (SS2) and Sun $-$ S1 (SS1) distances respectively (Fig. 3.1).

The heliocentric distances R_{sm} (m=1,2) and the topocentric distances R_{om} (m=1,2) were calculated from

$$R_{sm} = X_{sm} + Y_{sm} + Z_{sm}$$
$$= \left(X_{jm} + x_{sm}\right) + \left(Y_{jm} + y_{sm}\right) + \left(Z_{jm} + z_{sm}\right) \tag{3.5}$$
$$R_{om} = X_{om} + Y_{om} + Z_{om}$$
$$= \left(X_{sm} + X_{sun} - X_{obs}\right) + \left(Y_{sm} + Y_{sun} - Y_{obs}\right) +$$
$$\left(Z_{sm} + Z_{sun} - Z_{obs}\right) \tag{3.6}$$

where (X_{jm}, Y_{jm}, Z_{jm}), (x_{sm}, y_{sm}, z_{sm}), $(X_{sun}, Y_{sun}, Z_{sun})$ and $(X_{obs}, Y_{obs}, Z_{obs})$ are the heliocentric co-ordinates of Jupiter, Joviocentric co-ordinates of the satellites at time T_{sm}, geocentric co-ordinates of Sun, and the geocentric co-ordinates of observer at the time of observations T_{obs} respectively. The co-ordinate axes are earth's equatorial co-ordinates of 1950.0 epoch.

T_{s1} and T_{s2} were calculated iteratively from the observed mid time T_{obs} using Eqs. (3.4), (3.5) and (3.6). The solutions converged within three to four iterations.

The distance between the centres of the two satellites projected on the sky plane as seen from the Sun were obtained from

$$R = r_{s1s2}.sinu \tag{3.7}$$

where r_{s1s2} is the distance between the two points on space where S1 was at time T_{s1} and S2 at time T_{s2}, and u is the angle between S1 $-$ Sun and S1 $-$

35

S2 vectors; r_{s1s2} and u were obtained from the following equations:

$$x_{s1s2} = Y_{s2} - Y_{s1}$$

$$y_{s1s2} = Y_{s2} - Y_{s1}$$

$$z_{s1s2} = Z_{s2} - Z_{s1}$$

$$r_{s1s2} = \left(x_{s1s2}^2 + y_{s1s2}^2 + z_{s1s2}^2\right)^{1/2} \tag{3.8}$$

$$cosu = \left(-\frac{X_{s1}}{R_{s1}}\right)\frac{x_{s1s2}}{r_{s1s2}} + \left(-\frac{Y_{s1}}{R_{s1}}\right)\frac{y_{s1s2}}{r_{s1s2}} + \left(-\frac{Z_{s1}}{R_{s1}}\right)\frac{z_{s1s2}}{r_{s1s2}}. \tag{3.9}$$

The velocity V of the centre of S2 relative to the shadow centre projected on the plane of the sky as seen from the Sun were obtained from the set of equations,

$$V_{sm} = \dot{R}_{sm}$$

$$= \dot{X}_{sm} + \dot{Y}_{sm} + \dot{Z}_{sm}$$

$$= (\dot{X}_{jm} + \dot{x}_{sm}) + (\dot{Y}_{jm} + \dot{y}_{sm}) + (\dot{Z}_{jm} + \dot{z}_{sm})$$

$$V_{s1s2} = \left\{(Vx_{s1s2})^2 + (Vy_{s1s2})^2 + (Vz_{s1s2})^2\right\}^{1/2}$$

$$= \left[(\dot{X}_{s2} - \dot{X}_{s1})^2 + (\dot{Y}_{s2} - \dot{Y}_{s1})^2 + (\dot{Z}_{s2} - \dot{Z}_{s1})\right]^2$$

$$V = V_{s1s2}.sin\omega \tag{3.10}$$

where the dots refer to time derivatives, of the quantities defined in Eqs. 3.5, 3.6 and 3.8, ω is the angle between S1 − Sun and the relative velocity vector V_{s1s2} given by

$$cos\ \omega = \left(-\frac{X_{s1}}{R_{s1}}\right)\frac{Vx_{s1s2}}{V_{s1s2}} + \left(-\frac{Y_{s1}}{R_{s1}}\right)\frac{Vy_{s1s2}}{V_{s1s2}} + \left(-\frac{Z_{s1}}{R_{s1}}\right)\frac{Vz_{s1s2}}{V_{s1s2}}. \tag{3.11}$$

3.2.2 Types of Eclipses

The distance (R) obtained using Eq. 3.7 at closest approach is the impact parameter. The impact parameter determines the type of the eclipse if one occurs.

No eclipse is possible if $R > R_2 + R_p$

a)   If $R < R_2 + R_p$ and $R > R_2 + R_u$

a penumbral eclipse is possible. Fig. 3.3(a).

36

b)   If $R < R_2 + R_u$ and $R > |R_2 - R_u|$

Partial penetration into the umbra occurs. Fig. 3.3(b).

c)   If $R < |R_2 - R_u|$ and $R_2 > R_u$

the entire shadow core will be intercepted, since S2 is larger than the umbral radius the eclipse will be annular, Fig. 3.3(c).

d)   If $R < |R_2 - R_u|$ and $R_u > R_2$.

S2 will be entirely covered by the umbra. The eclipse will be total, Fig. 3.3(d).
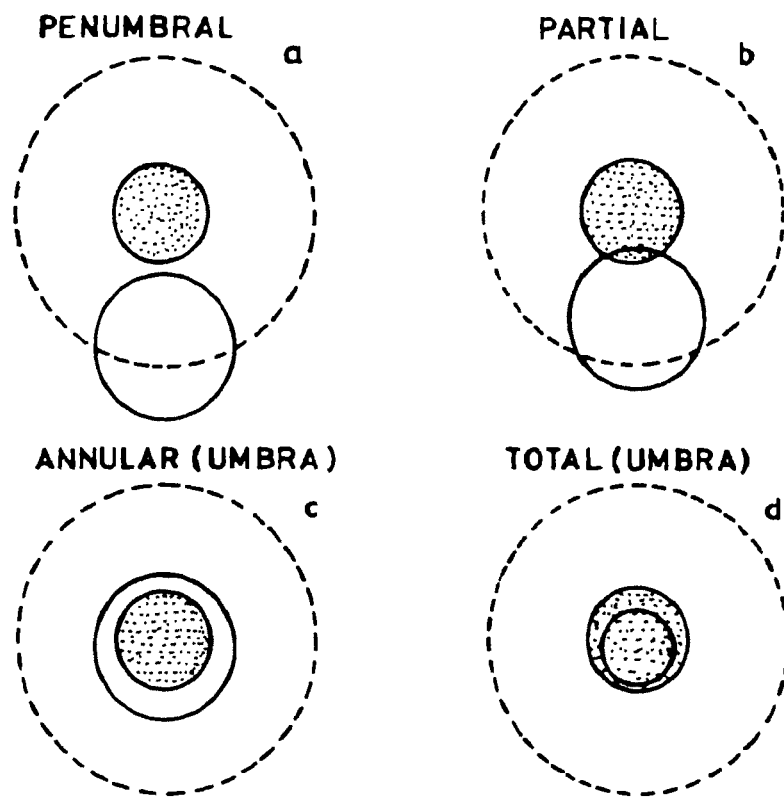
Fig. 3.3. Types of eclipses. The relative sizes of the penumbra (R_p), umbra (R_u), the radius of the eclipsed satellite (R_2) and its separation from the shadow axis (R) determine the type of the eclipse. The eclipse can be annular (c) if $R_2 > R_u$ or total (d) if $R_2 < R_u$.

3.2.3 The Occultation Geometry

A mutual occultation takes place when any two of the satellites are aligned with the observer, for example S1 (J2) and S2 (J3) in Fig. 3.1. Calculations of the occultation geometry is straightforward since the disc of S1 physically obstructs the view of S2. The correction for light travel time is taken into account by taking the position of S2 at time T_{s2} when light left it after reflection from its surface towards the observer reaching him at time T_{obs}, the position of S1 when the beam which started at T_{s2} from S2 was intercepted by it at time T_{s1}, and the observer's position at time T_{obs}. (Aksnes, Franklin, Magnusson 1986). Hence

$$
\begin{aligned}
T_{s2} &= T_{obs} - R_{o2}/c \\
T_{s1} &= T_{s2} + \frac{R_{o2} - R_{o1}}{c} \\
&= T_{obs} - R_{o1}/c
\end{aligned}
\tag{3.12}
$$

R_{o1} and R_{o2} were calculated using Eq. (3.6). The distance between the centres of S1 and S2 in the sky plane during the event is given by

$$
R^o = r^o_{s1s2} \cdot \sin(u^o)
\tag{3.13}
$$

where the superscripts refer to occultations. r^o_{s1s2} is the distance between the centres of S1 and S2, u^o is the angle between S1 $-$ observer and S1 $-$ S2 vectors. For the occultations one takes the topocentric aspect, r^o_{s1s2} and u^o were calculated using the equations

$$
\begin{aligned}
x^o_{s1s2} &= X_{o2} - X_{o1} \\
y^o_{s1s2} &= Y_{o2} - Y_{o1} \\
z^o_{s1s2} &= Z_{o2} - Z_{o1} \\
r^o_{s1s2} &= \left\{ (x^o_{s1s2})^2 + (y^o_{s1s2})^2 + (z^o_{s1s2})^2 \right\}^{1/2}
\end{aligned}
\tag{3.14}
$$

where (X_{o1}, Y_{o1}, Z_{o1}) and (X_{o2}, Y_{o2}, Z_{o2}) are the coordinates defined in Eq. 3.6 for times T_{s1} and T_{s2} obtained using Eq. (3.12) and

$$
\cos(u^o) = \left(-\frac{X_{o1}}{R_{o1}} \right) \frac{x^o_{s1s2}}{r^o_{s1s2}} + \left(-\frac{Y_{o1}}{R_{o1}} \right) \frac{y^o_{s1s2}}{r^o_{s1s2}} + \left(-\frac{Z_{o1}}{R_{o1}} \right) \frac{z^o_{s1s2}}{r^o_{s1s2}}.
\tag{3.15}
$$

The sky plane velocity V^o of S2 relative to S1 for a terrestrial observer is obtained from

$$V^o = V^o_{s1s2} \sin \omega^o \qquad (3.16)$$

where V^o_{s1s2} the velocity of S2 relative to S1 is given by

$$
\begin{aligned}
V^o_{s1s2} &= \dot{R}_{o2} - \dot{R}_{o1} \\
&= \left\{ \left(V^o x_{s1s2} \right)^2 + \left(V^o y_{s1s2} \right)^2 + \left(V^o z_{s1s2} \right)^2 \right\}^{1/2} \\
&= \left\{ \left(\dot{X}_{o2} - \dot{X}_{o1} \right)^2 + \left(\dot{Y}_{o2} - \dot{Y}_{o1} \right)^2 + \left(\dot{Z}_{o2} - \dot{Z}_{o1} \right)^2 \right\}^{1/2} \qquad (3.17)
\end{aligned}
$$

where $\left(\dot{X}_{om}, \dot{Y}_{om}, \dot{Z}_{om}, m = 1, 2 \right)$ refer to the time derivative of the quantities defined in Eq. 3.6 at time T_{sm}, ω^o in Eq. 3.16 is the angle between 'S1 – observer' vector and the relative velocity vector, it is calculated using the relation:

$$\cos(\omega^o) = \left(-\frac{X_{o1}}{R_{o1}} \right) \frac{V^o x_{s1s2}}{V^o_{s1s2}} + \left(-\frac{Y_{o1}}{R_{o1}} \right) \frac{V^o y_{s1s2}}{V^o_{s1s2}} + \left(-\frac{Z_{o1}}{R_{o1}} \right) \frac{V^o z_{s1s2}}{V^o_{s1s2}}. \qquad (3.18)$$

3.2.4 Types of Occultations

Occultation of a satellite of radius R_2 by another of radius R_1 is possible if the separation R between their centres projected on the topocentric sky plane satisfies the condition:

a) $R < R_1^1 + R_2$ where $R_1^1 = R_1 \frac{R_{02}}{R_{01}}$. The occultation will be partial if $R > |R_2 - R_1^1|$.

b)   The occultation will be total if $R < |R_2 - R_1^1|$.

c)   The occultation will be annular if $R < |R_2 - R_1^1|$ and $R_1 < R_2$.

3.3   Photometric Functions Used in the Study

3.3.1   Uniform Albedo Distribution

Fig. 3.4 shows geocentric view of the satellite S2. $S_2 N_7$ is along the normal to the orbital plane of the satellite. The point Q' on the surface of the satellite would be seen projected at Q on the disc of the satellite for a terrestrial observer. The intensity of light received by the observer from Q'

39

would depend not only on the viewing geometry but also on the scattering properties of the surface. It is assumed that the entire surface of the satellite has the same average albedo.
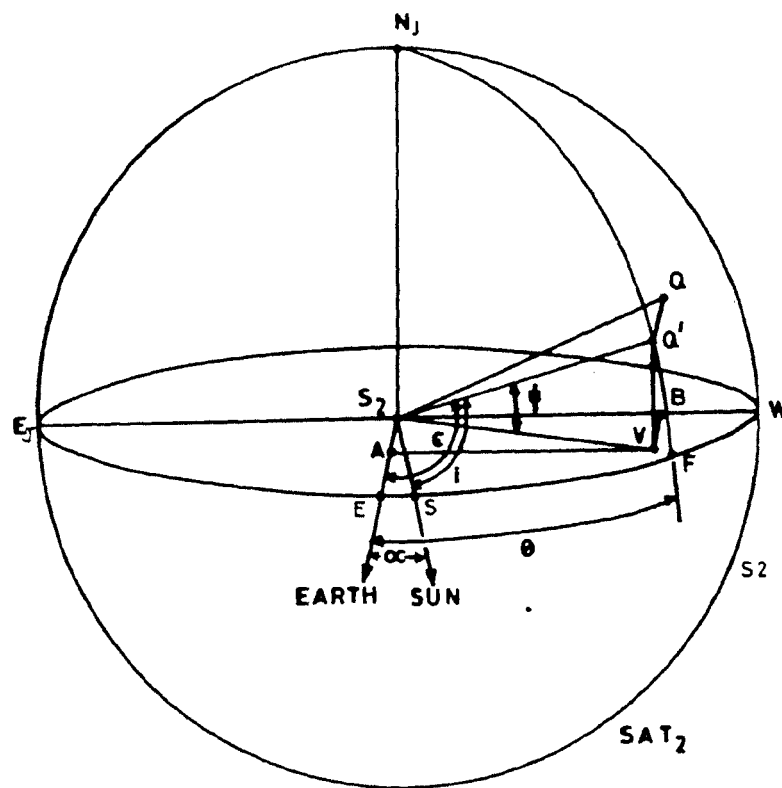
Fig. 3.4. Terrestrial view of the satellite. A point $Q'(\theta, \psi)$ on the surface of the satellite will be seen projected on the disc $(E_J N_J S_2 W)$ at the point Q. The angles of incidence and reflectance of sunlight at Q' are i and ϵ respectively.

The photometric function $I(\mu_0, \mu, \alpha)$ used in the estimation of light loss during the mutual eclipse is a measure of the light received from an elementary area on the surface of the satellite which is illuminated at an angle $\cos^{-1}(\mu_0)$ and viewed at an angle $\cos^{-1}(\mu)$ to the surface normal. Alpha is the solar phase angle . Several expressions have been worked out by various authors to explain the observed reflectance of solar system objects without atmosphere. Some of these are empirical relations (Hapke 1963; Irvin 1966; Minnaert 1941). Scattering laws for particulate surfaces of arbitrary albedo have been derived from radiative transfer by Lumme and Bowel (1981); Goguen (1981); Hapke (1981). The scattering laws most commonly used are given below:

1) Photometric function for lunar like surfaces developed by Hapke (1963) and Irvin (1966) which correctly describe the scattering from a dark porous surface like that of the moon is given by

$$I(\mu_0, \mu, \alpha) = F\left(\frac{\mu_0}{\mu_0 + \mu}\right).f(\alpha) \qquad (3.19)$$

where

F $\qquad = \quad$ incident solar flux and

$f(\alpha)$ $\qquad = \quad$ phase function of the surface.

This function closely approximates the scattering behaviour of many low albedo particulate materials. The angular characteristics of this function is the well known Lommel-Seeliger's law.

2) For very bright surfaces one can use Lambert's law given by

$$I(\mu_0, \mu, \alpha) = F r_n \mu_0 \qquad (3.20)$$

where r_n is the normal albedo. By definition, a Lambert surface appears equally bright when viewed from any angle and reflects all the light incident on it.

3) A widely used empirical photometric function is the Minnaert's function (Minnaert 1941) given by

$$I(\mu_0, \mu, \alpha) = B_0(\alpha).\mu_0^{k(\alpha)}.\mu^{k(\alpha)-1} \qquad (3.21)$$

41

where $B_0(\alpha)$ and $k(\alpha)$ are the two Minnaert's parameters which are functions of α and the wavelength. Goguen (1981) has shown that Eq. 3.21 is only a crude approximation to the scattering properties of real surfaces; however it has been found to be valid for near zero solar phase angles. Therefore Minnaert's law can be used as a convenient approximation (except very close to the limb) to study small phase angle data. Since the maximum solar phase angle at the distance of Jupiter is less than $12°$, this law has been used in the present study. It has been successfully used by Simonelli and Veverka (1986) to analyze Voyager observations of Io. In the extreme case when $k(\alpha)$ is equal to unity Eq. 3.21 represents Lambert's Law.
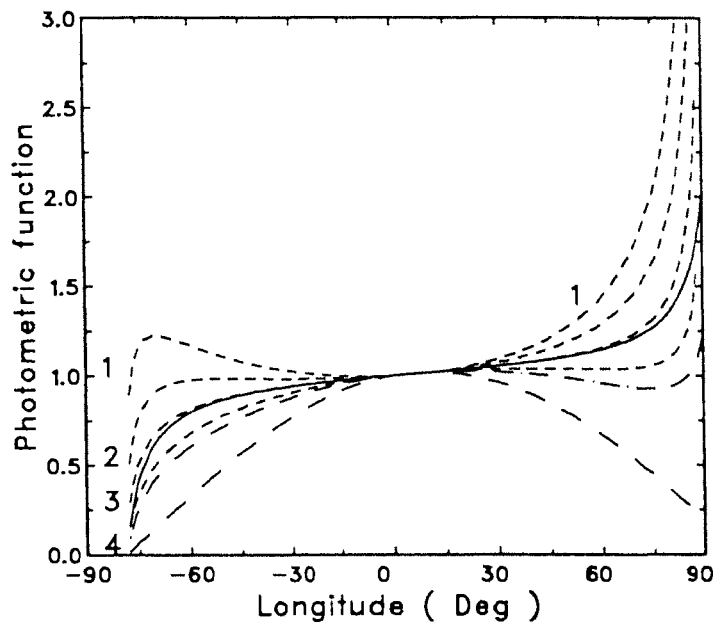
Fig. 3.5(a). Variation of the photometric function along the equator for a terrestrial observer, for a solar phase angle of $11°$. The continuous line is for Lommel-Seeliger's law; the long dashed line for Lambert's law; the dotted dashed line for Hapke's law for parameters for Io from Descamps et al. (1992); and the short dashed lines-Minnaert's law. For Minnaert's curves the labels 1-4 refer to values of $k(\alpha)$ from 0.3-0.6.

4) Hapke's function (without macroscopic roughness) has the form

$$I(\mu_0, \mu, \alpha) = \frac{w}{4\pi} \cdot \left(\frac{\mu_0}{\mu_0 + \mu}\right) \left[\left\{1 + B(\alpha, h)\right\} P(\alpha, g) + H(w, \mu) \times H(w, \mu_0) - 1\right]$$

$$(3.22)$$

where $B(\alpha, h)$ is the backscatter function (Hapke 1981); h is the compaction parameter, $P(\alpha, g)$ is the single particle phase function, w is the average single scattering albedo g is the asymmetry parameter for the Henyey-Greenstein phase function, and $H(w, \mu)$ and $H(w, \mu_0)$ are Hapke's approximations to functions tabulated by Chandrasekhar (1950) given by

$$H(w, \mu) = \frac{1 + 2\mu}{1 + 2\mu\sqrt{1 - w}}.$$
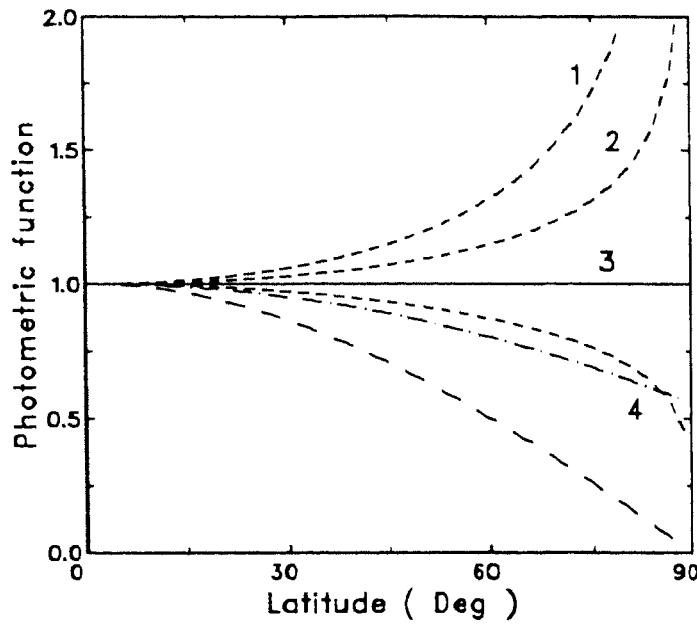
Fig. 3.5(b). Variation of the photometric function along the central meridian. Other details same as that for Fig. 3.5(a).

43

Table 3.1(a) Brightness ratios and boundaries used in the model for Io

Region	Latitude (b) on Io (deg)	Relative brightness[1]
Equatorial band	$0 < \|b\| > 50$	0.85 on the trailing hemisphere 0.90 on the leading hemisphere
Polar regions	$50 < \|b\|$	0.49
Overlapping regions	$50 < \|b\| < 60$	0.5 Equatorial + 0.5 polar
Scattering law	Minnaert's law	

1. Through R and I filters

Table 3.1(b) Features modelled on Ganymede

Feature	Relative[1,2] brightness
Perrine	0.765
Nicholson east and west	0.765
Bright ray Crater *Tros*	1.28
Bright Polar Caps	1.16

Scattering law : Lunar like
(Lommel-Seeliger's law)
Relative brightness of deafault regions = 0.86

1. Squyres and Veverka, 1981
2. Mallama 1991

44

Variation of the photometric functions given in 3.19–3.22 along the photometric equator and meridian are shown in the Fig.s 3.5.(a) and (b) respectively, for typical values of the constants.

3.3.2 Non Uniform Albedo Distribution

In the post Voyager era, the full potential of mutual event data can be exploited by taking into account the differences in albedo over different terrains on the surface of the satellites. Most of the events observed from VBO during the 1991 apparitions involved occultations or eclipses of Io by Europa. Io has a broad equatorial band, with brighter white markings and brown polar regions. The mutual event observations from VBO were carried out in R and I band. The Voyager imagery was carried out in the wavelength region 4000Å to 7000Å. We have therefore used the published values of the equator to pole albedo ratios by Simonelli and Veverka (1986) for the orange filter observations as the starting values. Best fits were obtained for the relative brightness values given in Table 3.1(a). For the single observation of occultation of Ganymede by Europa, the phase functions $f(\alpha)$ in Eq. (3.19) derived by Squyres and Veverka (1981) have been used. Albedo boundaries on Io and Ganymede used in the present study are given in Table 3.1(a,b).

3.4 Computation of Light Loss During the Mutual Events

3.4.1 Light Loss During an Eclipse

The light loss in the umbra and the penumbra were computed using the method described by Aksnes and Franklin (1976) modified to include the effect of limb darkening on the eclipsed satellite. Fig. 3.6 shows the geometry for a particular case as seen from the Sun. The eclipsed satellite totally encompasses the umbra UU' and part of the penumbra $LTIWMKL$. $S_2 S_2'$ is the track of S2 with respect to the shadow centre. Fig. 3.7 shows the heliocentric view of S2; S_2 is the centre of the eclipsed satellite, S and E are the sub-solar and sub-terrestrial points respectively.

The great circle perpendicular to SS_2 in the plane $E_J NS_2 W$ is repre-

sented as $(LTIIVMDL)$ in Fig. 3.6. The portions on S2 immersed in the umbra will be totally dark whereas the regions in the penumbra at a radial distance x from the shadow axis will have intensity $(l - lp(x))$ which varies from a value 0 at the inner surface to 1 at the outer surface of the penumbral cone. The penumbral intensity at any point was estimated by computing the area of the apparent disc of the Sun of radius R'_s, at the distance of the eclipsed satellite as seen from that point (Aksnes and Franklin, 1976). The limb darkening parameter on the Sun at the wavelength of observation used in the calculations were taken from Allen (1963).
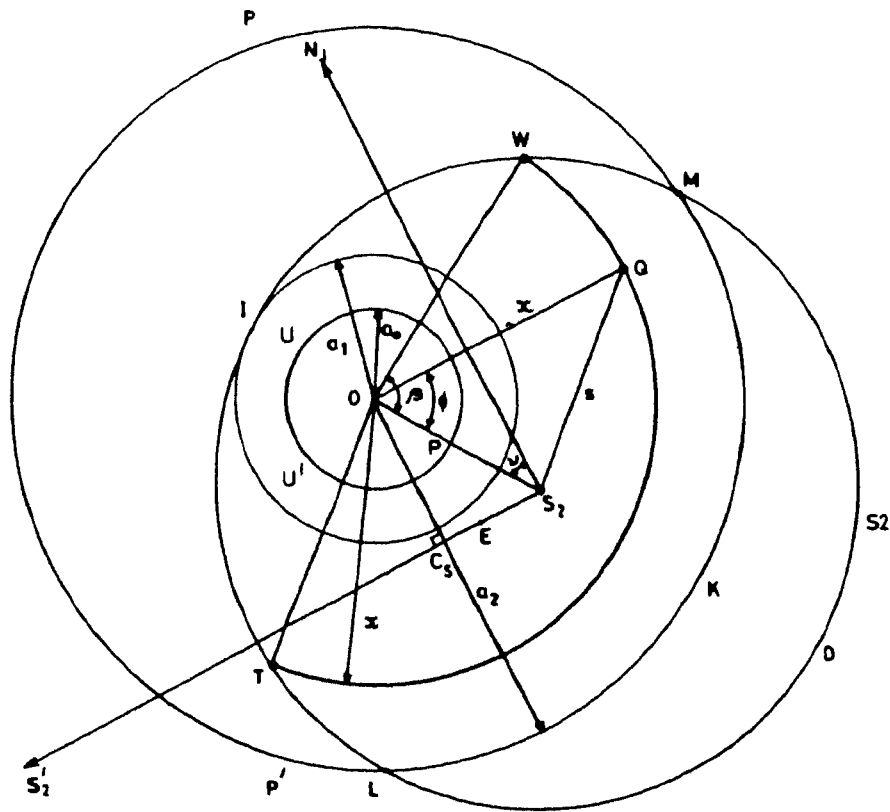
Fig. 3.6. Heliocentric view of an eclipse event. $S_2S'_2$ is the path of the eclipsed satellite relative to the shadow centre O. S_2N_J is parallel to the direction of north pole of Jupiter. C_S is the close approach point on the track. In this particular case the satellite is annularly eclipsed by the umbra UU' and partially eclipsed by the penumbra $LP'PMKL$.

46

In Fig. 3.7 i and ϵ are the angles of incidence and reflectance respectively and α is the solar phase angle (positive in this case) let

$$\mu_0 = \cos i$$

$$\mu = \cos \varepsilon$$

$$wi = 1.0 \qquad \text{for the limited regions on } S2 \qquad (3.23)$$

$$= 0.0 \qquad \text{for regions beyond the terminator}$$

The loss in light in the penumbra as seen by a terrestrial observer is calculated as follows.

Let da be an elementary area at Q' which on projection on the sky plane for a terrestrial observer-has a value da_e, and projection on the sky plane for a heliocentric observer has a value da_s such that

$$da_e = da.\mu$$

$$da_s = da.\mu_0$$

$$\text{hence} \qquad da_e = da_s.\frac{\mu}{\mu_0} \qquad (3.24)$$

$$= x\,d\phi\,dx.\frac{\mu}{\mu_0}$$

The shadow cone is along the S_2-Sun direction. One however views the event from the earth. The light loss when an elementary area da_e is covered by the penumbral cone will be

$$dL_p = l_p.wi.I(\mu_0, \mu, \alpha).da_e$$

where wi excludes the regions at the limb beyond the terminator and $I(\mu_0, \mu, \alpha)$ is defined in section (3.3.1). Using relations in Eq. 3.24

$$dL_p = l_p.wi.I(\mu_0, \mu, \alpha).da_s.\frac{\mu}{\mu_0}.$$

This is in accordance with the reciprocity principle (Minnaert 1941) given by

$$I(\mu, \mu_0, \alpha).da_s = I(\mu_0, \mu, \alpha).da_e. \qquad (3.25)$$

The total light loss in the penumbra will be

$$dL_p = \int \int lp(x).wi.I(\mu_0, \mu, \alpha).da_s.\frac{\mu}{\mu_0}. \qquad (3.26)$$

The light loss in Eq. 3.26 was computed in two parts following the method of Aksnes and Franklin (1976); the inner annular region bounded between the umbral boundary ($a_0 = R_u$) and circle of radius a_1 and an outer region bounded by radii a_1, a_2 and the limb of S2 ($LTIWMKL$) :

$$
L_p = \int\limits_{a_0}^{a_1} \int\limits_{0}^{2\pi} lp(x).wi.I(\mu_0, \mu, \alpha).x.d\phi.dx\frac{\mu}{\mu_0} +
$$

$$
\int\limits_{a_1}^{a_2} \int\limits_{-\beta}^{\beta} .lp(x).wi.I(\mu_0, \mu, \alpha).x.d\phi.dx.\frac{\mu}{\mu_0} \qquad (3.27)
$$

where $\beta = \angle WOS_2$. The limits of integration a_0, a_1, a_2 were calculated using the relations (Aksnes and Franklin 1976)

$$
a_0 = \min[R_p, \max(R_u, R - R_2)]
$$

$$
a_1 = \min[R_p, \max(a_0, R_2 - R_1)] \qquad (3.28)
$$

$$
a_2 = \min[R_p, R + R_2].
$$

Fig. 3.7. Heliocentric view of the satellite centred at S_2. The point Q on the disc of the satellite as seen from the Sun corresponds to the point $Q'(\theta, \psi)$ on the surface.

48

For the point Q' on S2 (Fig. 3.7)

$$\mu_0 = \cos \psi \cos \theta$$

$$\mu_1 = \cos \psi (\cos \theta + \alpha).$$

For eclipse events the longitude is measured more conveniently from S. The plane containing the centres of the Sun, Earth and the satellite is inclined by less than $0^{\circ}.5$ to the orbital plane of the satellites and the equatorial plane of Jupiter. Therefore motion of S2 would be very close to this plane; $S_2 N_J$ and $C_S O$ (Fig. 3.6) would be parallel to the spin axis of Jupiter (Aksnes, Franklin and Magnusson, 1986). Fig. 3.8 shows the terrestrial view of the sequence of the event; the defect of illumination on S2 would always be either at the leading or trailing limb, depending on the sign of the solar phase angle α. The co-ordinates (θ, ψ) of the point Q' (Fig. 3.7) can be calculated from the position (x, θ) of the corresponding point Q (Fig. 3.6) using the following relations.

$$
\begin{aligned}
\cos \psi \cos \theta &= \frac{QQ'}{S_2 Q'} \\
&= \sqrt{1 - (S_2 Q / R_2)^2} \\
&= \sqrt{1 - (s / R_2)^2} \\
\cos \psi \sin \theta &= -\frac{S_2 B}{R_2} \\
&= -\frac{S_2 Q}{R_2} \times \sin(N S_2 Q) \\
&= -\frac{s}{R_2} \times \sin(O S_2 Q - \nu) \\
\sin \psi &= \frac{S_2 Q}{R_2} \times \cos(N S_2 Q) \\
&= \frac{s}{R_2} \times \cos(O S_2 Q - \nu) \\
\nu &= \arctan(d / y)
\end{aligned}
\qquad (3.29)
$$
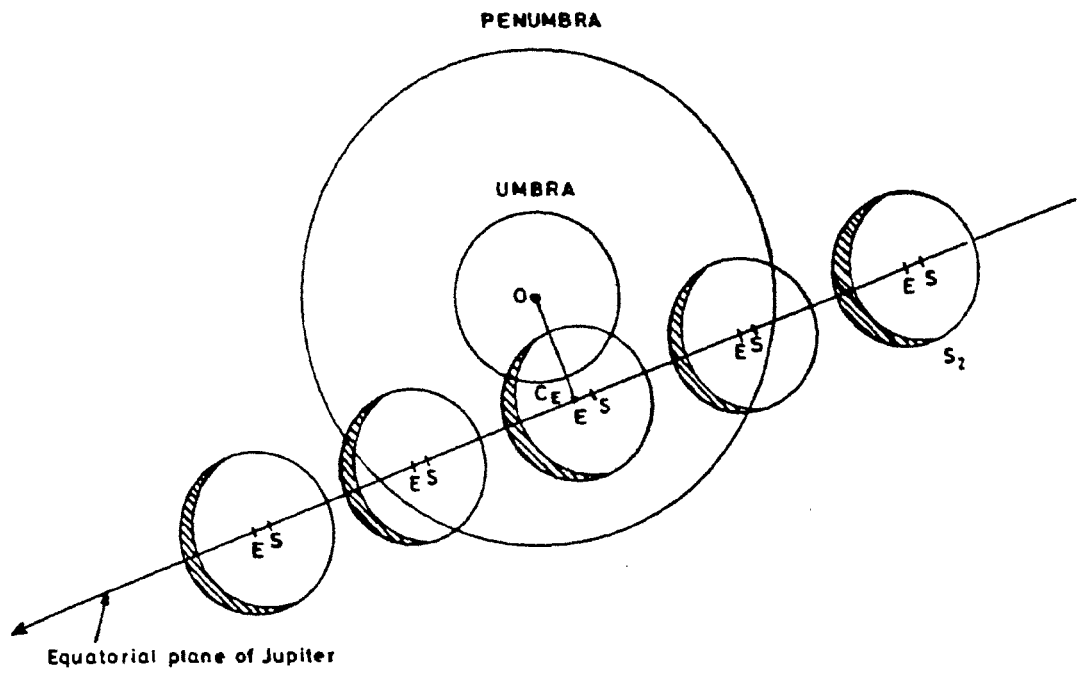
Fig. 3.8. Terrestrial view of the path of S_2 across the shadow cone. The defect of illumination on the disc of S_2 will be at the leading or trailing limb depending on the direction of its relative motion and the sign of the solar phase angle. C_E is the closest point.
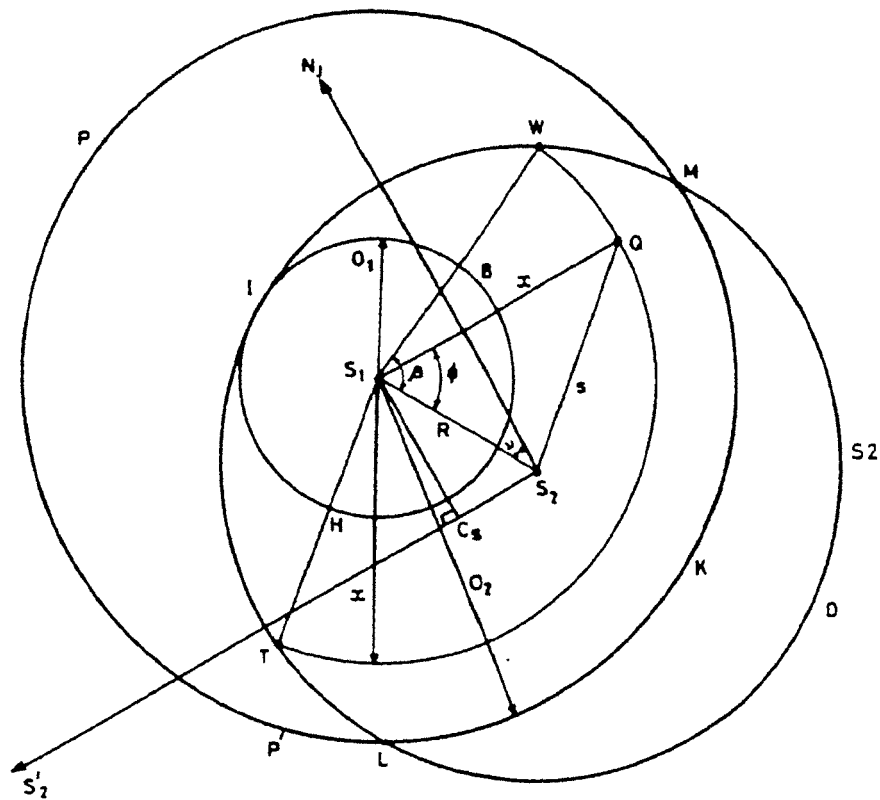
Fig. 3.9. Geocentric view of an occultation of the satellite S2 (LTIWMDL) centered at S_2 by the satellite S1 (LP′PMKL) centered at S_1, in the partial phase. $S_2 S_2'$ is the track of S2 relative to S1.

51

where R_2 is the radius of eclipsed satellite, d its distance (C_sS_2) from the closest approach point C_S (Fig. 3.6),and y the impact parameter. The light loss in the umbra is given by /

$$L_u = \int\limits_{u_0}^{u_1} \int\limits_0^{2\pi} wi.I(\mu_0,\mu,\alpha).x.d\phi.dx.\frac{\mu}{\mu_0} +$$

$$\int\limits_{u_1}^{u_2} \int\limits_{-\beta}^{\beta} wi.I(\mu_0,\mu,\alpha).xd\phi.dx.\frac{\mu}{\mu_0} \qquad (3.30)$$

where u_0, u_1, u_2 ,the limits of integration are determined for each instant as in case of the penumbral limits:

$$u_0 = \min\{R_u.\max(0.R - R_2)\}$$

$$u_1 = \min\{R_u.\max(u_0, R_2 - R)\}$$

$$u_2 = \min\{R_u, R + R_2\}. \qquad (3.31)$$

The total light loss in the umbra and penumbra was normalized with respect to the total light from the uneclipsed surface of S2, before comparison with the observed data.

Light from the uneclipsed satellite is

$$L = \int\limits_0^{R2} \int\limits_0^{2\pi} wi.I(\mu_0,\mu,\alpha).xd\phi.dx.\frac{\mu}{\mu_0}. \qquad (3.32)$$

The integrations were carried out using double 12 step Gaussian quadrature.

3.4.2   Light Loss During an Occultation

The geometry of a partial occultation is shown in Fig. 3.9. $LP'PMKL$ is the occulting satellite centered at S_1. LTIWMDL is the occulted satellite centered at S_2 which represents the sub earth point on the disc (Fig. 3.4).

52

$S_2 S'_2$ is the occultation track. $C's$ is the close approach point. The loss in light is equal to that is reflected from the area $LTIIVMKL$ from S2. As in the case of eclipse

$$L_o = \int\limits_{o0}^{o1} \int\limits_{0}^{2\pi} wi.I(\mu_0.\mu,\alpha).x.d\phi.dx +$$
$$\int\limits_{o1}^{o2} \int\limits_{-\beta}^{\beta} wi.I(\mu_0.\mu,\alpha).x.d\phi.dx. \qquad (3.33)$$

The elementary area at (x,ϕ) on the disc S2 is $xd\phi dx$ as seen by the observer. The limits of integration o_0, o_1, o_2 are obtained from

$$o_0 = \min[R_1', \max(0, R - R_2)]$$
$$o_1 = \min[R_1', \max(o_0, R_2 - R)]$$
$$o_2 = \min[R_1', R + R_2] \qquad (3.34)$$

wi is defined in Eq. 3.23. The light from the unocculted satellite will be

$$L = \int\limits_{0}^{R2} \int\limits_{0}^{2\pi} wi.I(\mu_0.\mu,\alpha).x.d\phi.dx. \qquad (3.35)$$

The light from the satellite either outside the occultation event calculated using Eq. (3.35) or outside eclipse using Eq. (3.32) should the same. This is indeed so because in Eq. (3.35)

$$x.d\phi.dx = da_e \qquad (3.36a)$$

where as in Eq. (3.32)

$$x.d\phi.dx = da_s \qquad (3.36b)$$

using the relation between da_e and da_s in Eq. (3.24) it is readily noticed that Eq. (3.32) and (3.35) are identical.

53

3.5 The Longitude Discrepancy and the Phase Correction

Due to proximity of the earth to the Sun compared to the distance between the Sun and the Jupiter system, mutual eclipses and occultations occur in pairs. The time interval between the two kinds of events depends on the solar phase angle – typically a few minutes near opposition to a few hours at larger solar phase angles. The orbital longitudes of the two satellites do not change appreciably during the time interval between the occultation and the corresponding eclipse. The error in longitude as determined from the (O-C) of the event mid time should be the same for the two kinds of events. For a satellite k eclipsing or occulting another satellite l let

Δx_{lk}^{ec} = residual in km, in the sense $(l - k)$, measured along the track of the satellite l with respect to the shadow centre.

Δx_{lk}^{oc} = residual in km, in the sense $(l - k)$ measured along the track of the satellite l with respect to the satellite k. Since the two events occur very close in time and in space, one expects

$$\Delta x_{lk}^{ec} \simeq \Delta x_{lk}^{oc}$$

However, from the analysis of the 1973 mutual event data, Aksnes and Franklin (1976) noticed that the difference $\Delta x_{lk}^{ec} - \Delta x_{lk}^{oc}$ increased steadily with the phase angle. Similarly Lieske (1980) noticed that, compared to the E-2 ephemeris, the mean residual in right ascension was +0.030 arcseconds for the eclipse events in 1973. The mean residual for occultation events had a much lower value of −0.005 arcseconds. It appeared to indicate that the eclipses took place before the predicted times but the occultations were close to the predicted times. Aksnes, Franklin and Magnusson (1986) resolved this longitude discrepancy by attributing it to the finite separation between the light centre and the geometric centre on the satellite disc. Fig. 3.10(a) shows the geometry of an occultation event when the geometric centre E, the sub earth point on the occulted satellite S2 is closest to the centre of the occulting satellite S1. EN$_J$ is normal to the equatorial plane of S2.

54
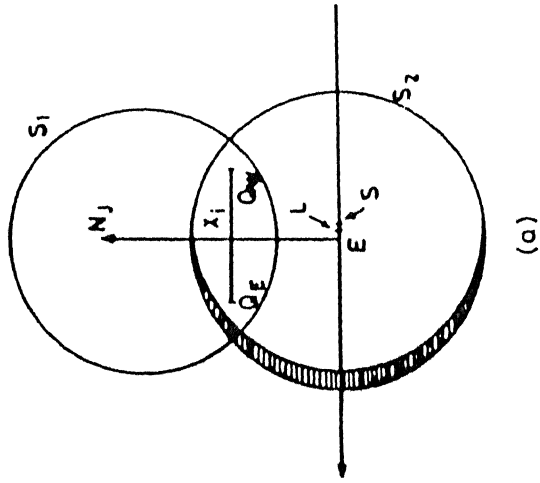
OCCULTATION

ECLIPSE
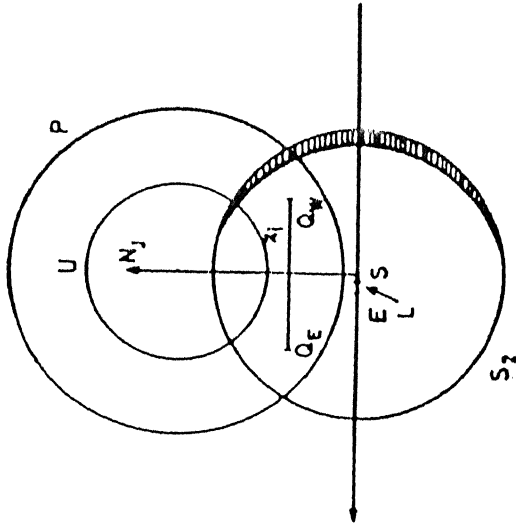
Fig.3.10. (a) The occultation geometry : For $\alpha > 0$ the sub Sun point S is to the west of the sub earth point E. The eastern hemisphere will appear fainter (Fig. 3.5a) in addition to the phase defect, the light centre according to definition in Eq. 3.37 will be to the west of E. (b) The eclipse geometry: For $\alpha > 0$, E is to the east of the sub sun point. From the earth the western hemisphere will appear brighter than the eastern hemisphere. The light centre L will therefore be to the west of E.

55

For a post opposition event the sub sun point S will be to the west of E. There exists asymmetry in light distribution on the two halves of the disc, the eastern half being relatively fainter in addition to the phase defect at the eastern limb. The distance of the light centre L from the geometric centre E for the unocculted disc of S2 can be obtained from the relation

$$\delta x_\alpha = \frac{\Sigma \vec{r_i}\, dE_i}{\Sigma dE_i} \qquad km \qquad (3.37)$$

where dE_i is the light flux from an elementary area at a distance of $\vec{r_i}$ from the polar axis EN$_J$ on S2. For a partial event, the summation is carried out only over the occulted portion of the disc. The position of L for partial events corresponds to the intersection of the meridian through the light centre of the occulted region on the equator. The effect of finite solar phase angle at the time of mutual event when the earth and Sun are very close to the equatorial plane of the satellites, introduces discrepancy in longitude and not in the latitude.

Let δx_α be the phase correction for an impact parameter y. The variation of δx_α with the impact parameter y for 102 and 201 events are shown in Fig. 3.11(a) and (b) respectively. The continuous line corresponds to Lommel-Seeliger's law and the dotted line corresponds to Lambert's law in the model. In the case of Lommel-Seeliger's law, for the 201 event, the phase correction first increases with increase in impact parameter. This is a consequence of the higher degree of asymmetry along the longitude at larger distances from the sub earth point in longitude (Fig. 3.5(a)). When the occulting satellite is smaller than the occulted one, the span of longitude coverage is larger when higher latitude regions are blocked, compared to the central annular events. As the occulted area gradually diminishes with increase in y, δx eventually begins to decrease.

For occultations, the aspect is topocentric [Fig. 3.12(a)]. If S2 is moving eastwards the light centre (L) will be occulted later than the predicted time which corresponds to close approach of the geometric centre E. Following the sign convention of Aksnes et al. (1986), δx_α is taken positive if L is displaced towards west from G.
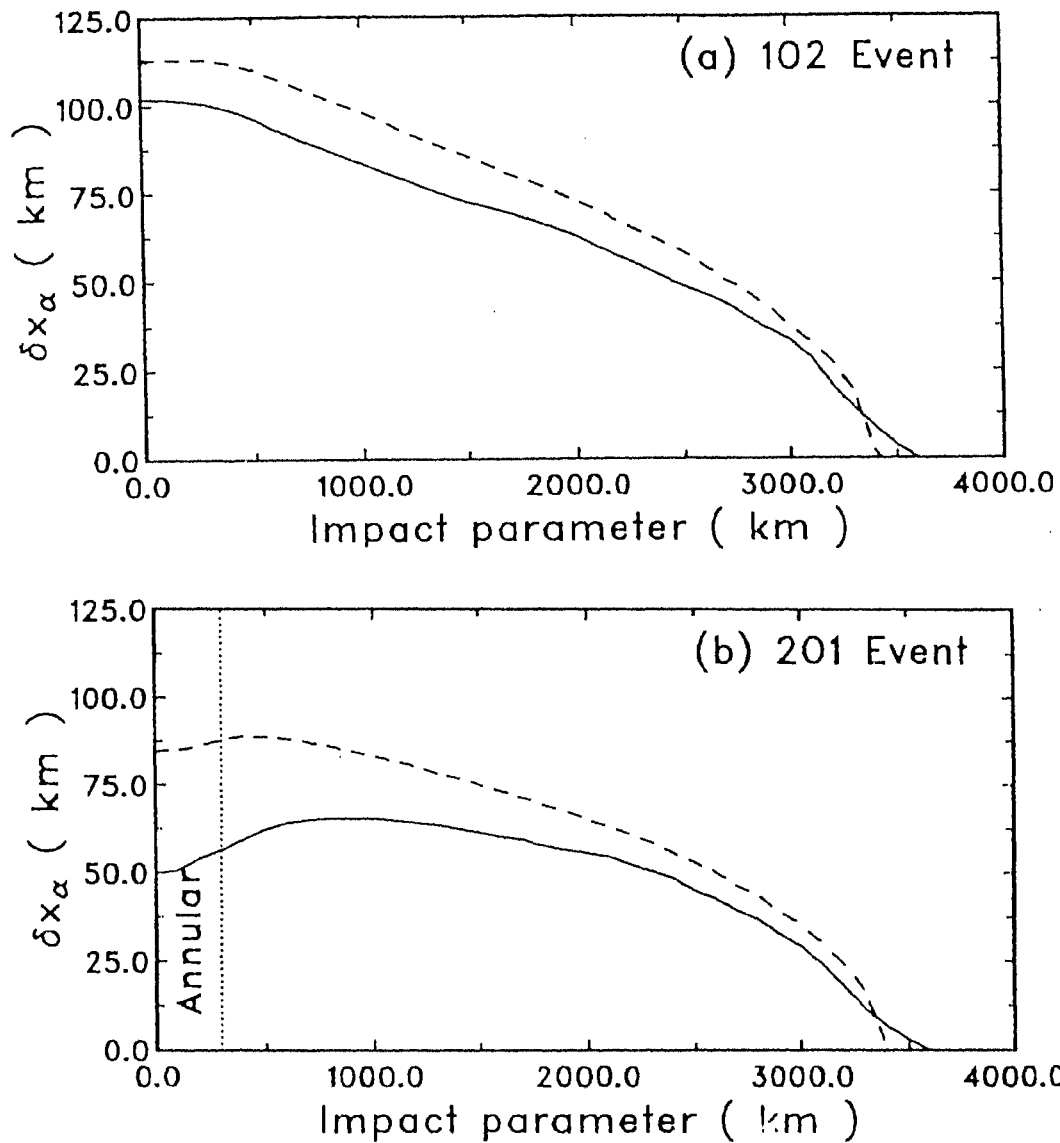
Fig. 3.11 Variation of the phase correction $\delta.r_\alpha$ with the impact parameter y for a solar phase angle of 11°; the continuous line is using Lommel-Seeliger's law and the dashed curve is using Lambert's law. (a) For the occultation of Europa by Io, (b) For the occultation of Io by Europa, the increase in $\delta.r_\alpha$ with y in the beginning is a consequence of higher degree of asymmetry at larger distances from the subearth point in longitude. (Fig. 3.5(a)). When the occulting satellite is smaller than the occulted one as in this case, the span of longitude coverage is larger when the higher latitude regions are blocked, compared to the central annular events. As the occulted area decreases with increase in y, $\delta.r_\alpha$ eventually begins to decrease.
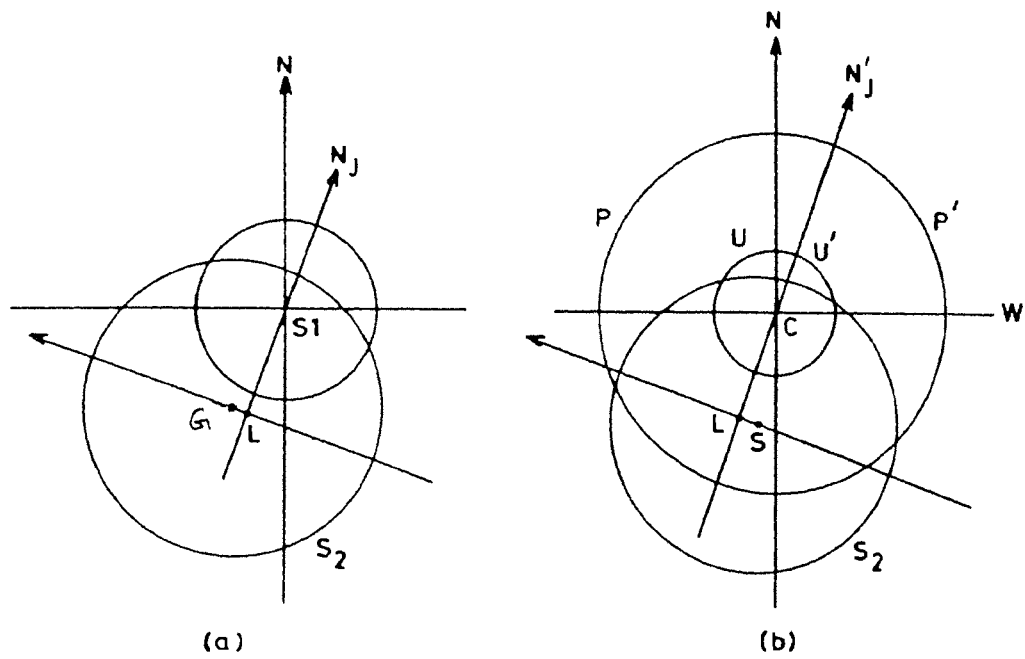
Fig. 3.12. Geometry illustrating the longitude discrepancy. The theory predicts mid time T_g of an event when the geometric centre passes closest to the target. The observations yield time of light minimum T_l when the light centre is closest to the target. (a) For occultations the target is the centre S_1 of S1, Geometric centre is the sub earth point E. (b) For eclipses the target is the centre C of umbra (U) or penumbra (P), the geometric centre is the sub Sun point (S). L is the light centre both kinds of events. When $\alpha > 0$, the occultation will be delayed if motion of S2 is eastward with respect to S1. Whereas the eclipse will occur earlier than the predicted time, for an eastward movement of S2 relative to the shadow.

58

For eclipses the aspect is heliocentric although one calculates the light loss as seen from the earth. In Fig. 3.12(b), S is the sub Sun point, for ($\alpha > 0$), L is east of the geometric centre (S), δx_α is therefore negative. For an eastward movement of S2 the light centre (L) will be eclipsed first followed by the geometric centre(S). For events before opposition the location of light centre will be on the opposite side. Aksnes et al. (1986) pointed out that, since all the eclipses save one of the 1973 season were post opposition events, a positive bias of the residuals compared to E-2 ephemeris was obtained. The occultations occurred with equal frequency before and after opposition. The mean residual was therefore a negligible quantity.

The longitude correction suggested by Aksnes et al. (1986) should be applied to both kinds of events. The correction should be applied to the observed time of light minimum T_l to obtain the time T_g of closest approach of the geometric centre to the target before comparing with theory. For occultations,

$$T_g = T_l - \delta T_\alpha \qquad (3.38)$$

where δT_α is the phase correction in time given by

$$\delta T_\alpha = \delta x_\alpha / V^o. \qquad (3.39)$$

If V^o is the sky plane velocity of the occulted satellite (S2) with respect to the occulting satellite (S1). If this relative motion is eastwards, V^o is positive.

The value of V^o is estimated using relation 3.16. δx_α is calculated by substituting the values of x_i and dE_i in Eq. 3.37.

For the occultation geometry in Fig. 3.9

$$\delta x_\alpha = \frac{LM_o}{L_o} \qquad (3.40)$$

where

$$LM_o = \int_{o0}^{o1} \int_0^{2\pi} \omega i . I(\mu_0, \mu, \alpha) . x \sin(\phi) . x d\phi . dx$$

$$+ \int_{o1}^{o2} \int_{-\beta}^{\beta} wi . I(\mu_0, \mu, \alpha) . x \sin(\phi) . x d\phi dx \qquad (3.41)$$

59

and L_o is given by Eq. 3.33.

For eclipses similarly

$$T_g = T_l - \delta T_\alpha \tag{3.42}$$

$$\delta T_\alpha = \delta x_\alpha / V \tag{3.43}$$

where V, the sky plane velocity of S2 relative to the shadow centre, is calculated using relation 3.10.

For the eclipse geometry in Fig. 3.6

$$\delta x_\alpha = \frac{LM_p + LM_u}{L_p + L_u} \tag{3.44}$$

where LM_p and LM_u are given by

$$LM_p = \int_{a0}^{a1} l_p(x) \int_0^{2\pi} wi.\, I(\mu_0, \mu, \alpha).\, x.\, \sin(\phi).\, x d\phi dx.\frac{\mu}{\mu_0}$$

$$+ \int_{a1}^{a2} l_p(x) \int_{-\beta}^{+\beta} wi.\, I(\mu_0, \mu, \alpha)x.\, \sin(\phi).\, x.d\phi.dx.\frac{\mu}{\mu_0} \tag{3.45}$$

$$LM_u = \int_{u0}^{u1} \int_0^{2\pi} wi.\, I(\mu_0, \mu, \alpha).\, x.\, \sin(\phi).\, x.d\phi.dx.\frac{\mu}{\mu_0}$$

$$+ \int_{u1}^{u2} \int_{-\beta}^{+\beta} wi.\, I(\mu_0, \mu, \alpha).\, x.\, \sin(\phi).\, x.d\phi.dx.\frac{\mu}{\mu_0} \tag{3.46}$$

3.6   Fit of the Observations to the Model

The light curves were recorded with time resolutions ranging between 0.15s to 0.3s for fast events and between 0.8 to 1.0s for slow events (section 2.2). To improve the signal to noise ratio the normalized intensity values at these time resolutions were binned such that the total light curve had approximately 100 data points. For the eclipse events the instantaneous separation R of the centre of eclipsed satellite to the shadow centre on the sky plane at the times T_{obs} corresponding to each of the data point was determined using Eq. (3.7). The light loss L_p in penumbra and L_u in the umbra

were calculated using Eqs. (3.27) and (3.30) respectively. For occultations the separation between the centres of the two satellites on the sky plane was calculated using Eq. (3.13) and the light loss using Eq. (3.33). The loss in light was then scaled in the range $0-1$ by normalizing with respect to the light from the uneclipsed or unocculted satellite using either Eq. (3.32) or Eq. (3.35), to obtain I_{th} corresponding to the time T_{obs}.

The observed (T_{obs}, I_{obs}) and theoretical (T_{obs}, I_{th}) light curves were fitted using Marquardt's technique. The free parameters in the fit were the impact parameter y and a shift δx along the track $S_2 S_2'$ (Fig. 3.6 for eclipse and Fig. 3.9 for occultation). This shift along the track is required to shift the theoretical geometric centre to the observed position of geometric centre $(O - C).X_g$ hence

$$(O - C).X_g^{ec} = \delta x^{ec} \quad \text{for eclipses}$$
$$(O - C).X_g^{oc} = \delta x^{oc} \quad \text{for occultatins} \tag{3.47}$$

3.7 Sky Plane Co-ordinates

The main aim of observing mutual events is to derive the astrometric positions of the satellite to refine the theory of motion of the satellites. The derived impact parameter 'y' yields the closest distance of the track of the occulted (eclipsed) satellite to the centre of the occulting satellite (shadow centre). At the time of light minimum T_l the light centre is closest. At the time T_g the geometric centre is closest.

3.7.1 Astrometric Positions During Occultations

The relative separation $(\Delta \alpha \cos \delta, \Delta \delta)$ at T_g between the centres of the two satellites during an occultation as seen by a terrestrial observer is

$$(\Delta \alpha \cos \delta)_g = y \sin P$$
$$(\Delta \delta)_g = y \cos P \tag{3.48}$$

where P is the position angle of the projection of the north pole N_J of Jupiter on the sky plane, measured from the celestial north.

61

These astrometric positions at time T_g of an occultation can be directly combined with photographic observations for updating the theory of motion of the satellites.

The published astrometric positions prior to 1986 refer to time of light minimum T_l (Fig. 3.12(a)). One can either correct the time by applying the correction given by Eq. 3.38, or alternatively the position of geometric centre at T_l can be obtained using the relations:

$$(\Delta \alpha \cos \delta)_g = (\Delta \alpha \cos \delta)_l - \delta x_\alpha \cos P$$
$$(\Delta \delta)_g = (\Delta \delta)_l + \delta x_\alpha \sin P \tag{3.49}$$

3.7.2 Astrometric Positions During Eclipses

The heliocentric separation $(\Delta \alpha \cos \delta, \Delta \delta)$ of the geometric centre of S2 from the shadow centre at T_g is

$$(\Delta \alpha \cos \delta)_g = y \sin P'$$
$$(\Delta \delta)_g = y \cos P' \tag{3.50}$$

where P' is the position angle of north point N'_j on S2 for heliocentric aspect.

The astrometric position of geometric centre can be obtained from position of light centre at T_l Fig. 3.12(b)

$$(\Delta \alpha \cos \delta)_g = (\Delta \alpha \cos \delta)_l - \delta x_\alpha \cos P'$$
$$(\Delta \delta)_g = (\Delta \delta)_l + \delta x_\alpha \sin P' \tag{3.51}$$

3.8 Summary

Theoretical eclipse and occultation light curves were generated using models described in the previous sections. the profile of the observed light curves were fitted with those obtained using the model. The fit yields correction to time in terms of the offset $(O - C)$ in distance along the track, and the impact parameter y. From the impact parameter the relative astrometric positions $(\Delta \alpha \cos \delta)_g$ and $(\Delta \delta)_g$ at time T_l were obtained. The results of the fit of the light curves observed during 1985 and 1991 from VBO are given in the next chapter.

4 Results of Observations of Mutual Events from VBO

4.1 Extraction of Astrometric Parameters

The light curves observed at VBO were corrected for sky background, atmospheric extinction and contribution of occulting or eclipsing satellite in the diaphragm and were normalized as explained in chapter 2. The normalized light curve at original time resolution was used for determining the time of light minimum. Since the entire light curve is utilized for fitting it was preferred to bin the data points obtained at high time resolutions to a set of about 100 points spanning the total duration of the main event. This improved the signal to noise ratio and also reduced computing time. The reconstructed light curve was fitted with the theoretical light curves generated using the model described in chapter 3. The source code for fitting the light curve uses fortran routines from Bevington's (1969) 'CURFIT' program which employs Marquardt's technique. For the good quality light curves the solutions converged within 3−4 iterations. The final solutions were found to be independent of the starting values.

The impact parameter y, the shift of the theoretical light curve δx were determined as free parameters when Lommel-Seeliger's and Lambert's scattering laws were used. For the mutual eclipses of 1985 series, comparison of solutions using these scattering laws and a uniform disc solution indicated best fit in terms of minimum χ^2 with model using Lommel-Seeliger's law (Vasundhara 1991). The fitted values y and δx for the 1985 series are given in Table 4.1. For the mutual events of series 1991, Minnaert's law was also used in the model, the Minnaert's parameter $k(\alpha)$ was derived during the fit. Most of the occultation light curves involving Io were fitted taking into account the albedo differences, between pole to equator and between the leading and trailing hemispheres. The brightness ratios given in Table 3.1(a) yielded best fit for the I and R bands of observations. The unusual shape of the light curve of the 203 event is due to the uncommon geometry shown

in Fig. 4.1(a). The positions of Ganymede and Europa are shown at the instant of close approach. The relative path of Ganymede between 15^h00^m to 22^h00^m is shown along the curved track. In addition to Lommel-Seeliger's law and Lambert's law this light curve was also fitted by modelling the polar caps, the regiones Nicholson west and east and the bright ray crater *Tros*. The albedo ratios and boundaries were adapted from Squyres and Veverka (1981) and Mallama (1991) for the phase angle of $-1°.1$ at the time of this event. The occultation and eclipse events on 91/01/29 which occurred close to the opposition ($\alpha = 0°.2$) followed in quick succession. Fig. 4.1(b) shows the geometry of this event. Fig. 4.2(d) shows the composite light curve. The blended light curve was fitted with theoretical composite light curves which were obtained by summing the light loss on Io, in the shadow (eclipse) and behind Europa (occultation). Regions which were both occulted and eclipsed shown dotted in Fig. 4.1(b) were considered to be only occulted. The phase correction according to the definitions by Eq. (3.40) for occultations and Eq. (3.44) for eclipses were calculated for all the events corresponding to the fitted values of the impact parameter using the different laws of scattering. The fitted value of δx corresponds to the distance between the predicted and actual positions of the geometric centres of the occulted or eclipsed satellite. The difference

$$
\begin{aligned}
\delta x_r^{oc} &= \delta x^{oc} - (T_l - T_p)V^o \\
&= \delta x_\alpha^{oc} \quad \text{[phase correction using Eq. (3.40)].}
\end{aligned}
\tag{4.1}
$$

similarly

$$
\begin{aligned}
\delta x_r^{ec} &= \delta x^{ec} - (T_l - T_p)V \\
&= \delta x_\alpha^{ec} \quad \text{[phase correction using Eq. (3.44)]}
\end{aligned}
\tag{4.2}
$$

T_l is an observed quantity, T_p is predicted from theory, δx's are derived from the fit and δx_α's are obtained using Eqs. (3.40) or (3.44). Therefore comparison of δx_r's and δ_α's provide additional check on the validity of Eqs (3.40) and (3.44). The calculated values of δx_α's and δx_r's given in Table (4.2) for most of the events appear to be in good agreement within the observational error. The fitted light curves are plotted in Figs. 4.2(a–p).

64

Table 4.1 Eclipse events during 1985 from VBO.
Fitted parameters using Lommel-Seeliger's law

Date	Event	δx_α	Impact Parameters		χ^2
			Fitted	Predicted	$\times 10^4$
		(km)	(km)	(km)	
(1)	(2)	(3)	(4)	(5)	(6)
85/09/24	1E2	-78	328	448	1.667
85/10/24	3E1	-86	1683	1738	0.505
85/10/12	1E2	-105	691	603	7.055
85/11/15	3E1	-118	336	369	8.688
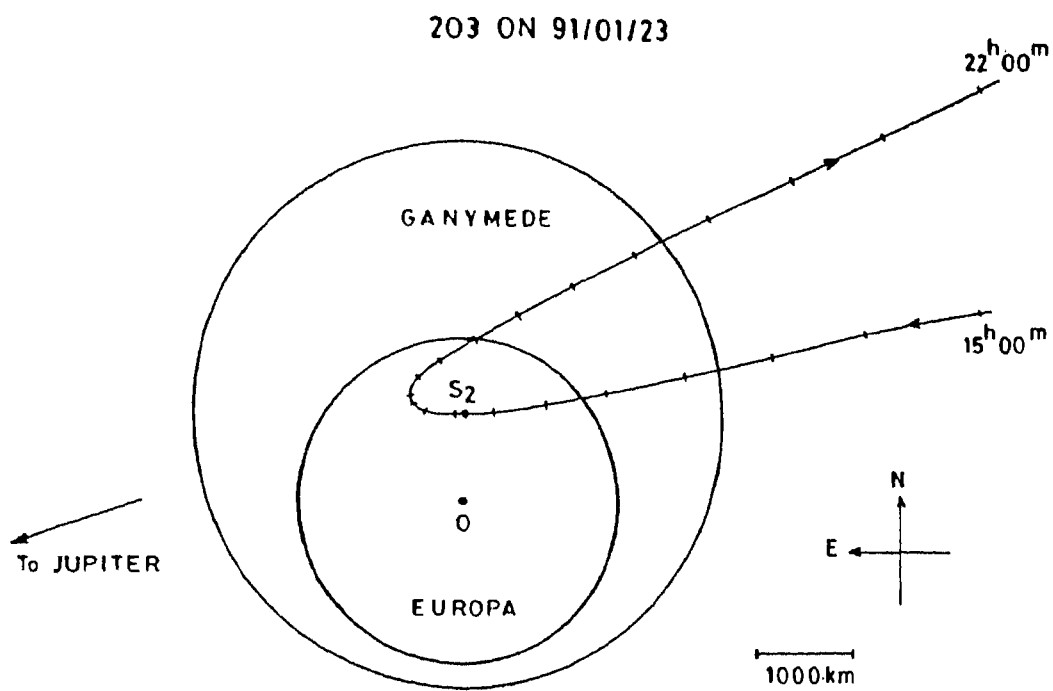
203 ON 91/01/23

Fig. 4.1(a). Geometry during the occultation of Ganymede centred at S2 by Europa centred at O at the instant of close approach on 91/01/23. The path of Ganymede between 15^h00^m UTC and 22^h00^m UTC is along the curved track. The tick marks indicate position of Ganymede at intervals of 15^m.
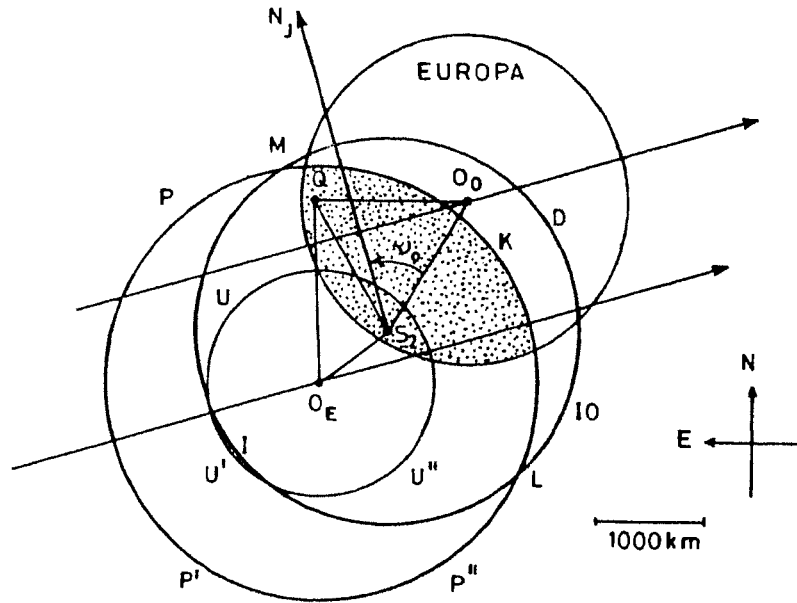
Fig. 4.1(b). Geometry during the composite occultation and eclipse events of Io by Europa on 91/01/29. The dotted area on Io (centred at S2) is occulted by Europa (Centred at O_O) and at the same time eclipsed by the umbra $(U''U'UU'')$ and the penumbra $(P''P'PP'')$ centered at O_E. The arrows indicate direction of motion of Europa and the shadow center relative to Io.

Table 4.2(a). Results of 2E1 event on 91/01/22, fitted parameters :

Scattering law	δx_r	δx_a	Impact parameter[1]	$k(\alpha)$	χ^2
	(km)	(km)	y(km)		$\times 10^4$
(1)	(2)	(3)	(4)	(5)	(6)
Lommel-Seeliger's law	8	15	+178		0.651
Lambert's law	11	21	+560		5.466
Minnaert's law	8	14	−6	0.461	0.595

1. Predicted impact parameter using E-3 : +220 km
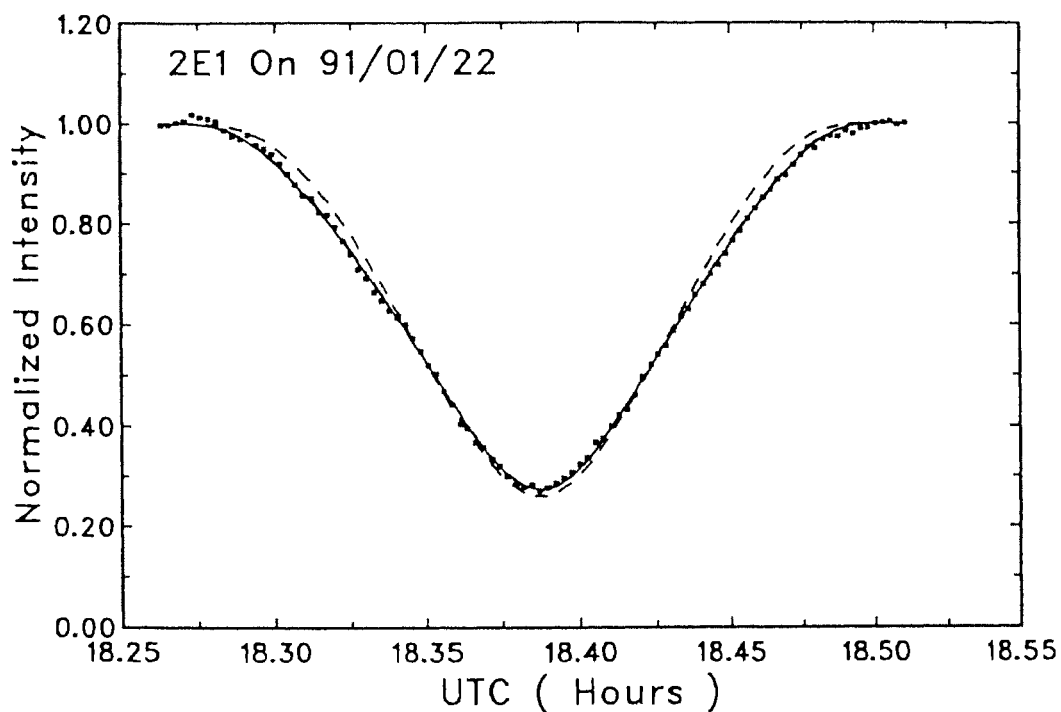
Fig. 4.2(a) Observed and fitted light curves. The dotted dashed line, short dashed line, continuous line correspond to models using Lommel-Seeliger's law, Lambert's law, Minnaert's law.

Table 4.2(b). Results of 2O1 event on 91/01/22, fitted parameters :

Scattering law	δx_r	δx_a	Impact Parameter	$k(\alpha)$	χ^2
	(km)	(km)	y(km)[1]		$\times 10^4$
(1)	(2)	(3)	(4)	(5)	(6)
Lommel-Seeliger's law	−17	−14	−1411		1.491
Lambert's law	−23	−18	−1430		5.955
Minnaert's law	−15	−13	−1405	.399	1.313
Minnaert's law with albedo variations[2]	−17	−14	−1400	.443	1.331

1. Predicted impact parameter using E-3 : −1349 km
2. Table 3.1(a)
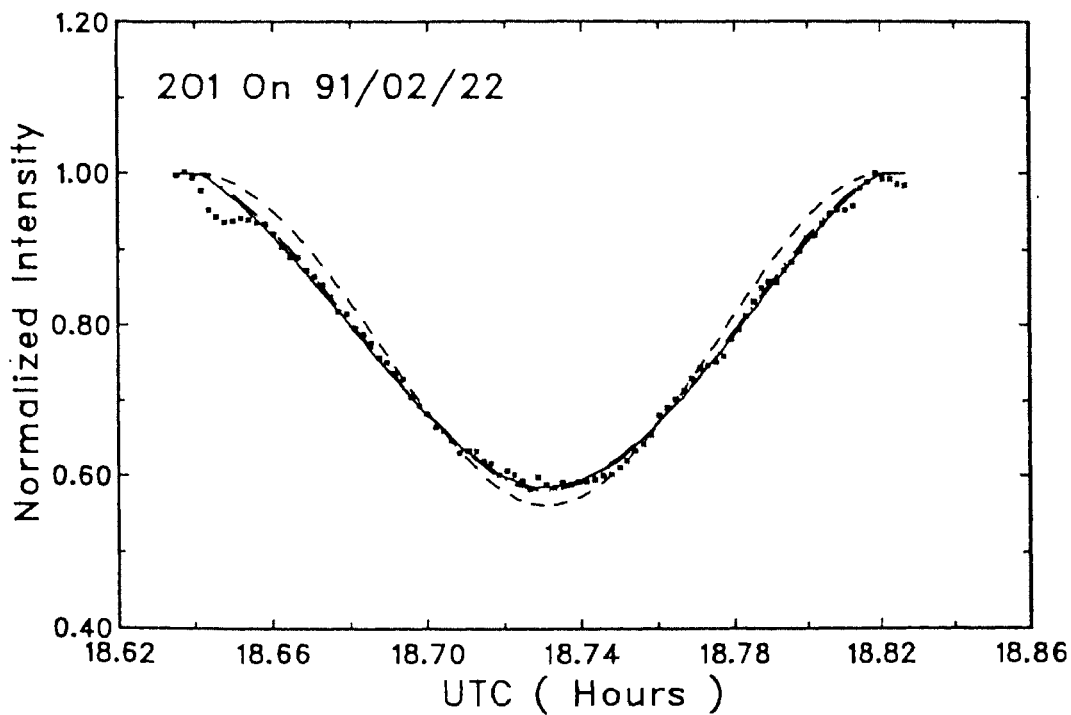
Fig. 4.2(b) Observed and fitted light curves. The dotted dashed line, short dashed line, continuous line and long dashed line correspond to models using Lommel-Seeliger's law, Lambert's law, Minnaert's law and model given in Table 3.1(a).

Table 4.2(c). Results of 203 event on 91/01/23, fitted parameters :

Scattering law	δx_r (km)	Impact Parameter $y(km)$[1]	χ^2
(1)	(2)	(3)	(4)
Lommel-Seeliger's law	336	+1111	4.344
Lambert's law	425	+1262	8.659
Lommel-Seeliger's law with albedo variations[2]	339	+1047	4.278

1. Predicted impact parameter using E-3 : +836 km
2. Table 3.1(b)
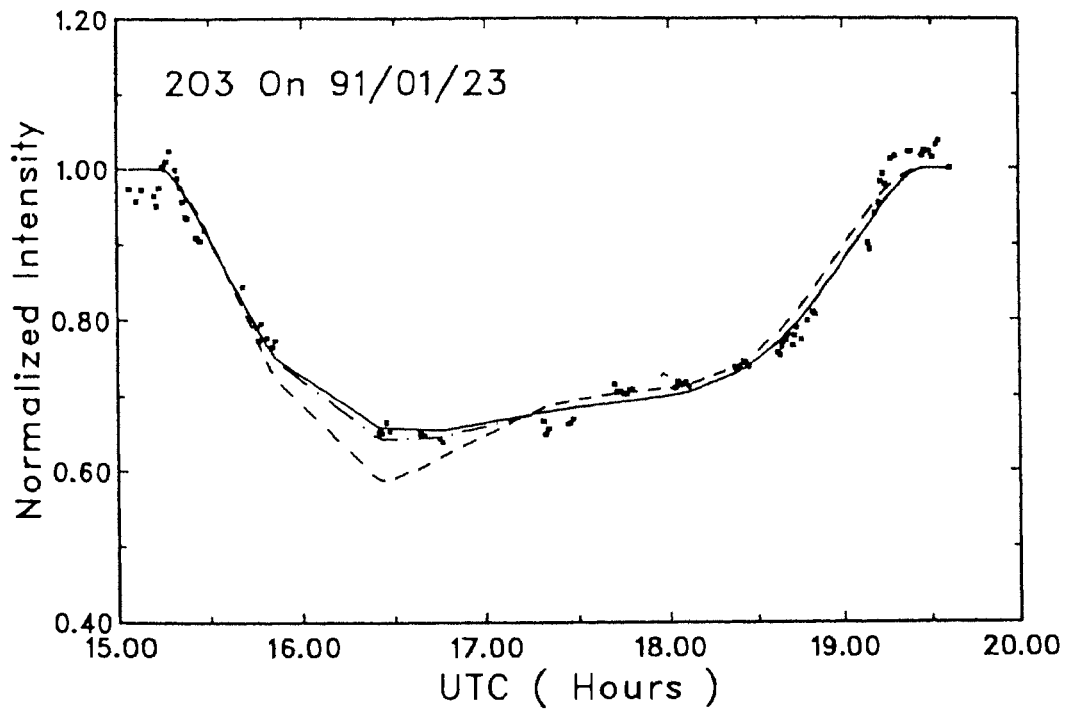
Fig. 4.2(c) Observed and fitted light curves. The dotted dashed line, short dashed line and continuous line correspond to models using Lommel-Seeliger's law, Lambert's law, and model given in Fig. 3.1(b).

Table 4.2(d) Results of 2O1 and 2E1 blended events on 91/01/29, fitted parameters

Scattering law	Impact Parameter[1] y(km)		$k(\alpha)$	$\chi^2 \times 10^4$
	2O1	2E1		
Lommel-Seeliger's law	-662	$+144$		2.979
Lambert's law	-994	$+540$		4.508
Minnaert's law	-656	$+121$	0.597	3.361
Minnaert's law with albedo variations[2]	-661	149	0.513	3.041

1. Predicted impact parameter using E-3 : Occulttion:-974 km
Eclipse:$+290$ km

201 and 2E1 On 91/01/29
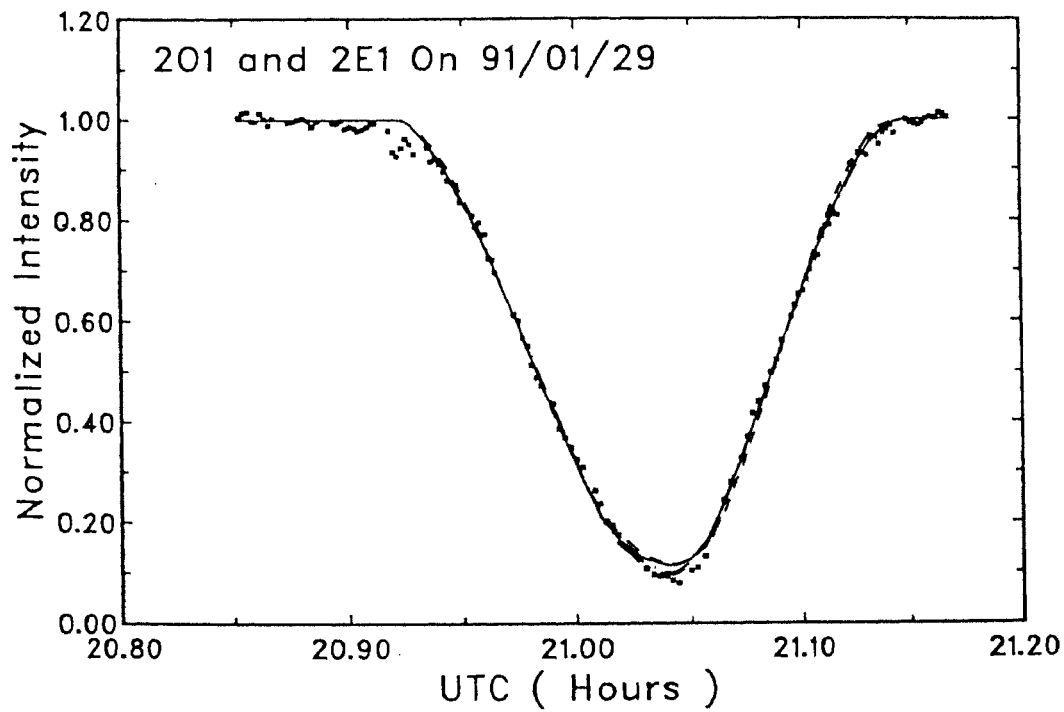
Table 4.2(e). Results of 2O1 event on 91/02/05, fitted parameters :

Scattering law	δx_r^2 (km)	δx_a (km)	Impact parameter[1] y(km)	$k(\alpha)$	χ^2 $\times 10^4$
(1)	(2)	(3)	(4)	(5)	(6)
Lommel-Seeliger's law		16	−262		74.1
Lambert's law		27	−567		83.1
Minnaert's law		11	+68	.357	72.7

1. Predicted impact parameter using E-3 : −558 km.
2. Unreliable due to noisy data.
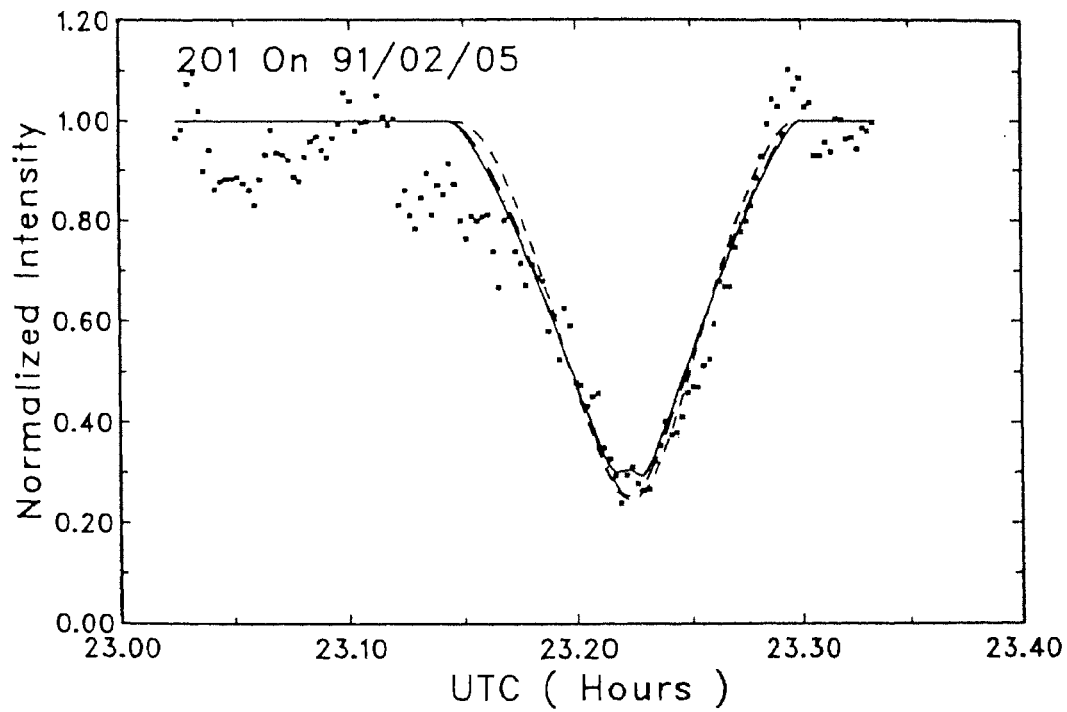
Table 4.2(f). Results of 2O1 event on 91/02/16, fitted parameters :

Scattering law	δx_r	δx_α	Impact Parameter[1]		χ^2
	(km)	(km)	y(km)	$k(\alpha)$	$\times 10^4$
(1)	(2)	(3)	(4)	(5)	(6)
Lommel-Seeliger's law	43	34	−4		2.381
Lambert's law	35	63	+433		5.201
Minnaert's law	33	39	−13	0.5821	1.454
Minnaert's law with albedo variations[2]	32	35	+105	0.5064	0.8530

1. Predicted impact parameter using E-3 : +118 km
2. Table 3.1(a)
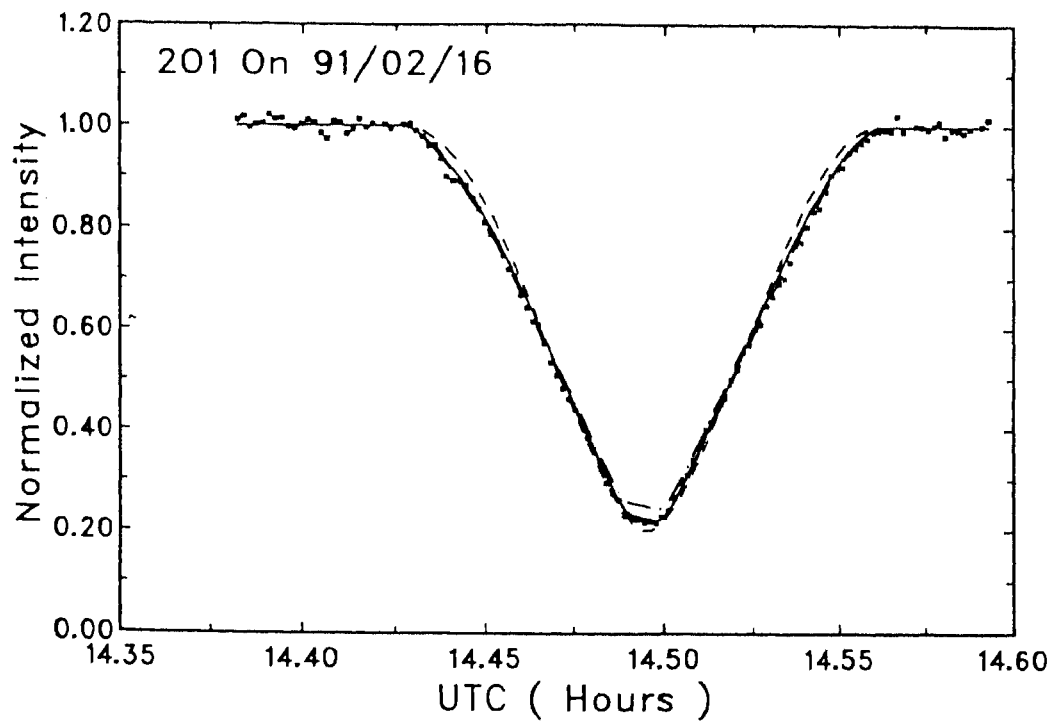
Table 4.2(g). Results of 2E1 event on 91/02/16, fitted parameters :

Scattering law	δx_r	δx_a	Impact parameter	$k(\alpha)$	χ^2
	(km)	(km)	y(km)[1]		$\times 10^4$
(1)	(2)	(3)	(4)	(5)	(6)
Lommel-Seeliger's law	−80	− 47	∼0		0.796
Lambert's law	−85	−63	488		3.934
Minnaert's law	−83	−49	∼0	.554	0.482

1. Predicted impact parameter using E-3 : +209 km.

2E1 On 91/02/16

Table 4.2(h). Results of 2Ol event on 91/02/23, fitted parameters :

Scattering law (1)	δx_r (km) (2)	δx_α (km) (3)	Impact Parameter y(km)[1] (4)	$k(\alpha)$ (5)	χ^2 $\times 10^4$ (6)
Lommel-Seeliger's law	61	59	+505		0.586
Lambert's law	66	81	+722		3.632
Minnaert's law	62	59	+515	0.516	0.584
Minnaert's law with albedo variations[2]	64	63	+587	0.564	0.700

1. Predicted impact parameter using E-3 : +590 km
2. Table 3.1(a)
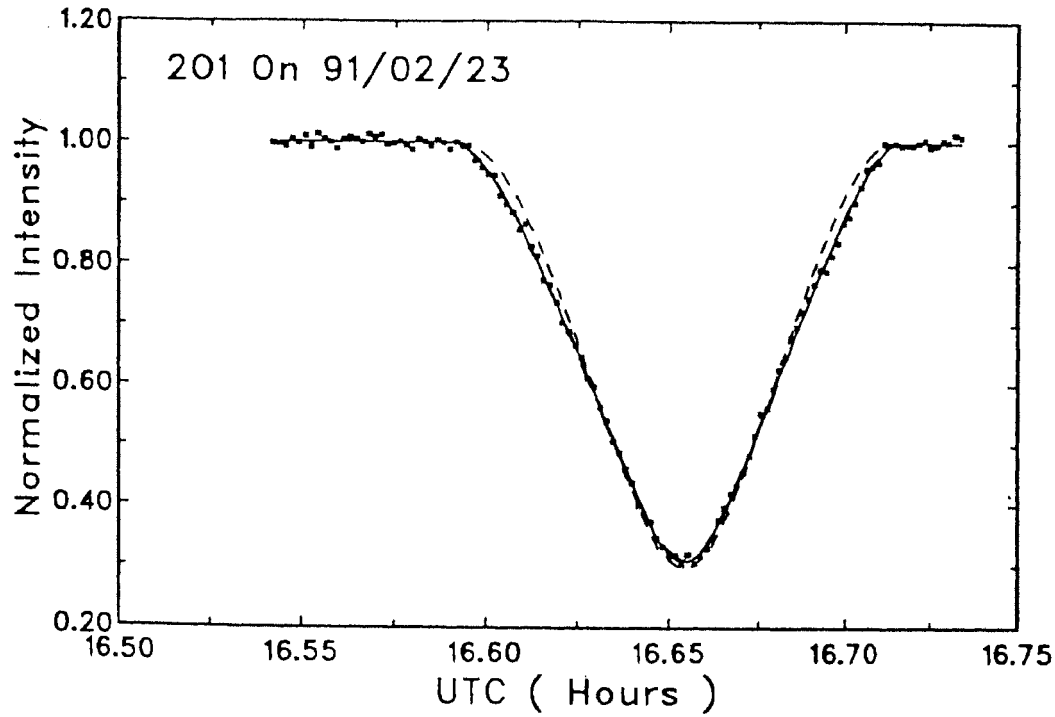
Fig. 4.2(h) Observed and fitted light curves. The dotted dashed line, short dashed line, continuous line and long dashed line correspond to models using

75

Table 4.2(i). Results of 2E1 event on 91/02/23, fitted parameters :

Scattering law (1)	δx_r (km) (2)	δx_a (km) (3)	Impact parameter y(km)[1] (4)	$k(\alpha)$ (5)	χ^2 ×10^{4} (6)
Lommel-Seeliger's law	−65	−63	∼0		1.839
Lambert's law	−69	−84	+434		3.698
Minnaert's law	−62	−69	∼0	0.589	0.742

1. Predicted impact parameter using E-3 : +590 km

76
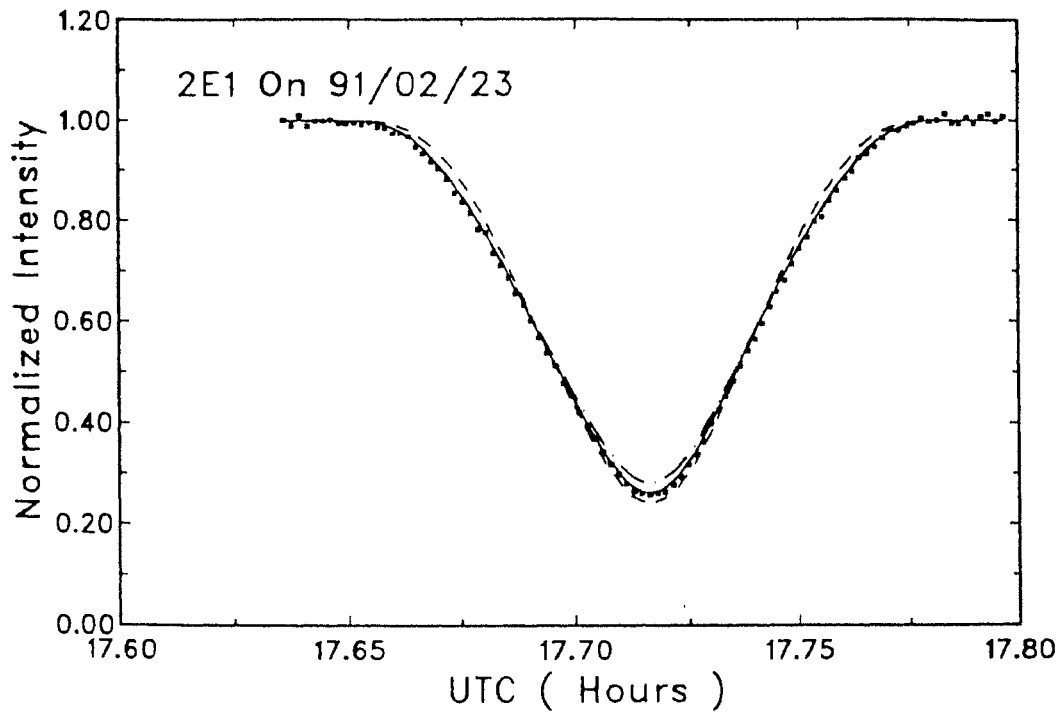
Table 4.2(j). Results of 201 event on 91/03/09, fitted parameters :

Scattering law (1)	δx_r (km) (2)	δx_a (km) (3)	Impact parameter y(km)[1] (4)	$k(\alpha)$ (5)	χ^2 ×10⁴ (6)
Lommel-Seeliger's law	99	81	1542		3.583
Lambert's law	109	101	1533		4.929
Minnaert's law	100	83	1540	.565	3.546
Minnaert's law with albedo variations[2]	105	85	1525	.617	3.547

1. Predicted impact parameter using E-3 : 1525 km
2. Table 3.1(a)
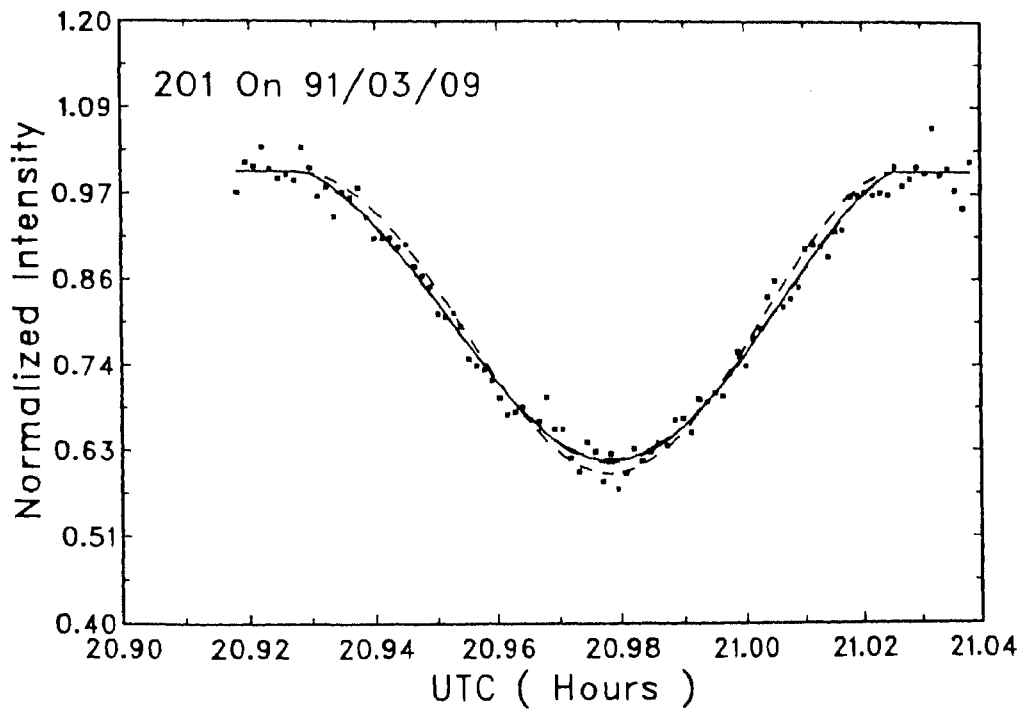
Fig. 4.2(j) Observed and fitted light curves. The dotted dashed line, short dashed line, continuous line and long dashed line correspond to models using Lommel-Seeliger's law, Lambert's law, Minnaert's law and model given in Table 3.1(a).

Table 4.2(k). Results of 4E2 event on 91/03/18, fitted parameters :

Scattering law (1)	δr_r (km) (2)	δr_o (km) (3)	Impact parameter $y(km)$[1] (4)	$k(n)$ (5)	χ^2 $\times 10^4$ (6)
Lommel-Seeliger's law	−149	−125	3027		1.116
Lambert's law	−161	−153	3006		1.003
Minnaert's law	−166	−157	3003	1.105	1.010

1. Predicted impact parameter using E-3 : 3094 km
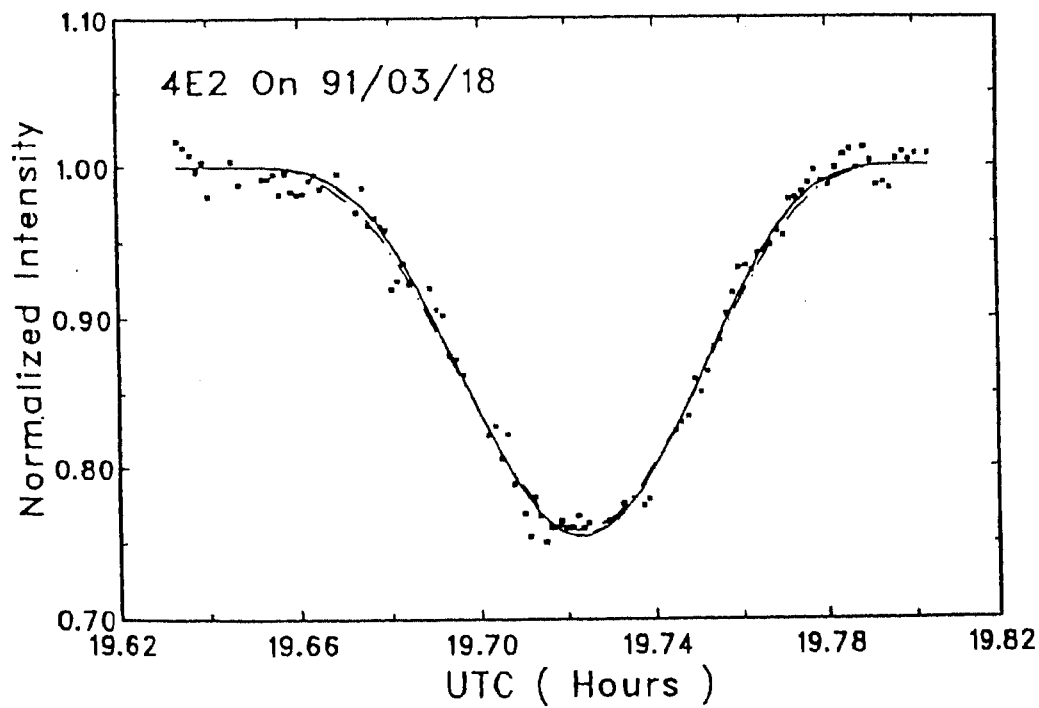
Fig. 4.2(k) Observed and fitted light curves. The dotted dashed line, short dashed line, continuous line correspond to models using Lommel-Seeliger's law, Lambert's law, Minnaert's law.

Table 4.2(1). Results of 2E1 event on 91/03/20, fitted parameters :

Scattering law (1)	δx_r (km) (2)	δx_o (km) (3)	Impact parameter $y(km)^1$ (4)	$k(\alpha)$ (5)	χ^2 $\times 10^4$ (6)
Lommel-Seeliger's law	−121	−112	−544		1.113
Lambert's law	−178	−142	−766		3.778
Minnaert's law	−85	−96	−331	0.310	0.627

1. Predicted impact parameter using E-3 = −681 km.
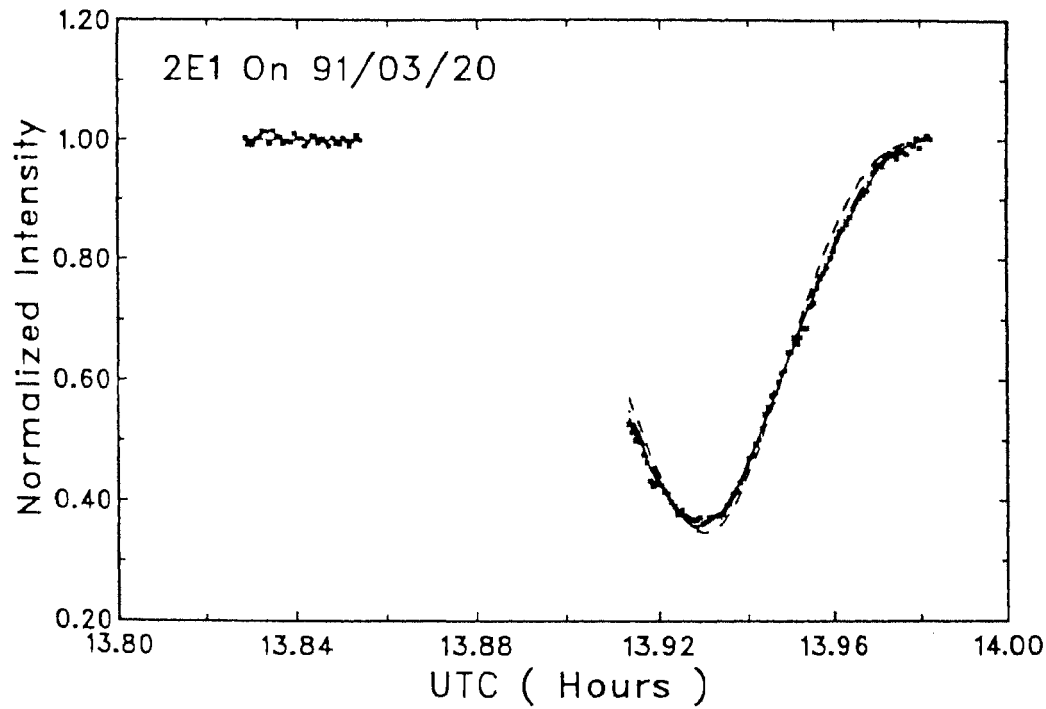
Fig. 4.2(1) Observed and fitted light curves. The dotted dashed line, short dashed line, continuous line correspond to models using Lommel-Seeliger's law, Lambert's law, Minnaert's law.

79

Table 4.2(m). Results of 201 event on 91/03/27, fitted parameters :

Scattering law	δx_r	δx_a	Impact parameter	$k(\alpha)$	χ^2
	(km)	(km)	$y(km)^1$		$\times 10^4$
(1)	(2)	(3)	(4)	(5)	(6)
Lommel-Seeliger's law	+39	+71	+2609		0.961
Lambert's law	+65	+94	+2476		1.053
Minnaert's law	+35	+71	+2670	0.327	0.963

1. Predicted impact parameter using E-3 = +2523 km.
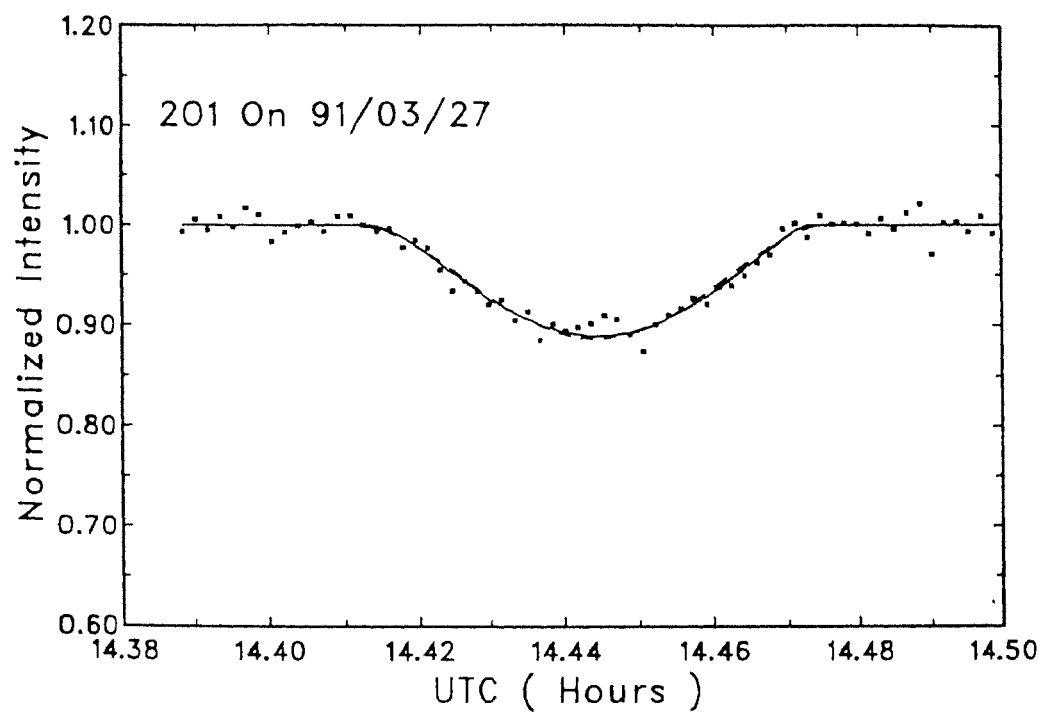
Fig. 4.2(m) Observed and fitted light curves. The dotted dashed line, short dashed line, continuous line correspond to models using Lommel-Seeliger's law, Lambert's law, Minnaert's law.

Table 4.2(n). Results of 2E1 event on 91/03/27, fitted parameters :

Scattering law	δx_r	δx_o	Impact parameter	$k(\alpha)$	χ^2
	(km)	(km)	y(km)[1]		$\times 10^4$
(1)	(2)	(3)	(4)	(5)	(6)
Lommel-Seeliger's law	-134	120	-924		0.571
Lambert's law	-139	149	-1027		2.192
Minnaert's law	-135	122	-934	0.544	0.564

1. Predicted impact parameter using E-3 = -986 km.
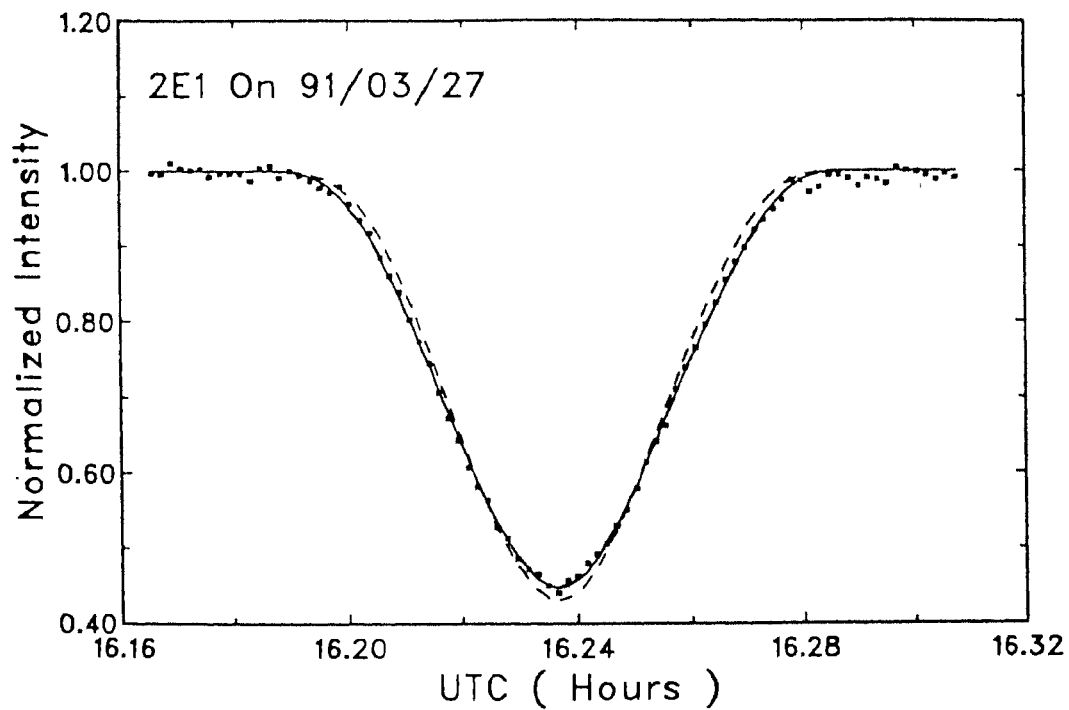
Fig. 4.2(n) Observed and fitted light curves. The dotted dashed line, short dashed line, continuous line correspond to models using Lommel-Seeliger's law, Lambert's law, Minnaert's law.

Table 4.2(o). Results of 2E1 event on 91/04/03, fitted parameters :

Scattering law	δr_r	δr_o	Impact parameter y(km)[1]	$k(\alpha)$	χ^2
	(km)	(km)			$\times 10^4$
(1)	(2)	(3)	(4)	(5)	(6)
Lommel-Seeliger's law	−151	−119	−1428		6.750
Lambert's law	−167	−150	−1440		9.304
Minnaert's law	−141	−108	−1425	0.325	6.488

1. Predicted impact parameter using E-3 = −1324 km.
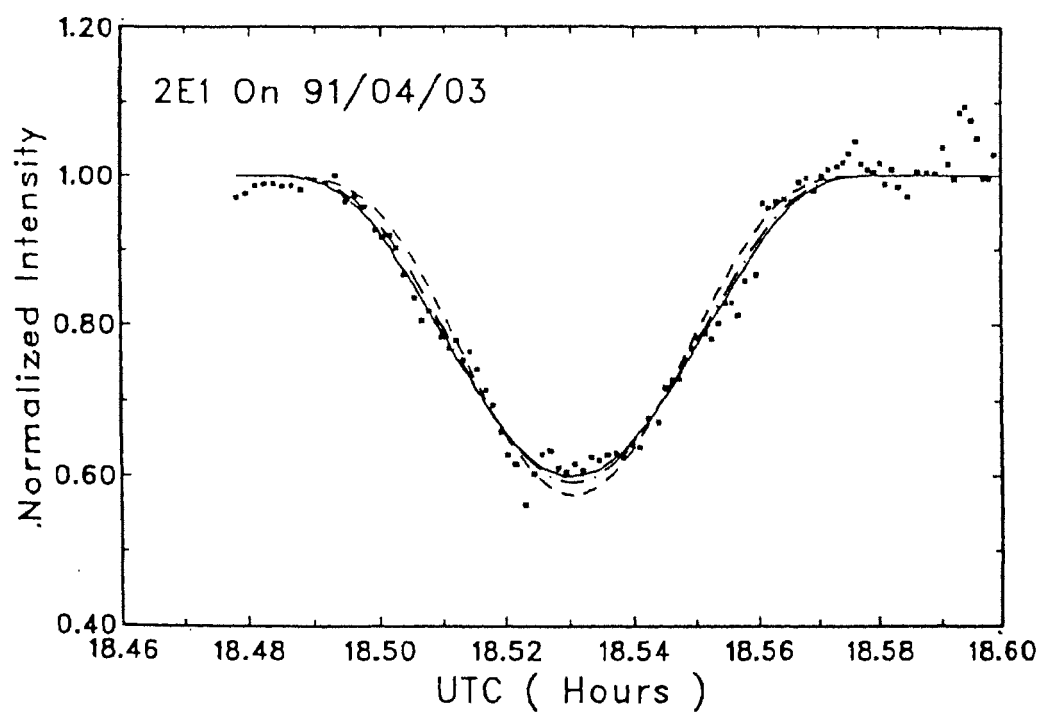
Fig. 4.2(o) Observed and fitted light curves. The dotted dashed line, short dashed line, continuous line correspond to models using Lommel-Seeliger's law, Lambert's law, Minnaert's law.

Table 4.2(p). Results of 1E2 event on 91/05/17, fitted parameters :

| Scattering law | δx_r | δx_o | Impact parameter | $k(\alpha)$ | χ^2 |
| | (km) | (km) | y(km)[1] | | $\times 10^4$ |
(1)	(2)	(3)	(4)	(5)	(6)
Lommel-Seeliger's law	−169	−157	−795		0.557
Lambert's law	−162	−181	−905		1.675
Minnaert's law	−167	−164	−826	0.620	0.463

1. Predicted impact parameter using E-3 = −811 km.
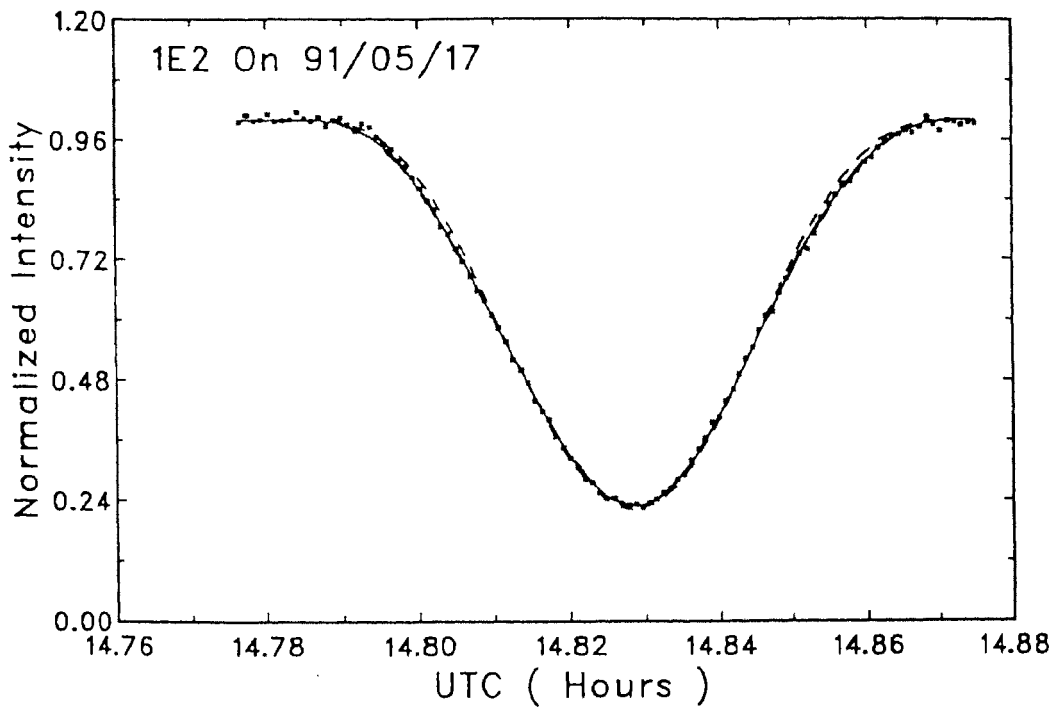
Fig. 4.2(p) Observed and fitted light curves. The dotted dashed line, short dashed line, continuous line correspond to models using Lommel-Seeliger's law, Lambert's law, Minnaert's law.

Table 4.3(a) Observed and predicted mid times for the 1985 series

Ut Date	Observed times		Predicted Mid Times		
Event	T_l	T_g		T_p	
			G-5	A-E	E-3
Air mass	hh:mm:ss	hh:mm:ss	hh:mm:ss	hh:mm:ss	hh:mm:ss
85/09/24	19:20:37.6	19:20:44.2	19:20:39	19:20:00	19:20:32
1E2	±2.0s	±2.0s			
85/10/12	13:33:20.2	13:33:25.7	13:33:17	13:32:42	13:33:11
1E2	±5.0s	±5.0s			
85/10/17	13:23:25.1	13:23:29.7	13:23:38	13:23:21	13:23:36
3E1	±2.0s	±2.0s			
85/10/24	16:17:14.0	16:17:18.9	16:17:26	16:17:21	16:17:30
3E1	±2.0s	±2.0s			
85/11/15	14:32:48.2	14:30:55.5	14:34:01	14:32:33	14:33:21
3E1	±25.0s	±25.0s			

84

Table 4.3(b) Observed and predicted mid times for the 1991 series

Ut Date	Observed times		Predicted Mid Times		
			T_p		
	T_l	T_g	G-5	A-F	E-3
Event	hh:mm:ss.s	hh:mm:ss.s	hh:mm:ss	hh:mm:ss	hh:mm:ss
91/01/22 2E1	18:23:12.7 ±0.5s	18:23:14.3	18:22:39	18:22:03	18:22:35.8
91/01/22 2O1	18:43:52.5 ±0.5s	18:43:53.9	18:43:20	18:42:42	18:43:16.2
91/01/23 2O3		16:42:19.1[1]	16:39:29	16:47:24	18:42:14.6
91/01/29 2O1		21:00:32.0[1]	21:00:03	20:59:30	20:59:59.4
91/01/29 2E1	±1.0s	21:03:23.6[1]	21:02:52	21:02:21	21:02:48.5
91/02/05 2O1	23:13:35.0 ±10.0s	23:13:34.1	23:13:06	23:12:36	23:13:01.6
91/02/16 2O1	14:29:41.9 ±0.5s	14:29:39.2	14:29:18	14:28:45	14:29:14.8
91/02/16 2E1	15:18:31.7 ±0.5s	15:18:35.0	15:18:05	15:17:45	15:18:12.3
91/02/23 2O1	16:39:16.1 ±0.5s	16:39:11.3	16:38:53	16:38:21	16:38:49.0
91/02/23 2E1	17:42:58.5 ±0.5s	17:43:02.7	17:42:45	17:42:12	17:42:41.5
91/03/09 2E1	20:58:40.5 ±1.5s	20:58:33.9	20:58:18	20:30:45	20:58:13.8
91/03/18 4E2	19:43:25.1 ±2.0s	19:43:33.3	19:43:28	19:42:33	19:43:19.6
91/03/20 2E1	13:55:45.3 ±0.5s	13:55:51.3	13:55:39	13:55:12	13:55:35.2
91/03/27 2O1	14:26:37.3 ±0.5s	14:26:33.7	14:26:20	14:25:51	14:26:16.8
91/03/27 2E1	16:14:11.7 ±0.5s	16:14:17.5	16:14:06	16:13:42	16:14:02.8
91/04/03 2E1	18:31:49.0 ±2.0s	18:31:53.7	18:31:49	18:31:18	18:31:45.4
91/05/17 1E2	14:49:41.7 ±1.5s	14:49:48.4	14:49:55	14:49:33	14:49:53.1

1. These mid times were derived directly from fit.

Table 4.4 Phase corrections and $(O-C)^1$ along the track

Date event	Phase α (deg)	Phase correction δx_o (km)	δT_o (sec)	(O-C)G-5 Time (sec)	distance (km)	(O-C)E-3 Time (sec)	distance (km)	Orbital longitudes θ_1	θ_2
(1)	(2)	(3)	(4)	(5)	(6)	(7)	(8)	(9)	(10)
91/01/22		14.8	−1.7	32.1	−288	34.9	−313		
2E1	−1.3	20.8	−2.3	36.4	−326	39.2	−351	218	265
		14.1	−1.6	35.7	−320	38.5	−345		
91/01/22		−14.1	1.5	34.4	−324	37.8	−356		
2O1	−1.3	−18.0	1.9	34.8	−328	38.2	−360	219	266
		−12.8	1.4	34.3	−323	37.7	−355		
		−14.0	1.5	34.4	−324	37.8	−356		
91/01/29 2O1	+0.2	≃ 0.0	≃0.00	31.6	−342	35.1	−380	219	271
91/01/29 2E1	+0.2	≃ 0.0	≃0.00	29.0	−316	32.6	−355	219	271
91/02/05		16.2	−1.3	28.1	−340	32.1	−388		
	+1.7	27.1	−2.2	27.2	−329	31.7	−377	219	275
2O1		11.1	−0.9	28.5	−345	32.5	−393		
91/02/16	+3.9	34.4	−2.5	21.5	−298	24.6	−341		
2O1		62.5	−4.5	19.5	−270	22.7	−314	218	281
		39.2	−2.8	21.5	−294	24.4	−338		
		35.3	−2.5	21.3	−296	24.5	−340		
91/02/16		−47.1	3.2	30.3	−449	22.6	−335		
2E1	+3.9	−63.0	4.3	31.4	−465	23.7	−351	218	284
		−49.2	3.3	30.4	−450	22.7	−336		
91/02/23		59.0	−3.9	18.8	−281	22.4	−335		
	+5.2	81.7	−5.5	17.2	−257	20.8	−310	217	284
2O1		59.8	−4.0	18.7	−279	22.3	−333		
		63.12	−4.2	18.5	−276	22.7	−339		
91/02/23		−62.5	3.9	17.8	−288	20.9	−338		
	+5.2	−84.5	5.2	19.1	−309	22.2	−359	217	288
2E1		−68.6	4.2	18.1	−292	21.2	−342		
91/03/09		82.0	−4.8	16.5	−281	20.2	−344		
	+7.5	101.3	−6.0	15.3	−261	19.0	−323	216	290
2O1		83.0	−4.9	16.4	−279	20.1	−342		
		85.2	−5.0	16.3	−277	20.0	−341		
91/03/18		−125.0	6.5	4.0	−77	12.0	−231		
4E2	+8.7	−152.6	8.0	5.1	−106	13.5	−260	168	37
		−156.6	8.2	5.3	−110	13.7	−264		

Table 4.4 continued

Date event	Phase α	Phase correction		(O-C)G-5		(O-C)E-3		Orbital longitudes	
		δx_α	δT_α	Time	distance	Time	distance	θ_1	θ_2
	(deg)	(km)	(sec)	sec)	(km)	(sec)	(km)		
(1)	(2)	(3)	(4)	(5)	(6)	(7)	(8)	(9)	(10)
91/03/20		-112.16	6.0	12.7	-256	16.1	-325		
2E1	+8.9	-141.96	8.8	15.5	-313	18.9	-382	213	300
		-95.7	4.2	10.9	-220	14.3	-289		
91/03/27		71.4	-3.7	14.0	-273	16.8	-327		
2O1	+9.6	93.9	-4.8	12.9	-251	15.7	-306	214	298
		70.8	-3.6	14.1	-275	16.9	-329		
91/03/27		-119.56	5.6	11.7	-248	14.5	-306		
2E1	+9.6	-149.2	7.0	13.1	-278	15.9	-336	212	304
		-122.1	5.8	11.7	-252	14.7	-311		
91/04/03		-119.3	5.4	5.2	-115	8.8	-195		
2E1	+10.2	-150.0	6.8	6.6	-146	10.2	-226	210	307
		-108.4	4.9	4.7	-104	8.3	-184		
91/05/17		-156.7	6.4	-6.5	$+159$	-5	$+123$		
1E2	+10.3	-181.4	7.4	-5.5	$+135$	-4	$+98$	225	335
		-163.5	6.7	-6.2	$+152$	-4.7	$+115$		

4.2 Discussions

A comparison of the fitted light curves in Fig. 4.2(a-p) indicates that Lambert's law solution (short dotted line) fails to give good fit at the centre and at the wings. Fits using Minnaert's law (solid line) and Lommel-Seeliger's law (dotted dashed line) are comparable. The long dashed line in Figs. 4.3 (b, f, h, and j) corresponds to the model including the albedo variations given in Table 3.1(a). This curve is not clearly discernible from the solid curve of Minnaert's law solution. The mean value of the Minnaert's parameter derived from the good quality light curve in the I band is $0.559 \pm .011$. Due to limited data its dependence on phase could not be evaluated.

The phase corrections δx_α for all the events using Eq. (3.40) or Eq. (3.44) in distance and in time are given in Table 4.4. The $(O - C)$ compared with predictions using G-5 and E-3 in time and distance, along the track are also given in this table. The first, second and third rows correspond to phase corrections derived using Lommel-Seeliger's law, Lambert's law and Minnaert's law. The fourth row if exists corresponds to the model using albedo variation given in Table 3.1(a). For the 2O3 event on 91/01/23, due to complex geometry δx_α was not derived. For the 2O1 and 2E1 events on 91/01/29 the phase corrections are very nearly zero ($\alpha = 0^\circ.2$), the reported $(O - C)$ values, correspond to the Minnaert's law solution. The last two columns give the orbital longitude of the satellites S1 and S2. All the events involving Io and Europa have an average residual of -341 km, -345 km and -338 km corresponding to fits using Lommel-Seeliger's law, Lambert's law and Minnaert's law. The differences in the longitude residual using different scattering laws is less than the observational scatter of $\sim \pm 25$ km. The fitted impact parameters are however affected to a larger extent on the nature of light distribution. The values of δ_r's calculated using Eq. (4.1) for occultations and Eq. (4.2) for eclipses are close to the corresponding values of δ_α's calculated using (3.40) or (3.44).

5 Fit to the Theory

5.1 Introduction

Sampson's theory (Sampson, 1921) of the motion of the Galilean satellites is the basis for computing their positions even today. Lieske (1974, 1977) revitalized Sampson's theory to enable one to use present day computers to perform the millions of algebraic computations. The salient features of Sampson's theory and the improvements by Lieske have been described in chapter I. Lieske's technique affords future revisions of the constants of the motion without having to recompute the entire process, when more observations are available. This has been possible by use of the partial derivatives of the observable quantities with respect to the constants. The partial derivatives help to determine the corrections to the constants which when added to the constants would best fit the observations.

5.2 The Present day Ephemerides

The excellent and extensive series of observations of the eclipses by Jupiter were made by E.C.Pickering, A.Searle and O.C.Wandell during the years 1878-1903 at Harvard. This data was the basis on which Sampson (1921) constructed his theory. Lieske reconstructed the Harvard data from the residuals published by Pickering (1907) relative to the American Ephemeris. The E-1 ephemeris was developed by Lieske (1978) using this data and additional photometric eclipse observations of half brightness made since then. Lieske further refined the theory by adding 1059 visual eclipses from 1903 to 1972, 74 mutual occultations and 96 mutual eclipses from 1973, and 2964 photographic observations from 1967 to 1978. The resulting E2 ephemerides (Lieske, 1980) were employed for the Voyager encounter, and were in error by less than 200 km at the time of close approach. The ephemeris E2x3 (Lieske, 1987) is based on the same 2964 photographic ex-

posures as in E-2, plus 112 mutual event pairs from 1973 and 1979, 183 pairs of data from Voyager optical navigation images and 15711 classical eclipses of the satellites by Jupiter from 1652 to 1983.

) used photographic observations made from 1891 to 1978 observations) to obtain the set of constants labled (G-5).

Table 5.1   Details of photographic data

Observer	Observatory	Year	No. of positions				Residual (arcsec)	
			J1	J2	J3	J4	G-5	I-32
Renz	Helsingfors	1891						
Renz	Helsingfors	1892-1897	171	175	184	174	0.126	0.111
Renz	Pulkovo	1895-1898						
Balanovsky	Pulkovo	1904-1910						
Chevalier	Zo-Sé	1917/1918	132	132	133	121	0.143	0.151
De Sitter	Greenwich	1918/1919						
De Sitter	The Cape	1924						
Petrescu	Bucarest	1934	85	104	106	118	0.221	0.223
Petrescu	Paris	1936						
Van Biesbroek	Yerkes	1961-1963						
Gorel	Nicolaiev	1962-1966						
Soulié	Bordeaux	1966-1974						
Gorel	Nicolaiev	1973-1974	284	282	318	307	0.395	0.390
Debehogne	Rio de Janeiro	1977/1978						
"	Uccle	1977/1978						
"	La Silla	1977/1978						
Ianna et al	Mc Cormick	1977/1978						
Pascu	Mc Cormick	1967/1968	836	875	883	940	0.081	0.086
"	USNO(Wash.)	1973-1978						
Pascu*		1986-1990						

* Private communication

90

5.3 The Observational Material for the Present Study

5.3.1 The Photographic Data

Most of the photographic data that were used by Arlot (1982) have been utilised in this study. Additional unpublished excellent photographic material covering the period 1986 to 1990 made by D.Pascu (private communication) were used in the study. This work was carried out at the Bureau des Longitudes, Paris. Table 5.1 gives the details of the photographic observations.

5.3.2 The Mutual Occultation Data

Two sets of mutual occultation data were used. Several events are common to the two sets. The data set (1) contains astrometric positions derived by Descamps et al. (1992), Descamps (1992a) using Hapke's law in his model. The statistics of the events for the four mutual event seasons 1973, 1979, 1985 and 1991 are given in Table 5.2(a).

Table 5.2(a)   Details of mutual occultation data set (1).

Year	Total events	No. of positions				Residuals (arcsec)	
		J1	J2	J3	J4	G5	I32
1973	21	20	21	1	0	0.022	0.019
1979	3	1	3	2	0	0.006	0.008
1985	23	11	14	15	6	0.019	0.020
1990-91	34	29	34	5	0	0.037	0.029

1. Source : Descamps (1992a)

The data set (2) contains astrometric positions derived by fitting light curves of 1985 (Arlot et al., 1992) and 1991 (data from VBO and from Arlot et al., 1993) using the model described in Chapter 3. In addition, the pub-

lished results of 1973 (Aksnes and Franklin, 1976),1979 (Aksnes et al., 1984) and 1985 (Franklin and the G S O, 1991) where used in the analysis after suitable modification. The reconstruction of the published data was considered necessary to correct for the longitude discrepancy (Aksnes, Franklin and Magnusson, 1986) for the 1973 and 1979 events. Further more the published values were derived using uniform disc model (1973, 1979 events) or Lambert's law (1985 events), whereas rest of the results were derived using either Hapke's law in set (1), or Lommel-Seeliger's law in set (2). The required corrections were determined in the following manner.

Table 5.2(b)   Details of mutual occultation data set (2).

Year	Total events	No. of positions				Residuals (arcsec)	
		J1	J2	J3	J4	G5	I32
1973[1]	34	31	34	3	0	0.015	0.014
1979[2]	6	3	6	3	0	0.022	0.023
1985[3]	16	7	9	10	6	0.023	0.020
1985[4]	85	52	41	56	21	0.028	0.029
1990-91[5,6]	21	17	20	4	1	0.039	0.034

Sources :
1. Aksnes and Franklin, 1976
2. Aksnes et al., 1984
3. Arlot et al., 1992
4. Franklin and GSO, 1991
5. Data from VBO
6. Arlot et al., 1993.

For the 1973 data, the published observed magnitude drop was used to derive the impact parameter y using the model described in Chapter 3. The model yields, in fact, the magnitude drop for a given impact parameter. The magnitude drops for a set of values for y close to the published value were first computed and the impact parameter corresponding to the observed magnitude drop was obtained by quadratic interpolation. The derived impact

parameter corresponds to the distance of the light centre of the occulted satellite to the centre of the occulting satellite at the published time (T_l). The position of the geometric centre at this instant was calculated using the method described in section 3.7.1.

The extensive astrometric data for the 1985 season by Franklin et al. (1991) correspond to the location of the geometric centre at the time of light minimum. These could in principle be used as such. However modification was required to transform the results from Lambert's law to Lommel-Seeliger's law. The published positions of the geometric centre (G) and the published phase corrections in time δT_α were used to obtain the position of the light centre (L), using the Eqs. 3.39 and 3.49.

The impact parameter using Lambert's law is then

$$y = (\Delta\alpha\cos\delta)_l^2 + (\Delta\delta)_l^2$$

The model described in Chapter 3 was first used with Lambert's law to estimate the magnitude drop for the impact parameter derived this way. Using this magnitude drop, the impact parameter for a satellite disc with light distribution given by Lommel Seeliger's law was determined by employing the method used for the 1973 data set. The 1979 data (Aksnes et al. 1984) were similarly transformed to the required form. Table 5.2(b) gives the statistics of the data sets of the four mutual event seasons. Table 5.3 gives the relative astrometric positions of the centres of the satellites at the time reported in the 3rd column. Entries in columns 1 and 2 refer to the occulting and occulted satellites respectively. The last two columns give the position of occulting satellite S2 relative to occulted satellite S1 at the given UT date.

Table 5.3   Relative astrometric positions for S1OS2 events.

Satellite				UT Date				$\Delta\alpha\cos\delta$	$\Delta\delta$
S1	S2	Dy	Mo	Yr	Hr	min	Sec	arcsec	arcsec
1	2	10	06	73	09	10	00.0	0.2201	−0.7423
1	2	10	06	73	09	09	58.0	0.2155	−0.7344
1	2	17	06	73	11	15	51.0	0.1730	−0.6287
1	2	17	06	73	11	15	53.0	0.1698	−0.6155
1	2	24	06	73	13	20	50.0	0.1409	−0.5232
1	2	28	06	73	02	22	41.0	0.1458	−0.5397
1	2	08	07	73	17	27	52.0	0.0996	−0.3917
1	2	08	07	73	17	28	06.0	0.0777	−0.3266
1	2	12	07	73	06	29	36.0	0.0777	−0.3104
1	2	12	07	73	06	29	23.0	0.0883	−0.3475
1	2	12	07	73	06	29	28.0	0.0915	−0.3584
1	2	12	07	73	06	29	24.0	0.0871	−0.3412
1	2	19	07	73	08	32	22.0	0.0739	−0.2794
1	2	22	07	73	21	34	06.0	0.0713	−0.2633
1	2	22	07	73	21	34	02.0	0.0731	−0.2664
1	2	26	07	73	10	35	32.0	0.0675	−0.2393
1	2	02	08	73	12	39	25.0	0.0749	−0.2381
1	2	13	08	73	03	48	09.0	0.0713	−0.1918
1	2	13	08	73	03	48	12.0	0.0619	−0.1610
1	2	16	08	73	16	51	42.0	0.0669	−0.1605
1	2	20	08	73	05	56	28.0	0.0633	−0.1333
1	2	20	08	73	05	56	28.0	0.0651	−0.1447
1	2	27	08	73	08	07	50.0	0.0652	−0.1155
1	2	03	09	73	10	23	19.0	0.0575	−0.0743
1	2	06	09	73	23	32	28.0	0.0691	−0.0466
1	2	10	09	73	12	44	23.0	−0.0437	−0.0551
1	2	21	09	73	04	31	37.0	−0.0262	0.0431
1	2	21	09	73	04	31	36.0	0.0284	0.0776
1	2	24	09	73	17	55	32.0	0.0182	0.1466
1	2	28	09	73	07	25	08.0	0.0151	0.1818
2	1	21	12	73	00	32	25.0	0.1733	−0.4721
3	2	24	09	73	01	45	18.0	0.2593	−0.8688
3	2	24	09	73	01	45	05.0	0.2392	−0.8194
3	2	01	10	73	06	05	55.0	0.2753	−0.9769
1	2	01	10	79	04	23	41.0	−0.1286	−0.2411
1	2	01	10	79	04	23	38.0	−0.1219	−0.2284
1	2	01	10	79	04	23	36.0	−0.1419	−0.2769
2	3	14	01	79	23	39	40.0	0.2739	1.1827
2	3	28	01	79	07	53	29.0	0.0783	0.3047

Table 5.3 Contd.

Satellite		UT Date						$\Delta\alpha\cos\delta$	$\Delta\delta$
S1	S2	Dy	Mo	Yr	Hr	min	Sec	arcsec	arcsec
1	2	21	09	85	03	48	24.9	0.2863	−0.9283
1	2	04	12	85	17	18	13.3	0.1991	−0.5890
1	2	04	12	85	17	18	18.0	0.2027	−0.5997
1	3	03	08	85	07	41	09.8	0.2972	−0.9108
1	3	22	09	85	03	19	14.4	0.2982	−1.0051
1	4	16	06	85	04	09	27.8	0.3720	−1.0534
1	4	19	07	85	04	19	11.3	0.1665	−0.4846
2	4	29	05	85	04	11	20.0	+0.0029	−0.0078
3	2	03	06	85	07	07	05.9	+0.2315	−0.6420
3	2	10	06	85	10	13	36.1	0.1225	−0.3481
3	2	16	07	85	01	14	29.2	−0.1859	0.5362
3	2	23	07	85	04	11	39.3	−0.2039	0.5962
3	2	30	07	85	07	09	47.7	−0.2163	0.6419
3	4	17	06	85	01	45	10.6	+0.3547	−1.0149
4	3	12	07	85	00	39	58.3	0.2081	−0.6161
4	3	12	07	85	00	40	10.0	0.2074	−0.6140
1	2	6	09	85	21	50	51.4	0.2920	−0.9607
1	2	14	09	85	01	4	44.6	0.2605	−0.9121
1	2	14	09	85	01	4	44.4	0.2639	−0.9214
1	2	14	09	85	01	4	22.5	0.2693	−0.9330
1	2	17	09	85	14	28	2.9	0.2607	−0.9236
1	2	21	09	85	03	48	36.9	0.2539	−0.9144
1	2	21	09	85	03	48	33.0	0.2750	−0.9821
1	2	21	09	85	03	48	37.2	0.2631	−0.9371
1	2	4	12	85	17	18	22.1	0.1846	−0.6212
1	2	4	12	85	17	18	16.4	0.1869	−0.6230
1	2	15	12	85	08	55	7.1	0.1101	−0.3508
1	2	15	12	85	08	55	10.0	0.1101	−0.3508
1	3	13	07	85	00	32	8.2	0.3299	−0.8609
1	3	27	07	85	05	17	39.7	0.3081	−0.8897
1	3	27	07	85	05	17	45.6	0.3037	−0.8828
1	3	3	08	85	07	41	13.9	0.3154	−0.9588
1	3	3	08	85	07	41	11.9	0.3142	−0.9539
1	3	3	08	85	07	41	07.4	0.3178	−0.9671
1	3	3	08	85	07	41	08.3	0.2964	−0.9006
1	3	10	08	85	10	6	30.9	0.3079	−0.9885
1	3	10	08	85	10	6	23.4	0.3142	−1.0108
1	3	10	08	85	10	6	29.7	0.3150	−1.0115
1	3	24	08	85	15	7	03.4	0.3174	−1.1167
1	3	31	08	85	17	45	58.5	0.3145	−1.1420

Table 5.3   Contd.

Satellite			UT Date					$\Delta\alpha\cos\delta$	$\Delta\delta$
S1	S2	Dy	Mo	Yr	Hr	min	Sec	arcsec	arcsec
1	3	7	09	85	20	34	04.9	0.3414	−1.1611
1	3	14	09	85	23	38	01.4	0.2855	−1.1136
1	3	14	09	85	23	37	43.5	0.3034	−1.1630
1	3	14	09	85	23	37	59.3	0.2896	−1.1204
1	3	22	09	85	03	19	33.8	0.2689	−1.0605
1	3	22	09	85	03	19	51.2	0.2611	−1.0412
1	3	22	09	85	03	19	33.5	0.2635	−1.0477
1	3	22	09	85	03	19	40.8	0.2623	−1.0375
1	4	16	06	85	04	9	19.0	0.3863	−0.9498
1	4	6	09	85	05	57	11.3	0.3214	−1.1285
1	4	6	09	85	05	57	11.3	0.3458	−1.1190
2	4	30	05	85	10	38	06.5	0.2147	−0.3863
2	4	30	05	85	10	38	05.8	0.2140	−0.3813
3	1	3	06	85	11	07	31.3	0.3460	−0.8905
3	1	10	06	85	14	13	25.4	0.2378	−0.6148
3	1	10	06	85	14	13	29.4	0.2350	−0.6266
3	1	17	06	85	17	43	27.5	0.1846	−0.4833
3	1	22	11	85	01	14	35.9	0.2622	−0.9103
3	1	29	11	85	04	54	19.5	0.1733	−0.5799
3	1	29	11	85	04	54	20.5	0.1743	−0.5864
3	2	3	06	85	07	06	58.5	0.2336	−0.6057
3	2	10	06	85	10	13	29.0	0.1030	−0.2913
3	2	10	06	85	10	13	29.8	0.0970	−0.2771
3	2	10	06	85	10	13	28.9	0.1069	−0.2996
3	2	10	06	85	10	13	29.5	0.1030	−0.2940
3	2	8	07	85	22	17	20.1	−0.1425	0.4075
3	2	16	07	85	01	14	25.0	−0.1625	0.4781
3	2	16	07	85	01	14	25.5	−0.1567	0.4617
3	2	23	07	85	04	11	47.5	−0.1895	0.5693
3	2	23	07	85	04	11	44.5	−0.1937	0.5748
3	2	30	07	85	07	09	44.4	−0.1946	0.5882
3	2	30	07	85	07	09	45.5	−0.2036	0.6165
3	2	30	07	85	07	09	47.5	−0.1872	0.5667
3	2	06	08	85	10	10	13.1	−0.2026	0.6136
3	2	06	08	85	10	10	14.2	−0.2115	0.6421
3	2	06	08	85	10	10	12.8	−0.2048	0.6210
3	2	06	08	85	10	10	17.1	−0.2013	0.6115
3	2	06	08	85	10	10	14.1	−0.1977	0.6002
3	2	13	08	85	13	13	24.0	−0.2118	0.6500
3	2	13	08	85	13	13	24.2	−0.2097	0.6401
3	2	27	08	85	19	37	14.8	−0.2293	0.7164
3	2	27	08	85	19	37	9.1	−0.2435	0.7465

Table 5.3   Contd.

Satellite				UT Date				$\Delta\alpha\cos\delta$	$\Delta\delta$
S1	S2	Dy	Mo	Yr	Hr	min	Sec	arcsec	arcsec
3	2	03	09	85	23	03	44.8	−0.2400	0.7475
3	2	11	09	85	02	48	11.2	−0.2950	0.9047
3	2	25	09	85	18	57	44.5	−0.3176	0.9558
3	4	17	06	85	01	44	59.3	0.4086	−1.0443
3	4	17	06	85	01	44	37.3	0.3949	−1.0134
4	1	06	06	85	22	04	34.2	0.3494	−0.8830
4	1	10	07	85	09	37	20.7	0.0825	−0.2441
4	1	10	07	85	09	37	20.9	0.0850	−0.2455
4	1	10	07	85	09	37	19.7	0.0796	−0.2325
4	1	10	07	85	09	37	21.8	0.0826	−0.2428
4	1	10	07	85	09	37	23.5	0.0729	−0.2180
4	1	27	07	85	17	08	19.0	0.3459	−1.0277
4	1	27	07	85	17	08	24.1	0.3439	−1.0202
4	1	24	12	85	01	18	39.8	−0.1415	0.4114
4	1	24	12	85	01	18	42.0	−0.1591	0.4456
4	1	25	12	85	02	38	07.2	−0.0355	0.0976
4	2	06	06	85	17	55	57.6	0.3709	−0.9552
4	2	26	07	85	12	34	16.6	0.0156	−0.0503
4	3	12	07	85	00	39	54.3	0.2306	−0.6058
4	3	12	07	85	00	39	58.5	0.2137	−0.5590
2	1	01	01	91	06	27	55.7	0.1621	−0.5325
2	1	01	01	91	06	29	58.6	−0.1575	−0.5174
2	1	19	01	91	05	34	06.7	−0.1448	−0.4627
2	1	22	01	91	04	57	04.9	0.0897	0.3718
2	1	22	01	91	18	43	54.0	−0.1336	−0.4310
2	1	05	02	91	23	13	33.7	−0.0239	−0.0802
2	1	09	02	91	12	19	28.6	−0.027	−0.1109
2	1	13	02	91	01	24	21.7	−0.0280	−0.0958
2	1	13	02	91	01	24	26.0	−0.0301	−0.1032
2	1	16	02	91	14	29	39.5	0.0092	0.0319
2	1	20	02	91	03	34	21.0	0.0353	0.1233
2	1	23	02	91	16	39	11.4	0.0501	0.1764
2	1	27	02	91	05	43	41.3	0.0712	0.2529
2	1	09	03	91	20	58	25.9	0.1238	0.4491
2	1	09	03	91	20	58	35.3	0.1235	0.4475
2	1	09	03	91	20	58	34.1	0.1242	0.4503
2	1	27	03	91	14	26	33.6	0.1972	0.7260
2	3	25	12	90	22	07	12.6	−0.0864	−0.2683
2	3	02	01	91	01	39	49.2	−0.0810	−0.2569
2	3	23	01	91	16	42	19.1	0.0999	0.3191
3	4	21	02	91	02	00	29.7	0.1878	0.8188

5.4   Correction to the Constants

The method developed by Arlot (1982a) was used for the present analysis, and is described briefly:

The finite values of difference in the values of the sky plane co-ordinates $\Delta\alpha\cos\delta$ and $\Delta\delta$ between observations (O) and theory (C) come partly from error in observations which is of statistical nature and is eliminated in the least square fit and partly from the theory itself, thus if X_j and Y_j denote the values of these observed co-ordinates

$$(O)X_j \neq (C\{C_k, C_{k'}\})X_j$$

but

$$= \Big[C\{C_k(1+\varepsilon_k),(C_{k'}+\beta_{k'})\}\Big]X_J \qquad (5.1)$$

where C_k and $C_{k'}$ (k = 1-28 and k' = 1-22) are the constants of motion of the Galilean satellites (Lieske 1977), ε_k and $\beta_{k'}$ are the corrections required to update the constants in order to fit the observations. The constants C_k are listed in Table 5.4(a) (Lieske 1977). The parameters ε's represent relative variation of Sampson's generic value A_0 (column 3), such that the revised value will be

$$A = A_0(1+\varepsilon)$$

or

$$\varepsilon = (A - A_0)/A_0 \qquad (5.2)$$

All the ε values are dimensionless parameters. The constants $C_{k'}$ are listed in Table 5.4(b) (Lieske 1977). The corrections to $C_{k'}$ are the $\beta_{k'}$ values. The β's are in degrees and are added to the generic values (column 3).

The problem now lies in deriving ε, β values, such that the updated constants of the theory would best fit the set of (N) observations in the least square sense. A careful adjustment is possible by use of the partial derivatives:

$$(O-C)X_j^i = \sum_{k=1}^{28} \frac{\delta X_j^i}{\delta\varepsilon_k}.\Delta\varepsilon_k + \sum_{k'=1}^{22} \frac{\delta X_j^i}{\delta\beta'_k}.\Delta\beta_{k'}$$

$$(O-C)Y_j^i = \sum_{k=1}^{28} \frac{\delta Y_j^i}{\delta\varepsilon_k}.\Delta\varepsilon_k + \sum_{k'=1}^{22} \frac{\delta Y_j^i}{\delta\beta'_k}.\Delta\beta_{k'} \qquad (5.3)$$

98

Table 5.4(a) Details of the 28 ε values, extraced from Lieske (1977)

Index	Symbol $\varepsilon( )$	Generating Value A_o * $\varepsilon = (A - A_o)/A_o$	Name
1	m_1	449,7	Mass of Satellite I relative to Jupiter
2	m_2	252,9	Mass of Satellite II relative to Jupiter
3	m_3	798,8	Mass of Satellite III relative to Jupiter
4	m_4	450,4	Mass of Satellite IV relative to Jupiter
5	S/J	1047.355	Mass of Sun relative to Jupiter system
6	n_1	203.48895 4208	Mean motion of Satellite I, deg/day
7	n_2	101.37472 3445	Mean motion of Satellite II, deg/day
8	n_4	21.57107 1403	Mean motion of Satellite IV, deg/day
9	λ_A	0†	Libration phase angle amplitude
10	n_J	8.30912 15712 $\times 10^{-2}$	Mean motion of Jupiter, deg/day
11	J_2	0.01484 85	Jupiter J_2
12	J_4	-8.107×10^{-4}	Jupiter J_4
13	R_J	71420	Radius of Jupiter, km
14	P_J	9.924825	Jupiter period of rotation, hr
15	3(C-A)/2C	0.111	Ratio Jupiter moments of inertia
16	e_{11}	465,	Primary eccentricity of Satellite I, rad
17	e_{22}	825,	Primary eccentricity of Satellite II, rad
18	e_{33}	15164,	Primary eccentricity of Satellite III, rad
19	e_{44}	73725,	Primary eccentricity of Satellite IV, rad
20	e_J	0.04846 02472	Eccentricity of Jupiter
21	c_{11}	4756,	Primary sine inclination of Satellite I
22	c_{22}	81490,	Primary sine inclination of Satellite II
23	c_{33}	31108,	Primary sine inclination of Satellite III
24	c_{44}	47460,	Primary sine inclination of Satellite IV
25	I_J	3.10401	Inclination of Jupiter orbit to equator, deg
26	J	1.30691	Inclination of Jupiter orbit to ecliptic, deg
27	ϵ	23° 26' 44.84"	Obliquity of ecliptic at 1950.0
28	n_S	3.34597 33896 $\times 10^{-2}$	Mean motion of Saturn, deg/day

Notes: *Nominal value are $\varepsilon = 0$
A comma denotes the seventh decimal (e.g. 449,7 = 449.7 × 10⁻⁷)
†This phase angle amplitude for libration is an absolute quantity (i.e. $\varepsilon_9 = \lambda_A$), measured in radians. Sampson value: $\lambda_A = 0$.
Form of free libration is $\lambda_A \sin (\mu t + \phi_\lambda)$ where $\mu = \sqrt{L}$ and $\phi_\lambda = \beta_5$

Note: If, in evaluating the latitude series ζ_j, $(= Z/a)$, the "time-completed" is employed by means of
$$t_j^+ = t_o + \Delta t_j$$
$$\Delta t_j^+ = v_j/n_j$$
$$t_o = \text{ephemeris time}$$
then the resultant series represents $s_j^+ = Z_j/a_j (1 + \xi_j^+) = Z_j/\rho_j$ complete through second order and the second order terms in s_j^+ (ZZ-DEG) should not be applied. The second-order terms in J'_j should be employed only if the time-completed feature is not utilized.

Table 5.4(b) Details of the 22 β values, extracted from Lieske (1977)

Index	Symbol	Epoch Value (JD 2443000.5)*	Rate (deg/day)	Name
1	ℓ_1	$106°.03042 + \beta_1$	$203.48895\ 4208\ (1 + \epsilon_6)$	Mean longitude of Satellite I
2	ℓ_2	$175°.74748 + \beta_2$	$101.37472\ 3445\ (1 + \epsilon_7)$	Mean longitude of Satellite II
3	ℓ_3	$120°.60601 - 1/2\ \beta_1 + 3/2\ \beta_2$	$50.31760\ 80635\ [1 - 2\epsilon_6 + 3\epsilon_7 - 2.20451\ 8497 \times 10^{-2}\ (\epsilon_6 - \epsilon_7)]$	Mean longitude of Satellite III
4	ℓ_4	$84°.51861 + \beta_4$	$21.57107\ 1403\ (1 + \epsilon_8)$	Mean longitude of Satellite IV
5	ϕ_λ	$0 + \beta_5$	$\sqrt{L}\quad (= 0.1719\ 0889 + \cdots)$	Libration phase angle See Table A.30
6	π_1	$4°.51172 + \beta_6$	$\dot{\pi}_1\quad (= 0.1612\ 2004 + \cdots)$	Proper periapse of Satellite I See Table A.12
7	π_2	$74°.53051 + \beta_7$	$\dot{\pi}_2\quad (= 0.0476\ 3124 + \cdots)$	Proper periapse of Satellite II See Table A.17
8	π_3	$174°.85831 + \beta_8$	$\dot{\pi}_3\quad (= 0.0069\ 7450 + \cdots)$	Proper periapse of Satellite III See Table A.20
9	π_4	$336°.02667 + \beta_9$	$\dot{\pi}_4\quad (= 0.0018\ 7351 + \cdots)$	Proper periapse of Satellite IV See Table A.22
10	Π	$13°.30364 + \beta_{10}$	0	Longitude of perihelion of Jupiter
11	ω_1	$242°.73706 + \beta_{11}$	$\dot{\omega}_1\quad (= -0.1340\ 1884 + \cdots)$	Proper node of Satellite I See Table A.23
12	ω_2	$95°.28556 + \beta_{12}$	$\dot{\omega}_2\quad (= -0.0327\ 4001 + \cdots)$	Proper node of Satellite II See Table A.25
13	ω_3	$125°.14673 + \beta_{13}$	$\dot{\omega}_3\quad (= -0.0070\ 1735 + \cdots)$	Proper node of Satellite III See Table A.26
14	ω_4	$317°.89250 + \beta_{14}$	$\dot{\omega}_4\quad (= -0.0018\ 0387 + \cdots)$	Proper node of Satellite IV See Table A.28
15	ψ	$316°.73369 + \beta_{15}$	$\dot{\psi}\quad (= -0.0000\ 0229 + \cdots)$	Longitude of origin of coordinates (Jupiter's pole) See Table A.29
16	G'	$31°.97852\ 80244 + \beta_{16}$	$3.34597\ 33896 \times 10^{-2}\ (1 + \epsilon_{28})$	Mean anomaly of Saturn
17	G	$30°.37841\ 20168 + \beta_{17} + 6G^\dagger$	$8.30912\ 15712 \times 10^{-2}\ (1 + \epsilon_{10})$	Mean anomaly of Jupiter
18	ϕ_1	$172°.84\ (1 - 0.014\ \epsilon_{20}) + \beta_{18}$	0	Phase angle occurring in solar $(A/R)^3$ with angle $2G' - G$
19	ϕ_2	$47°.03\ (1 - 0.156\ \epsilon_{20}) + \beta_{19}$	0	Phase angle occurring in solar $(A/R)^3$ with angle $5G' - 2G$
20	ϕ_3	$259°.18 + \beta_{20}$	0	Phase angle occurring in solar $(A/R)^3$ with angle $G' - G$
21	ϕ_4	$157°.12\ (1 + 0.0014\ \epsilon_{20}) + \beta_{21}$	0	Phase angle occurring in solar $(A/R)^3$ with angle $2G' - 2G$
22	Ω_J	$99°.95326 + \beta_{22}$	0	Longitude of ascending node of Jupiter's orbit

Notes: *All parameters β are measured in degrees. Nominal values are $\beta = 0$.

$\dagger 6G = 0°.03439\ \sin\ (2G' - G + 0°.76699) + 0°.33033\ \sin\ (5G' - 2G - 0.0227694694\ t_y + 64°.26288)$ where $t_y = (JD - 2443000.5)/365.25$
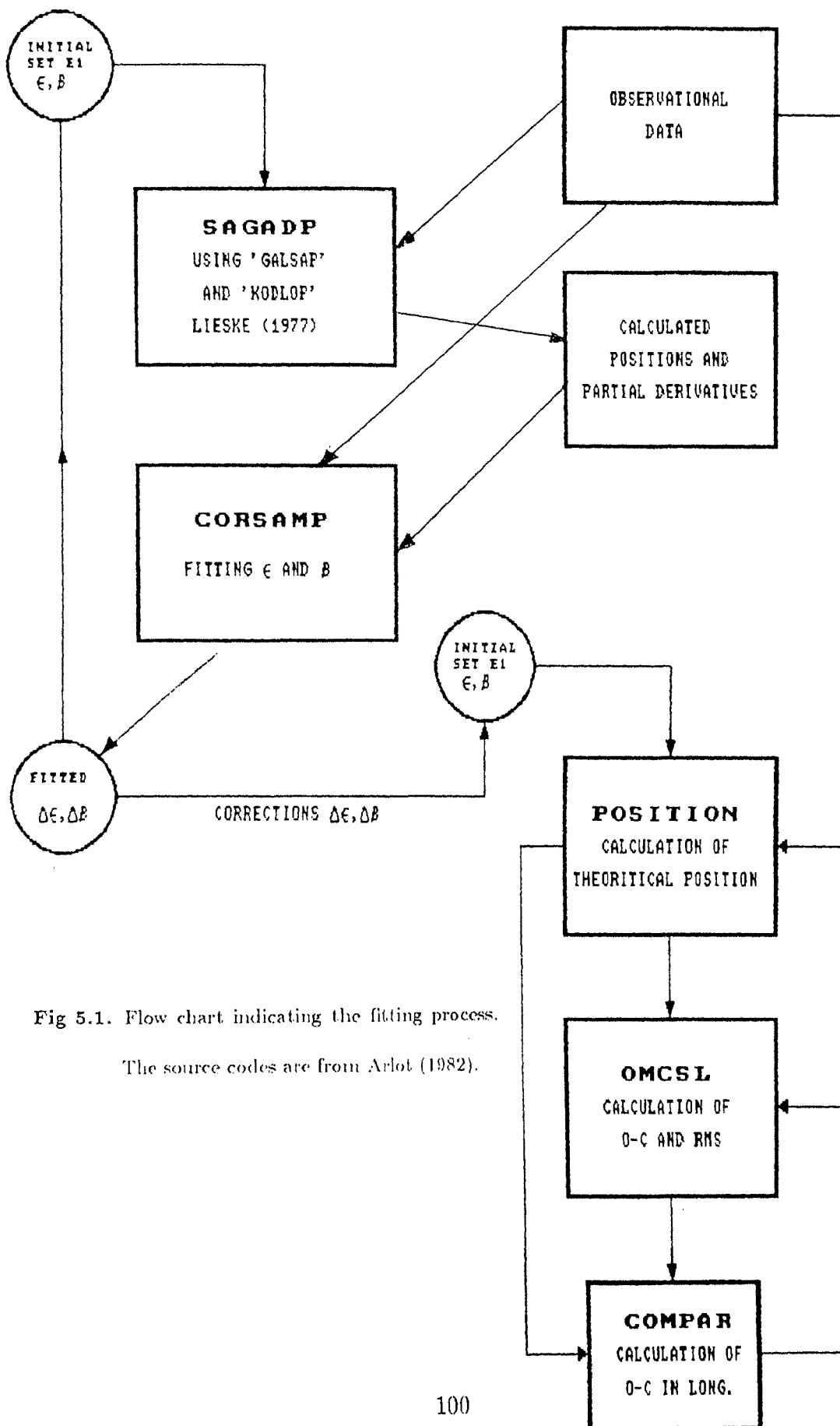
Fig 5.1. Flow chart indicating the fitting process. The source codes are from Arlot (1982).

100

where $i(1 \rightarrow N)$ is running index of the observation, and j identifies the satellite. Mutual occultations provide relative positions between the satellites, therefore the O-C values of their relative positions were used in the fit. Similarly the satellite-satellite positions of the photographic data were used. From the sets of conditional Eqs. (5.3), all the 28 ε's and 22 β's can be derived. However it is not possible and also not necessary to make corrections to all the constants of the theory. In the present work only the mean motions ($\varepsilon_6 - \varepsilon_8$), primary eccentricities ($\varepsilon_{16} - \varepsilon_{19}$), primary sine inclinations ($\varepsilon_{21} - \varepsilon_{24}$), mean longitudes ($\beta_1, \beta_2, \beta_4$) proper perijoves ($\beta_6 - \beta_9$) proper nodes ($\beta_{11} - \beta_{14}$), libration phase angle amplitude (ε_9) and the libration phase angle (β_5) were fitted. The software developed by Arlot (1982, 1982a) to derive his G-5 ephemeris was used for solving Eqs. 5.3. A minor modification was made for adding the corrections from successive iterations. The flow chart in Fig 5.1 describes the sequence of the fitting procedure.

The programme 'SAGADP' calculates the theoretical positions and the partial derivatives $\left(\frac{\delta X}{\delta \varepsilon_k}, \frac{\delta Y}{\delta \varepsilon_k}, \frac{\delta X}{\delta \beta_{k'}}, \frac{\delta Y}{\delta \beta_{k'}} \right)$ using the fortran routines 'GALSAP' and 'KODLOP' by Lieske (1977). The starting ephemeris for the fit was E-1. The mutual events were assigned a weight of 50, whereas the weight assigned to the photographic data ranged from 1 to 2 depending on the plate scale and r.m.s. of the residuals. The mutual event data were given larger weight because the mutual events are inherently accurate and yield positions of the satellites accurate to about a few tens of kilometers.

The observations are reported in universal time (UT). However, the theoretical positions are calculated with respect to the TT (Terrestrial time) close to the former definition of ET (Ephemeris time) and physically made by measuring TAI (International atomic time) so that TT=TAI+32.184s. In order to look for possible changes in the mean motions of the satellites over the time span of 100 years, it is of utmost importance to know the difference, $\Delta T = TT - UT$, precisely. The values of ΔT used in the present study were taken by Arlot (1982a) from various sources and is shown as continuous line in Fig 5.2. For comparison, the ΔT values by Stephenson and Morrison (1984) are shown as dotted line (American Ephemeris 1992). The ΔT values of the two sets differ by a maximum of 1.5 seconds.

101
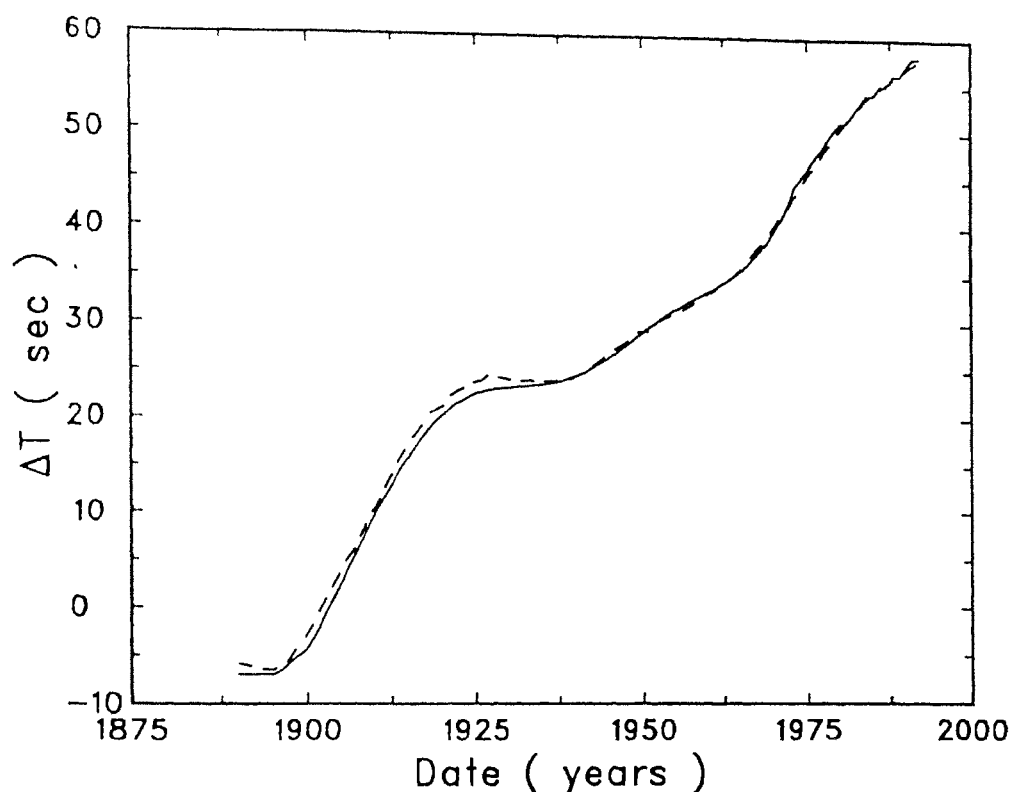
Fig 5.2. ΔT values used in the present work is from Arlot (1982), shown as the continuous line. The dashed line is from Stephenson and Morrison (1984).

The program 'CORSAMP' carries out the fit in the least square sense and determines the corrections $\Delta\varepsilon_k$ and $\Delta\beta_{k'}$ to original $(\varepsilon_k, \beta_{k'})$ set. The positions and partial derivatives were recalculated with the modified ε, β values in 'SAGADP' and fit was repeated. Four iterations were carried out. The selected resulting ephemeris labeled I-32 is given in Table 5.5. The residuals σ for the positions of the satellites at the time of observation were calculated compared to G-5 and I-32 ephemerides where

$$\sigma = \sqrt{\frac{\sum\limits_{i=1}^{N}\sum\limits_{j=1}^{4}\left[\left(X_i^j\right)^2 + \left(Y_i^j\right)^2\right]}{2 \times 4 \times N}} \tag{5.4}$$

102

These are given in the last two columns of Table 5.1, and Tables 5.2(a&b). Comparison of the residuals using the two ephemerides shows only a marginal difference.

Table 5.5 $\varepsilon - \beta$ values for I32 ephemeris.

ε	β
$(\varepsilon_1 = +0.041590 \pm 0.0098)$	$\beta_1 = +0.042422 \pm 0.004659$
$(\varepsilon_2 = -0.002461 \pm 0.0200)$	$\beta_2 = -0.015043 \pm 0.000928$
$(\varepsilon_3 = -0.0231890 \pm 0.0076)$	—
$(\varepsilon_4 = +0.256938 \pm 0.0084)$	$\beta_4 = -0.068653 \pm 0.000270$
$(\varepsilon_5 = \{+2.067082138 \pm 0.095\}.10^{-4})$	$\beta_5 = 182.843830 \pm 0.003527$
$\varepsilon_6 = \{+0.1914605 \pm 0.07028\}.10^{-8}$	$\beta_6 = 81.260641 \pm 20.77448$
$\varepsilon_7 = \{1.0620350 \pm 0.044363\}.10^{-8}$	$\beta_7 = 86.913295 \pm 2.068978$
$\varepsilon_8 = \{-4.3762173 \pm 0.12171\}.10^{-8}$	$\beta_8 = 14.509744 \pm 0.184138$
$\varepsilon_9 = \{14.2286 \pm 0.064061\}.10^{-4}$	$\beta_9 = -0.690772 \pm 0.022813$
$(\varepsilon_{10} = \{+0.1620 \pm 0.063)\}.10^{-4}$	$(\beta_{10} = +0.166755 \pm 0.05)$
$(\varepsilon_{11} = -0.007778 \pm 0.00054)$	$\beta_{11} = +62.543522 \pm 1.509104$
$(\varepsilon_{12} = -0.275934 \pm 0.024)$	$\beta_{12} = +5.805040 \pm 0.083225$
$(\varepsilon_{13} = -0.000308 \pm 0.0006)$	$\beta_{13} = -5.466685 \pm 0.126572$
$(\varepsilon_{14} = \{0.0950 \pm 2.80\}.10^{-4})$	$\beta_{14} = +4.468895 \pm 0.054777$
$(\varepsilon_{15} = 0.00 \pm 0.15)$	$(\beta_{15} = -0.233589 \pm 0.19)$
$\varepsilon_{16} = -0.761448 \pm 0.068703$	$(\beta_{16} = 0.0 \pm 0.4)$
$\varepsilon_{17} = +0.963303 \pm 0.061752$	$(\beta_{17} = -0.140391 \pm 0.03)$
$\varepsilon_{18} = -0.056173 \pm 0.003330$	$(\beta_{18} = +15.610 \pm 3.1)$
$\varepsilon_{19} = -0.0018711 \pm 0.000411$	$(\beta_{19} = +5.135 \pm 4.2)$
$(\varepsilon_{20} = +0.002781 \pm 0.0005)$	$(\beta_{20} = -1.719 \pm 2.1)$
$\varepsilon_{21} = +0.460587 \pm 0.040296$	$(\beta_{21} = -7.784 \pm 1.8)$
$\varepsilon_{22} = -0.009496 \pm 0.001377$	$(\beta_{22} = +0.04428 \pm 0.007)$
$\varepsilon_{23} = +0.048456 \pm 0.002255$	
$\varepsilon_{24} = -0.078446 \pm 0.000904$	
$(\varepsilon_{25} = +0.005384 \pm 0.011)$	
$(\varepsilon_{26} = -0.000133 \pm 0.00011)$	
$(\varepsilon_{27} = \{0.0 \pm 0.0047\}.10^{-4})$	Parameters within the
$(\varepsilon_{28} = \{0.0 \pm 0.0010\}.10^{-4})$	paranthesis were not fitted

5.5 Residual in Longitude

The programs 'POSITION', 'OMCSL' and 'COMPAR' were used to calculate the $(O-C)$ in longitudes, using the G-5 and I-32 ephemerides. The $(O-C)$ in longitudes in units of minutes of time are given for the four satellites in Table 5.6(a) and (b). (1) only photographic; (2) photographic and the mutual events of set (1) and lastly (3) all the data sets. A curious trend is noticed in the residuals of data sets with mutual occultations with respect to the G-5 ephemeris. Whereas Io is delayed Europa is in advance. A trend in the increase in residuals from 1973 through 1991 is also seen in Tables 5.2(a&b). Mallama (1992) reported a net projected along-track positional error for Europa relative to Io, which increased rather smoothly from -12 km in 1973 to -308 km in 1991, compared to E-3 ephemeris.

Table 5.6(a)   Error in longitude (minutes of time) compared to G5.

Data Set	dT(J1) (min)	dT(J2) (min)	dT(J3) (min)	dT(J4) (min)
Photographic	0.054	0.017	0.047	0.059
	±0.010	±0.012	±0.015	±0.020
(N)* =	(1508)	(1568)	(1624)	(1660)
Photographic and	0.052	−0.001	0.044	0.059
mutual occultations	±0.010	±0.012	±0.015	±0.019
set (1)				
N =	(1569)	(1640)	(1647)	(1666)
Photographic and	0.051	−0.016	0.035	0.062
mutual occultations	±0.010	±0.011	±0.014	±0.018
set (1) and (2)				
N =	(1679)	(1750)	(1723)	(1694)

*N = Total number of data points.

104

The I-32 ephemeris improves the residuals in longitude in case of photographic observations and also the combined data set. The paucity of observations of Callisto in the mutual occultation set leads to unreliable corrections to the constants related to this satellites. The residuals using I-32 for J4 have worsened compared to that using G-5.

Table 5.6(b)   Error in longitude (minutes of time) compared to I32.

Data Set	dT(J1) (min)	dT(J2) (min)	dT(J3) (min)	dT(J4) (min)
Photographic	0.019	0.010	0.039	0.267
	±0.015	±0.017	±0.021	±0.027
(N)* =	(1508)	(1568)	(1624)	(1660)
Photographic and	0.018	0.006	0.038	0.267
mutual occultations	±0.014	±0.017	±0.020	±0.027
set (1)				
N =	(1569)	(1640)	(1647)	(1666)
Photographic and	0.019	0.002	0.034	0.268
mutual occultations	±0.014	±0.016	±0.020	±0.026
set (1) and (2)				
N =	(1679)	(1750)	(1723)	(1694).

*N = Total number of data points.

105

5.6 Search for Secular Changes in Mean Motions

The direction of secular changes in the mean motion of the Galilean satellites can yield valuable clue to the evolution of the satellite system itself. It is of great interest to the planetary scientists to determine whether Io moves towards Jupiter ($\dot{n}_1 > 0$) or away from it ($\dot{n}_1 < 0$), where n_1 is the mean motion of Io . A positive value of $\dot{n}_1/n_1$ implies that the tides raised on Io by Jupiter are dominating. If $\dot{n}_1/n_1$ is negative, the tides raised on Jupiter by Io dominate the evolution. The values of $\dot{n}_1/n_1$ has been estimated by several groups (deSitter, 1928; 1931: Brouwer and Clemence, 1961; Goldstein, 1975; Goldstein and Jacob, 1985, 1986; Lieske 1987).

The longitude $(O-C)$ values of the data sets used in the present study using I-32, were fitted with a quadratic equation of the form

$$(O - C) = A + B(T - T_o) + C(T - T_o)^2 \tag{5.5}$$

The $(O - C)$'s are in minutes of time. The parameter A in units of minutes is a measure of a constant offset in the longitude, B (min.yr^{-1}) is indicative of a constant error in the estimation of the mean motions, and C (min.yr^{-2}) is a measure of the acceleration along the orbit. T_o was taken to be 1961, the approximate mean epoch of the data set. The constants A, B and C were determined by using the program 'COMPAR'. The derived values of constants are given in Table 5.7, for the three combinations of the data sets. From the photographic data alone, Io appears to be advancing whereas Europa is lagging by a small amount. When the occultation data set (1) is included the coefficient C decreases for both the satellites. This trend increases further when both the occultation data sets are included in the analysis. The constant C in Eq. 5.5 is in fact $\frac{1}{2}\dot{n}_i$ where i =1, 4 for Io through Callisto.

The values of q_1 and q_2 given by (Lieske 1987)

$$q_1 = 10^{11}\dot{n}_i/n_i$$
$$q_2 = 10^{11}(\dot{n}_1 - 2\dot{n}_2)/n_1 \tag{5.6}$$

were determined using the derived constants. For the photographic data set

this yields

$$q_1 = 24.79 \pm 7.89$$

$$q_2 = 30.17 \pm 12.14.$$

The value of $\dot{n}_1/n_1$ is $(24.79 \pm 7.89)10^{-11}$ yr^{-1}.

Table 5.8 gives the previous determinations of $\dot{n}_1/n_1$ extracted from (Lieske 1987) along with the results of this analysis.

For the photographic and both the occultation data sets

$$q_1 = 21.65 \pm 7.44$$

$$q_2 = 45.61 \pm 11.17.$$

The values of q1 and q2 appear to depend significantly on the type of data set used in the analysis. Therefore a cautious approach will be not to take the results as conclusive.

Table 5.7 Error in longitude (minutes of time) compared to I-32.

Data set	Satellite	$\Delta T =$	A (min)	$+ B(\text{min yr}^{-1})(T - T_o)$	$+C(\text{min yr}^{-2})(T - T_o)^2$
1 Ph	1		$-0.04(\pm0.02)$	$0.00161024(\pm0.00077271)$	$0.00006519(\pm0.00002074)$
	2		$0.02(\pm0.03)$	$0.00178567(\pm0.00090356)$	$-0.00001421(\pm0.00002443)$
	3		$0.00(\pm0.03)$	$0.00313965(\pm0.00104315)$	$0.00003933(\pm0.00002932)$
	4		$0.48(\pm0.04)$	$-0.00879705(\pm0.00137827)$	$-0.00023561(\pm0.00003800)$
2 Ph	1		$-0.04(\pm0.02)$	$0.00140722(\pm0.00075431)$	$0.00006048(\pm0.00002028)$
and MO	2		$0.05(\pm0.03)$	$0.00039328(\pm0.00085611)$	$-0.00004814(\pm0.00002321)$
Set (1)	3		$0.01(\pm0.03)$	$0.00291842(\pm0.00102259)$	$0.00003442(\pm0.00002882)$
	4		$0.48(\pm0.04)$	$-0.00860459(\pm0.00135970)$	$-0.00023151(\pm0.00003953)$
3 Ph	1		$-0.03(\pm0.02)$	$0.00128284(\pm0.00072480)$	$0.00005693(\pm0.00001956)$
and MO	2		$0.06(\pm0.02)$	$-0.00029429(\pm0.00081090)$	$-0.00006326(\pm0.00002201)$
Sets (1)	3		$0.01(\pm0.03)$	$0.00239246(\pm0.00098022)$	$0.00002376(\pm0.00002786)$
and (2)	4		$0.48(\pm0.04)$	$-0.00839037(\pm0.00131764)$	$-0.000227751(\pm0.00003653)$

Table[1] 5.8   Previous determination of $\dot{n}_1/n_1$ in units of 10^{-11} yr^{-1}.

$\dot{n}_1/n_1$	Author	Remarks
+25.2	deSitter (1928)	Empirical secular terms
+33.0	Brouwer and Clemence (1961)	Quotation of deSitter 1928 analysis
+2.58 ±5.6	deSitter (1931)	$\Delta\lambda_{Sun} = 1".83$ excess over 1".65 in 1928 analysis
+ 7.58 ±5.9	deSitter (1931)	$\Delta\lambda_{Sun} = 2".16$ excess over 1".65 in 1929 analysis
$|\dot{n}_1/n_1| < 11$	Goldstein (1975)	Adopted Picard-Roemer vs Innes
+58. ±10	Goldstein and Jacobs (1985)	Preliminary with $\Delta T = 45".39(T - 18.751)^2$
+46. ±9	Goldstein and Jacobs (1986)	Final with $\Delta T = 45".39(T - 18.751)^2$
−0.74 ± 0.87	Lieske (1987)	
+24.79 ±7.89	This work	(Photographic data set)
+21.65 ±7.44	"	(Photographic and mutual occultations)

[1] Extracted from Lieske (1987)

6. Concluding Remarks and Future Prospects

6.1 Evaluation of the New Ephemeris

The I-32 ephemeris was derived using all of the data of Arlot (1982) except deSitter's observations during 1913-1928. The additional 243 pairs of mutual occultations and extension of the photographic data set till 1990 have not appreciably altered the G-5 ephemeris. There is only marginal improvement in the residuals as can be seen from Table 5.1 and 5.2 (a&b). A comparison shows that the residuals in longitude have improved for Io, Europa and Ganymede. The effect of assigning higher weight to mutual occultation data involving Callisto has resulted in the degradation of the constants associated with this satellite primarily because of very small number of occultations involving this satellite.

Fig 6.1 shows the comparison of E0(■), E-1(□), E-2 ($\triangle$), G-5 ($\times$), E2x3 ($\odot$) and I-32 ($+$) ephemerides.

For Io, the mean motion derived using this work is larger than that of G-5 but smaller than E2x3. The eccentricity correction ε_{16} is lower than G-5, but closer to E-2 and E2x3 values. Whereas the primary sine inclination (ε_{21}), mean longitude (β_1) are very nearly same as those of G-5, E2x3, and E-2 values. The proper node β_{11}(is significantly higher than G-5 and E2x3 but closer to E-2.

For Europa no significant change in mean motion (β_7) is apparent compared to the other recent ephemerides. The primary eccentricity (ε_{17}) has increased by $\sim$100% compared to E0 and $\sim$50% compared to G-5. The other fitted parameters for the satellite are close to the G-5 values.

In case of Ganymede, I-32 yields slightly lower primary eccentricity (ε_{18}) compared to G-5 but it is closer to E2x3. The primary sine inclination correction (ε_{23}) is between the G-5 and E2x3 values. The proper periapse (β_8) and the proper node (β_{13}) corrections are close to that of G-5 ephemeris.

110

I-32 yields correction for mean motion (ε_8) for Callisto larger than by about 22% compared to G-5, but it is closer to that of E2x3. The corrections to mean longitude (β_4), proper periapse (β_9) and proper node (β_{14}) are not very different from G-5 and E2x3. The large residuals for this satellite [Table 5.6(b)] may be a result of significantly different correction to the mean motion (ε_8) primary eccentricity (ε_{19}) and the primary sine inclination (ε_{24}) for this satellite.

It is interesting to note that the residuals in longitude for photographic and the combined data sets using I-32 have improved compared to G-5 except for Callisto. However no significant improvement is noticable in the residual of the sky plane co-ordinates given in Tables 5.1 and 5.2(a&b).

One possible reason may be a consequence of higher weight assigned to the mutual events, and the difference in the accuracy attainable in the relative longitudes and latitudes of the satellites. The timings of the mutual events can be determined from the light curves with an accuracy of about one second. The correction to the longitude will be of the order of a few tens of kilometers. The accuracy of the relative latitude derived from mutual event on the other hand depends largely on the proper sky subtraction and the evaluation of the contribution of the occulting satellite (Section 2.5). The results of the fit presented in Tables 4.2(a-p) indicate that the derived parameter is also significantly model dependent. For good quality events, the fitted impact parameter using the model with albedo variation are close to be predicted values. Mallama (1992) arrived at residuals as low as $0''.013$ for the events in 1991 using CCD. The mutual events have therefore the potential of yielding accurate latitude information but are degradable due to reasons mentioned above.

Taking an average value of 1.5 as the weight for the photographic data set and 50 for the mutual events, the relative fraction of mutual event set to the total set is 8550:10762 for Io, 9100:11452 for Europa, 4950:6574 for Ganymede and 1700:3360 for Callisto. Except for Callisto, for which the mutual event data are insufficient, the derived mean motion and longitudes of the other three satellites would be expected to be more accurate than the inclinations and the nodes. The lower residuals in longitude with I-32 [Tables 5.6 (a&b)]

111

and only marginal improvement in the sky plane co-ordinates [Tables 5.1, 5.2(a&b)] would follow naturally.

Examination of the coefficients A, B and C given in Table (5.5) indicates that the mutual events appear to influence their estimation to a large extent, because of the higher weight assigned to them. Therefore a cautious approach will be not to take the results as conclusive; the mutual events, however, definitely show good potential.

6.2 Future Prospects

6.2.1 The Jovian Phenomena

In the present study only the mutual occultation data have been used. The mutual eclipses have not been included in the present analysis for the following reason. A mutual eclipse is in fact the occultation of the Sun by the eclipsing satellite as seen by the eclipsed satellite (Arlot 1986). Another problem pointed out by Arlot (1986) is that it is erroneous to assume that the cone of umbra or penumbra that is carried across the eclipsing satellite is aligned in the Sun-satellite direction. This would be the case if the eclipsing satellite were stationary with respect to the Sun, or in a frame of reference moving with the satellite. The $(\Delta\alpha\cos\delta, \Delta\delta)_g$ value for eclipse corresponds to the separation of the geometric centre of the eclipsed satellite from the shadow centre as seen from the Sun. Unlike occultations these astrometric positions cannot be directly combined with the photographic data set. The position of the eclipsing satellite on the sky plane has to be inferred after suitably correcting for the light travel time. Except near opposition, the mutual eclipses are recorded by monitoring only the eclipsed satellite. The magnitude drop can therefore be determined with better accuracy (section 2.5). The full potential of mutual events can be utilized if the mutual eclipses are also incorporated in the data set after accounting for the tilt of the shadow cone and aberration.

112

6.2.2 Phenomena of the Saturnian Satellites

The equatorial plane of Saturn corsses the inner solar system once in about 15 years — the next such crossing is centered around 1995. Eclipses of the satellites by the planet, occultations by the rings, mutual eclipses and occultations, during the forth-coming apparition have been predicted by Thuillot et al., 1992. It is proposed to observe all the events that are accessible for observations from India. Enceladus-Dione, Mimas-Tethys and Titan-Hyperion are locked in orbital resonances of 1:2, 1:2 and 3:4 respectively. For Mimas-Tethys, $2\lambda_1 - 4\lambda_3 + \Omega_1 + \Omega_3$ librates about 0° where the λ's are the mean longitudes and Ω's are the longitudes of ascending node. For Enceladus-Dione, $\lambda_2 - 2\lambda_4 + \tilde{\omega}_2$ librates about 0°. Determination of the libration amplitudes are important for dynamical purposes (Aksnes et al., 1984; Thuillot, 1992). Secular acceleration of Mimas can be determined if mutual events over several seasons are combined with photographic observations, similar to the present work for the Jovian satellites.

The astrometric observations of the inner faint satellites are difficult due to scattered light from the rings. Imaging in the deep molecular absorption bands will dim the light from the planet but the light from the satellites can only be reduced when these astrometric observations are carried out during the time of ring plane crossings. It is proposed to carry out the astrometric observations of the inner satellites during 1995 to understand their dynamical behaviour.
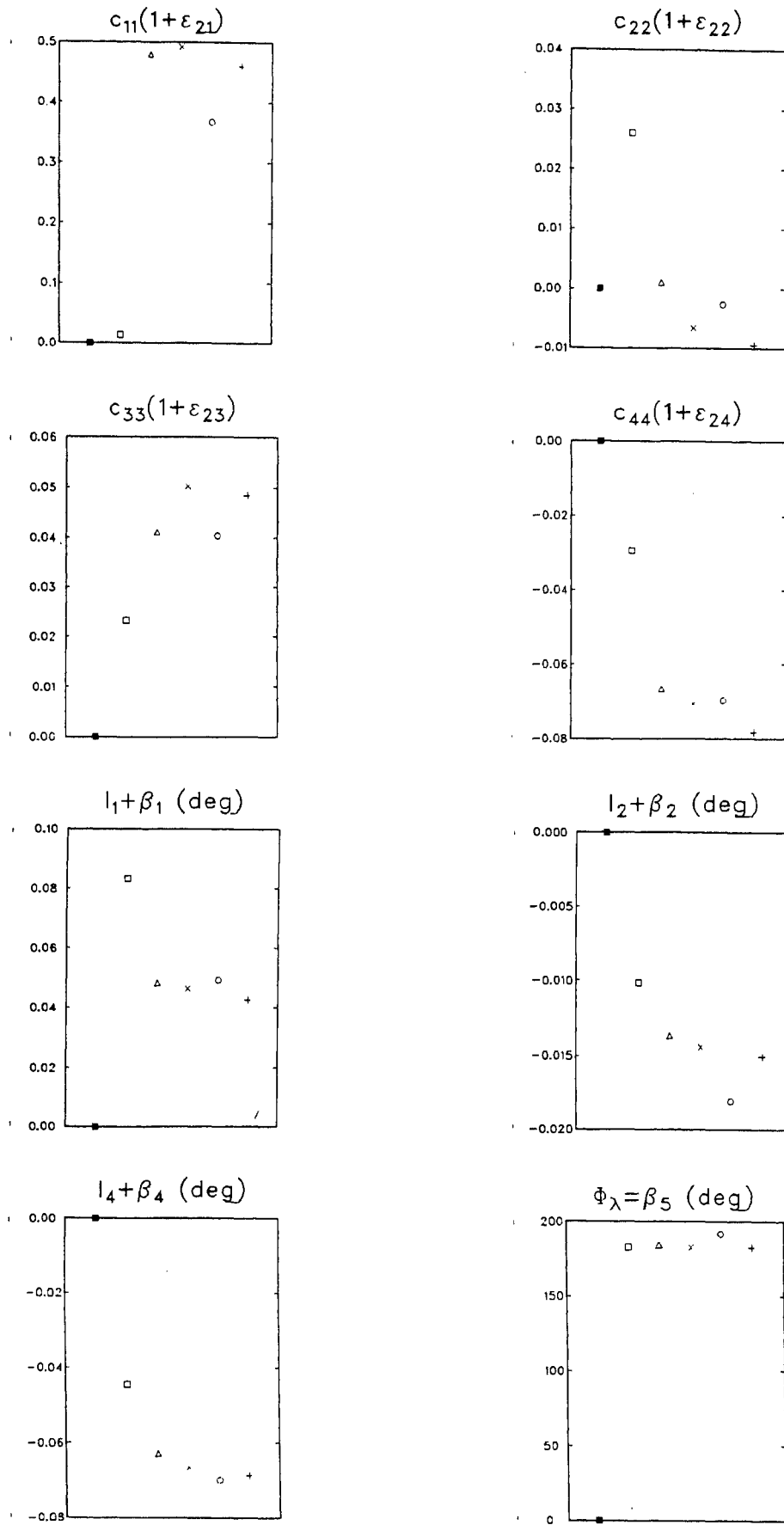
n$_1$(1+ε_6)deg/day

X 10^{-8}

1.0

0.5

0.0

-0.5

n$_2$(1+ε_7)deg/day

X 10^{-8}

1.5

1.0

0.5

0.0

n$_4$(1+ε_8)deg/day

X 10^{-8}

2.5

0.0

-2.5

-5.0

-7.5

$\lambda_A=\varepsilon_9$ radian

X 10^{-4}

15.0

10.0

5.0

0.0

e$_{11}$(1+ε_{16})

0.00

-0.25

-0.50

-0.75

-1.00

e$_{22}$(1+ε_{17})

1.00

0.75

0.50

0.25

0.00

e$_{33}$(1+ε_{18})

0.000

-0.025

-0.050

-0.075

e$_{44}$(1+ε_{19})

0.000

-0.002

-0.004

-0.006

Fig.6.1. Comparison of E0 (■), E-1 (□), E-2 (△), G-5 (×), E2x3 (⊙) and I-32 (+).

Fig.6.1. (Continued) Comparison of E0 (■), E-1 (□), E-2 (△), G-5 (×), E2x3 (⊙) and I-32 (+).
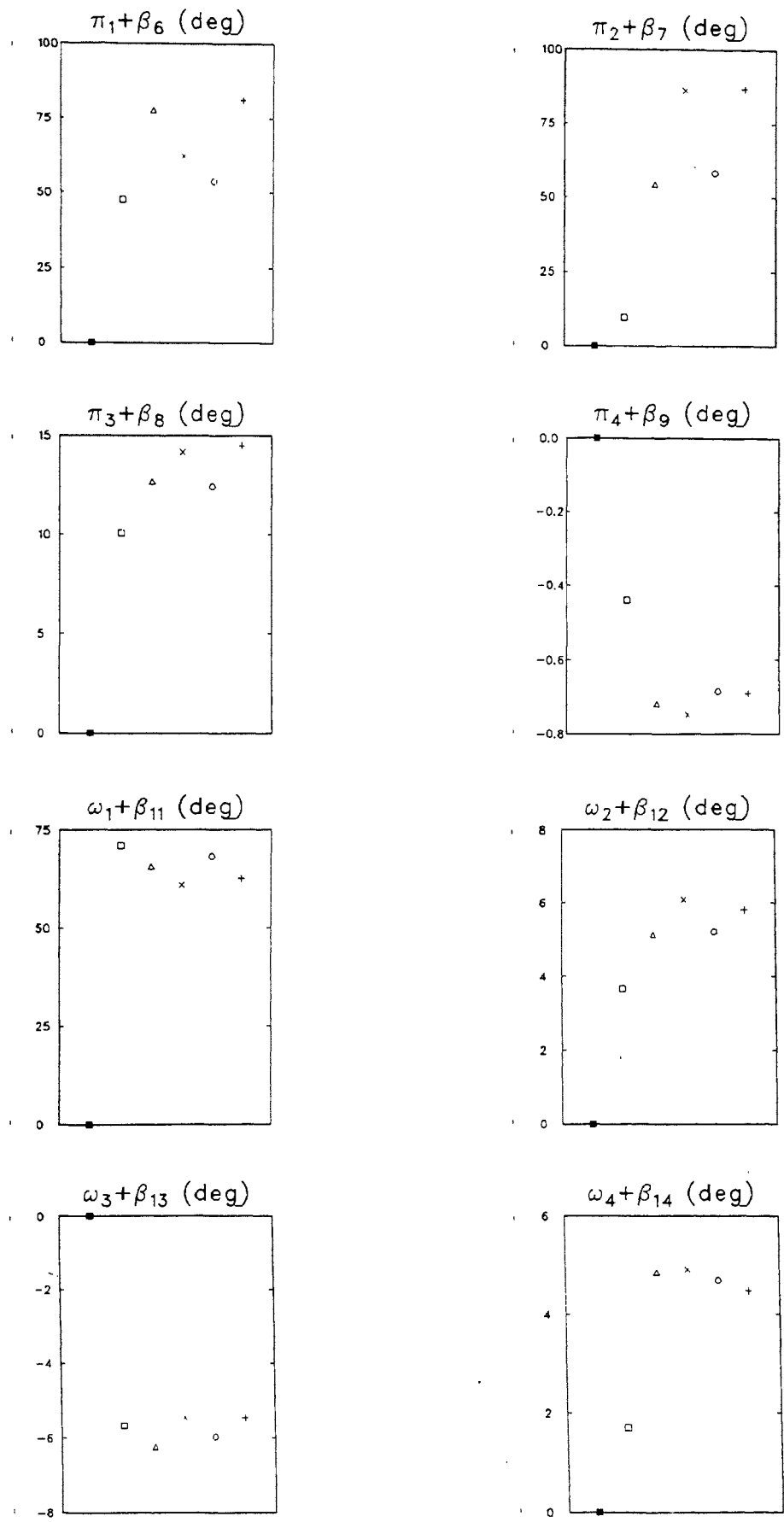
Fig.6.1. (Continued) Comparison of E0 (■), E-1 (□), E-2 (△), G-5 (×), E2x3 (◉) and I-32 (+).

References

Aksnes,K.A., and Franklin,F., 1976, *Astron. J* **81**, 464.

Aksnes, K., Franklin, F., Millis, R., Birch, P., Blanco, C., Catalano, S., Piironen, J., 1984, *Astron. J.* **89**, 280.

Aksnes, K., Franklin, F., Magnusson, P. 1986, *Astron. J.* **92**, 1436.

Aksnes,K.A., and Franklin,F., 1984, *Icarus* **60**, 180.

Aksnes,K.A., Franklin,F., Millis,R., Birch,P., Blanco,C. et al, 1984, *Astron. J.* **89**, 280.

Aksnes,K.A., and Franklin,F., 1990, *Icarus* **84**, 542.

Allen, G.W., 1963, *Astronomical Quantities*, University of London. The Athlone Press.

Andersson, L.E., 1978, *Bull. Am. Astron. Soc.* **10**, 586.

Arlot, J.E., Bernard, A., Bouchet, P., Daguillon, D., Dourneau, G., Figer, A., Helmer, G., Lecacheux, J. Merlin, Ph., Meyer, C., Mianes, P., Morando, B., Neves, D., Rousseau, J., Soulié, G., Terzan, A., Thulliot, W., Vapillon, L., Wlérick, G., 1982, *Astron. Astrophys.* **111**, 151.

Arlot, J.E., 1982, *Astron. Astrophys.* **107**, 305.

Arlot, J.E., 1982a, Ph.D. Thesis.

Arlot, J.E., 1984, *Astron. Astrophys.* **138**, 113.

Arlot, J.E., 1986, Note technique n° 33, RCP n° 754 du CNRS PHEMU 85. Bureau des Longitude, Paris.

Arlot, J.E., 1990, *Astron. Astrophys.* **237**, 259.

Bevington,P.R., 1969. Data Reduction and Error Analysis for the physical sciences. McGraw-Hill, New York.

Binzel, R.P., Tholen, D.J., Tedesco, E.F., Buratti, B.J., Nelson, R.M., 1985, *Science* **228**, 1193.

117

Blanco, C., and Catalano, S., 1974, *Astron. Astrophys.* **33**, 303.

Brinkmann, R.T., 1973, *Icarus* **19**, 15.

Brinkmann, R.T., and Millis, R.L., 1973, *Sky and Telescope* **45**, 93.

Brouwer, D., Clemence, G.M., 1961, in *Planets and Satellites*, Eds. G.P.Kuiper, B.M.Middlehurst, U.Chicago Press, Chicago), pp.31.

Brown, R.A., 1974, in *Explanation of the Planetary System*, Eds. A.Woszczyk and C.Iwaniszewska, Reidel, Dordrecht.

Christy, J.W., Harrington, R.S., 1978, *Astron. J.* **85**, 168.

Colas, F. and Laques, P., 1990, in Proceedings of the PHEMU91 workshop, held in Teramo (Italy) on November 6 and 7, 1990, 29.

de Haerdtl, E. de, 1892, *Bull. Astron.* **9**, 212.

Descamps, P., Arlot, J.-E., Thuillot, W., Colas, F., Vu, D.T., Bouchet, P., and Hainaut, O., 1992, *Icarus* in press.

Descamps, P., 1992a, Ph.D. Thesis.

Descamps, P., and Thuillot, W., 1993, *Icarus*, in press.

deSitter, W., 1928, *Ann. Sterrew, Leiden* **16**, Part 2.

deSitter, W., 1931, *M. N. R. A. S.* **91**, 706.

Franklin, F., 1991, *Astron. J.* **102**, 806.

Greenberg, R., 1982, In *Satellites of Jupiter*, ed. David Morrison, (Tucson: Univ. of Arizona Press), 65.

Greenberg, T., Goldstein, S.J.Jr and Jacobs, K.C., 1986, *Nature* **323**, 789.

Goguen, J.D., Sinton, W.M., Matson, D.L., Howell, R.R., Dyck, H.M., Johnson, T.V., Brown, R.H., Veeder, G.J., Lane, A.L., Nelson, R.M. and McLaren, R.A., 1988, *Icarus* **76**, 465.

Goldreich, P., 1965, *MNRAS* **130**, 159.

Goldstein, S.J.Jr., 1975, *Astron. J.* **80**, 532.

Goldstein, S.J.Jr., Jacobs, K.C., 1985, *Bull. Am. Astron. Soc.* **17**, 873.

Goldstein, S.J.Jr., Jacobs, K.C., 1986, *Astron. J.* **92**, 199.

118

Hapke, B., 1963, *J. Geophys. Res.* **68**, 4571.

Hapke, B., 1966, *Astron. J.* **71**, 333.

Hapke, B.W., 1984, *Icarus* **59**. 41.

Hapke, B., 1981,*J. Geophys.Res.* **86**,3039.

Hardie, R.H., 1962, in *Astronomical Techniques*, ed. W.A.Hiltner (Chicago: Chicago Univ. Press) p.178.

Harington, R.S., Christy, J.W., 1980, *Astron. J.* **85**, 168.

Harington, R.S., Christy, J.W., 1981, *Astron. J.* **86**, 442.

Harris, D.L., 1961, in *The Solar System* (eds: G.P.Kuiper and B.M.Middlehurst) 272. Univ. of Chicago Press.

Innes, R.T.A., 1910, *Observatory* **33**, 478.

Johnson, T.V., 1970, Ph.D. Thesis Cal. Tech.

Kupo, I., Mekler, Y. and Eviatar, A., 1976, **Astrophys. J. 205**, L.51.

Levin, A.E., 1931, *Mem. Brit. Astron. Assoc.* **30**, 149.

Lieske, J.H., 1973, *Astron. Astrophys.* **27**, 59.

Lieske, J.H., 1974, *Astron. Astrophys.* **31**, 137.

Lieske, J.H., 1977, *Astron. Astrophys.* **56**, 333.

Lieske, J.H., 1978, *Astron. Astrophys.* **65**, 83.

Lieske, J.H., 1980, *Astron. Astrophys.* **82**, 340.

Lieske, J.H., 1986, in *Relativity in Celestial Mechanics and Astronomy*, (eds. J.Kovalevsky, V.A.Brumberg), Reidel, Dordrecht, p.117.

Lieske, J.H., 1987, *Astron. Astrophys.* **176**, 146.

Lieske, J.H., 1987a, Private communication of E-3 computer code.

Mallama, A., 1991, *Icarus* **92**, 324.

Mallama, A., 1992, *Icarus* **95**, 309.

Mc Ewen, A.S., Matson, D.L., Johnson, T.V. and Soderblom, L.A., 1985, *J. Geophys. Res.* **90**, 12345.

Milbourn, S.W., and Carey, J.V., 1973, *Handbook of the British Astrnomical*

Association, p.36.

Minnaert, M., 1941, *Astron. J.* **93**, 403.

Morrison, D., Morrison N.D. and Lazarevicz, A.R., 1974 Four colour photometry of the Galilean satellites. *Icarus* **23**, 399-416.

Nakumara, T.W., and Shibasaki, H., 1990, in Proceedings of the PHEMU91 workshop, held in Teramo (Italy) on November 6 and 7, 1990, 41.

Nicolet, B. and Ch.Nitschelm, 1990, in Proceedings of the PHEMU91 workshop, held in Teramo (Italy) on November 6 and 7, 1990, 83.

Owen, F.W. and Lazor, F.J., 1973, *Icarus* **19**, 30.

Peale, S.J., Cassen, P., Reynolds, R.T., 1979, *Science* **203**, 892.

Pilcher, C.B., and Morgan, J.S., 1979, *Science* **205**, 297.

Simonelli, D.P., and Veverka, J., 1986, *Icarus* **66**, 403.

Squyres, S.W., and Veverka, J., 1981, *Icarus* **46**, 1981.

Srinivasan, R., Nagaraja Naidu, B., Vasundhara, R., 1993, *Indian Journal of Pure and Appl. Phys.* in press.

Stephenson, F.R., Morrison, L.V., 1984, *Phil. Trans. Roy. Soc., London* **A 313**, 47.

Thuillot, W., Arlot, J.-E., Vu, D.T., 1990, in proceedings of the PHEMU91 workshop, held in Teramo (Italy) on November 6 and 7, 1990, 33.

Thuillot,W., Arlot, J.-E., Colas, P.,Descamps,P.,Vu,D.T, 1992, Private communication.

Vasundhara, R., 1991, *J. Astrophys. Astr.* **12**, 69.

Wasserman, L.H., Elliot, J.L. and Veverka, J., 1976, *Icarus* **27**, 91.

Yoder, C.F., 1979, *Nature* **279**, 767.

Yoder, C.F., Peale, S.J., 1981, *Icarus* **47**, 1.

120